Geology and Geothermal Setting of Tompaso Geothermal System, Indonesia, with Comparisons of Andesite Alteration Patterns with Wairakei, New Zealand

By

Kartika Palupi Savitri

A thesis
submitted to Victoria University of Wellington
in partial fulfillment of requirements for the degree of
Master of Science in Geology

School of Geography, Environment and Earth Sciences
Victoria University of Wellington

2016

Abstract

Tompaso geothermal system is a typical volcanic arc geothermal system in North Sulawesi, Indonesia. Although situated close to the Tondano caldera, subsurface lithologies and structures do not show any evidence for caldera-related features and the system is inferred to be related to the andesitic Soputan volcano. The subsurface geology of Tompaso consists of Tuff B unit, Rhyolite unit, Andesite B unit, Pitchstone unit, Pyroclastic Breccia unit,Andesite A unit, Pumice unit, and Tuff A unit, respectively, from the oldest penetrated unit. The silicic Pitchstone and Rhyolite units are presumed to be sourced from the same magma chamber. Petrological and mineralogical observations using binocular and petrographic microscopy, short-wave infrared (SWIR) analysis, and back-scattered electron (BSE) imaging combined with energy dispersive X-ray spectroscopy (EDS) have been applied to cuttings and limited core material from three boreholes: LHD-26, LHD-27, and LHD-32. Age dating has not been undertaken and, thus, conclusions on correlations between subsurface geology inferred here with surface formation groupings from previous works cannot be drawn.

Tompaso geothermal system is characterised primarily by variations in the fracturing within the reservoir. Secondary mineralogy and the structure of present-day temperature of the system suggest that the movement of hydrothermal fluids at Tompaso is controlled by faults: the Soputan, Tempang, and A-A' faults, the last defined for the first time in this thesis. Soputan Fault controls the outflow of the system. On the other hand, the influence of Tempang and A-A' faults is dominant only in the upper portion of the system. The A-A' fault likely acts as a channel for cooler meteoric surface water, while the Tempang Fault is inferred to have experienced self-sealing and appears to be an impermeable structure in the system. The self-sealing process of the Tempang Fault and/or the introduction of meteoric water through the A-A' fault may be related to the cooling of the northern and western part of the system.

The challenges in identifying protoliths in active geothermal areas is addressed here through studies of the influence of andesite textures on the preferences of hydrothermal alteration processes. Wairakei andesites were chosen for comparison to Tompaso andesites, especially because of its different geological setting and geothermal reservoir structure. The results suggest that mineral composition and arrangement affect the preference of hydrothermal alteration on andesites.

Acknowledgement

Firstly, I am grateful for Geothermal Research Centre, Universitas Gadjah Mada (UGM), for encouraging and giving me a recommendation and full support for me to pursue my Master's study. Thanks are also expressed to Faculty of Engineering (UGM), Geological Agency of Indonesia, Indonesian Society of Economic Geologists and GNS Science of New Zealand for giving me recommendations, without which I would not have received my scholarship. The Ministry of Foreign Affairs and Trade (MFAT) of New Zealand funded my study in Victoria University of Wellington (VUW) through a New Zealand ASEAN Scholars (NZAS) Award in 2013-2016.

I would like to thank my primary supervisor, Prof. Colin Wilson. I am privileged to get a chance to be guided by and to have learned from you. You have taught me not only geology and volcanology, but also how to be a researcher and a teacher. It was a pleasure to work with you. I especially thank my co-supervisor Dr. Isabelle Chambefort for random questions and discussion about petrology, mineralogy, and geothermal systems. I also thank my co-supervisor Dr. Sarah Milicich for discussions about geology and geothermal systems and helping me with Leapfrog Geothermal software. Thanks also go to my third co-supervisor, Dr. Greg Bignall, for helping me during the initial phase of my research. I also thank you for flying to Indonesia to help me with permit application for the use of my samples.

PT Petamina Geothermal Energy (PGE) has given me access to Tompaso Geothermal Field and permission to use its core, cuttings, and other relevant data. Messrs. Imam Rahardjo, Eben Siahaan, Imam Prasetyo, Yustin Kamah, and Sardiyanto and Ms. Vivi Nusantara have been the key persons of this substantial process. The Directorate General of New Energy and Renewable Energy Conservation as part of the Ministry of Energy and Mineral Resources of Indonesia has approved the usage of Tompaso samples and made this work possible. I would like to thank Contact Energy along with GNS Science for giving me access and permission to use cores and cuttings from Wairakei Geothermal Field.

Thanks to Mark Simpson for teaching me the Short Wave Infrared (SWIR) analysis as well as GNS Science for giving access to the instrument as well as its related software. Thanks also go to Fiona Sanders for the helpful discussions on Wairakei. David Flynn through the School of Chemistry and Physical Sciences VUW gave me access to and trained me to use the Scanning Electron Microscopy and Energy Dispersive X-Ray (SEM-EDS) system: your help was invaluable. I thank Stewart Bush for undertaking the polished thin section preparation

and helping me polishing grain mounts. I would also like to thank Ian Schipper for undertaking probe analysis on the pitchstone samples.

I would like to acknowledge the support from ARANZ Geo Ltd. for granting me a year licence to use Leapfrog Geothermal software which made this thesis work possible. Thanks also go to AusSpec International for supporting the TSG Viewer software for SWIR analysis.

I appreciate all the Minahasan people at Tompaso for allowing me to access their land and giving me helpful insights during my fieldwork. I thank the Geothermal Research Centre for facilitating all the fieldwork instruments. Thanks also go to Mr. Tondo Wicaksono for your assistance during sample collection in Kamojang core shed.

I thank Andrea Blair and Mauro Passarella for letting me stay in their lovely house during my lab work in Wairakei. I would also like to thank my ISO, Helena Cook, for always be my ear for the last two years. Thanks to Lorena, Sandra, Pete, and Ti for being such lovely office mates. Jill Fernandes, thank you for being a fantastic study-mate and flatmate.

Thank you for all Indonesian friends in New Zealand for always providing a heart-warming place I could call home. Malia, Esti, Lina, Dika, Amalia, and many other friends living 7000 km away, thanks for always willing to pick up my calls and reply my messages even at the most ridiculous times, day and night; thank you for random questions and discussions and specially thank you for keeping me from falling when the road was not smooth. I am grateful for my mentor, Mrs. Pri Utami, for putting your trust in me and helping me gain my self-esteem back when I need it the most.

Last but not least, to my mother, my father and my brother, thank you for your endless love, encouragement, and support. My father especially; thanks for always being my geology partner and accompanying me doing fieldwork. My dear partner Adityo; thanks for being a source of spirit boost, inspiration, and motivation. I could never have done it without you!

Contents

Figures

Tables

CHAPTER ONE

INTRODUCTION

1.1. Background

Following the recent growth of geothermal energy as a 'green' or 'renewable' source of energy, increasing attention has been paid to developing this energy as an alternative to fossil fuels, particularly to generate electricity. Indonesia is located in an active volcanic area, considered to have the largest geothermal resources in the world with a total potential of ~29 Gigawatt electric (GWe) (Geological Resource Centre, 2014). Geothermal systems with a potential productivity of 3,248 Megawatt electric (MWe) exist within North Sulawesi, yet only 80 MWe had been developed by 2014 (Geological Resource Centre, 2014). It is apparent that developing geothermal systems in North Sulawesi offers attractive prospects for indigenous development of resources to satisfy increasing demands for electricity supplies. The exploration and development of a geothermal system relies on understanding the geological and geothermal settings of the system.

The main focus of this thesis is a study of the geological and geothermal settings of one of the geothermal fields in North Sulawesi: Tompaso. By observing the petrology and mineralogy of the subsurface rocks, this thesis aims to evaluate the subsurface geology as well as geothermal characteristics of Tompaso geothermal system. This study will give valuable knowledge about its geothermal system structures and properties. This knowledge is essential to assist the future development of Tompaso geothermal resources for electricity generation.

Another challenge in developing geothermal systems is that in active geothermal systems, the lithologies are commonly altered and it is difficult to identify the protoliths. To address this issue, the control of lithology on the distribution of hydrothermal products has also been investigated, with the focus of investigation is on rock textures. The term 'rock textures' used in this thesis include the arrangement of rock components and mineralogy composition. As Tompaso consists predominantly of andesite lithologies, this part of the work is limited to this type of rock. While most of previous studies highlighted the presence of fractures/microfractures as the main feature controlling hydrothermal alteration

processes (Roberts et al., 2000; Siratovich et al., 2012), this thesis studies the possibility that rock textures can also affect the precipitation of hydrothermal minerals.

Andesite is the most common lithology in volcanic arc geothermal systems, including Tompaso, and its alteration properties are complex. Thus, andesite from Wairakei geothermal system has been studied also in this thesis for comparison to the andesite from Tompaso. Wairakei Geothermal Field in New Zealand is also located in a volcanic arc setting, and although the lithologies are mainly silicic volcanic rocks (section 2.2.1), andesite lithologies are also present. Material from the Waiora Valley Andesite (WVA) has been made available through an ongoing research programme by GNS Science and Contact Energy. The results of this thesis will contribute towards their research work on the hydrothermal alteration.

1.2. Study Locations

The main work in this thesis has been undertaken on samples from Tompaso geothermal system in Indonesia. The Tompaso geothermal system is situated in North Sulawesi, Indonesia (Fig. 1.1), in a volcanic arc setting created by subduction zones on the eastern of Sulawesi Island (section 2.1.1). Tompaso is likely to be the next area of interest for development as a source of electricity in Sulawesi, with ownership of the resource in the field belonging to PT Pertamina Geothermal Energy (PGE). Even though the Tompaso system has not yet been exploited for production, it is estimated to have a geothermal potential output equivalent to as much as 220 MWe (Handoko, 2010). To date, eight wells have been drilled at Tompaso, grouped into three clusters based on their location (section 3.3.1). The characteristics of its geothermal system have not been studied in depth beyond internal, confidential company reports.

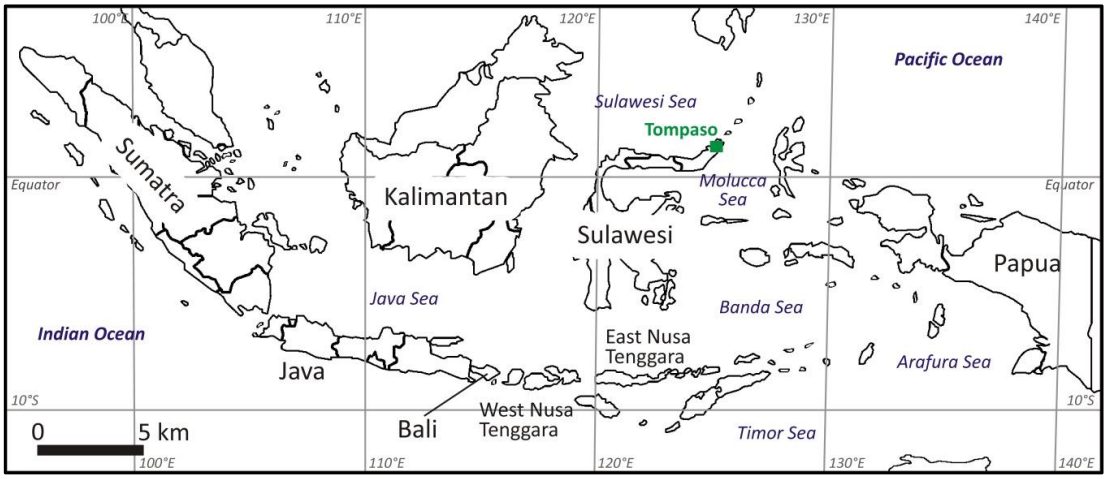

Figure 1.1. Location of the Tompaso geothermal system in Indonesia.

The second part of this thesis compares Tompaso to Wairakei andesites. The Wairakei geothermal system is located in North Island, New Zealand (Fig. 1.2). It is situated within Taupo Volcanic Zone (TVZ), the onshore southern end of the Tonga-Kermadec arc, associated with subduction of the Pacific plate under the Australian plate (section 2.2.1). The Wairakei Field has been operating for >50 years and has the longest operating history and the largest installed capacity (375 MWe) in New Zealand (Sepulveda et al., 2014). This field belongs to Contact Energy and is part of the bigger Wairakei-Tauhara geothermal system. The Wairakei-Tauhara system is estimated to have heat potential output as much as 420 MWe (Bibby et al., 1995). Despite a dominance of silicic lithologies, two andesite units are found in Wairakei: a member of the older Tahorakuri Formation and the younger Waiora Valley Andesite (WVA) intercalated in the Waiora Formation (section 2.2.2, 2.2.3) (Sanders et al., 2013).

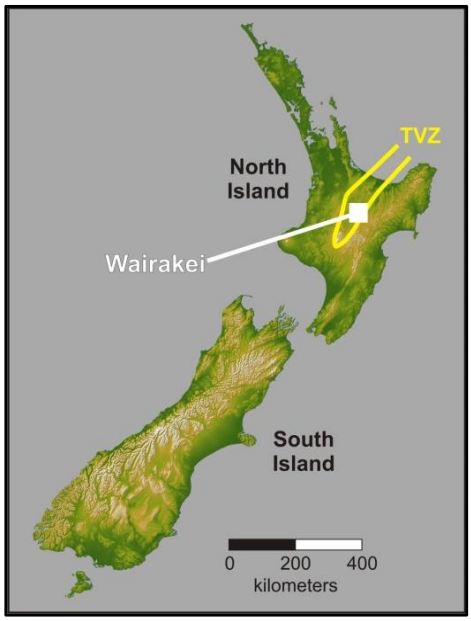

Figure 1.2. Location of Wairakei geothermal system, New Zealand.

1.3. Thesis Aims

The purpose of this research is to understand the characteristics of the Tompaso geothermal system. This research aims to produce a conceptual model of Tompaso geothermal system which is to help in the future development of the field with minimum risk. In addition, this thesis is expected to give ideas of the influence of andesite texture on hydrothermal alteration processes by comparing Tompaso and Wairakei samples. The research specifically aims to address these following questions:

(a) What is the subsurface geological setting of Tompaso geothermal system?
(b) What are the factors controlling permeability in Tompaso geothermal systems?
(c) What is the configuration of hydrology and thermal structure of the Tompaso geothermal system?
(d) What is the conceptual model of Tompaso geothermal system and, according to it, what area is likely suitable for the next targeted area?
(e) How does the distribution of hydrothermal alteration products relate to the textural characteristics of the andesite lithologies in Tompaso and Wairakei systems?
(f) What do the relationships considered under question (d) reveal about the controls of andesite textures on the preference of hydrothermal alteration processes?

1.4. Thesis Roadmap

This thesis investigates samples from Tompaso geothermal systems. Aspects of the Tompaso geothermal system have been investigated, including its geology, surface and subsurface features, hydrothermal alteration, and hydrological and thermal characteristics. These have been studied through hand specimen and binocular observation, petrography (primary geology and hydrothermal alteration), short wave infrared (SWIR) analysis, back-scattered electron (BSE) imaging combined with energy dispersive X-ray spectroscopy (EDS), and 3-dimensional (3D) geological modelling. Macroscopic, binocular, and petrographic examination has been undertaken on the cuttings and (limited) core (section 3.3.1) collected from three geothermal wells (LHD-26, LHD-27, and LHD-32) to observe rock types and mineralogy compositions. The results were then compared to the geological well data provided by PGE to understand the stratigraphy of each well. The compiled

stratigraphy was visualised in 3D using Leapfrog Geothermal software (section 4.1.1) and used as a guide to select samples for the next stages of the work.

In addition to being used to create a 3D geological visualisation, the petrographic results have been combined with data from SWIR and BSE-EDS to define and vertically map the distribution of hydrothermal minerals within the wells (section 4.1.3). Macroscopic and SWIR analyses have also been done on surface samples to give information about the lateral distribution of surficial hydrothermal minerals. Hydrothermal minerals provide information about the conditions in the geothermal system at the time they formed, including the position(s) and temperature(s) of upflow zones. Comparisons of temperatures recorded by hydrothermal minerals to measured well temperatures gives insight into the temperature configuration of the modern geothermal system as well as possible natural changes that have been experienced by the system (section 5.2.3). Surface geothermal manifestations have been studied during fieldwork, with observations such as temperature and pH of geothermal fluids recorded (section 4.1.2). The types of manifestation, and their temperature, pH and fluid composition can indicate position of each surface thermal manifestation relative to the overall system. Geothermal manifestations observed include hot springs, hot pools, warm springs, mud pots, fumaroles, and steaming ground. Comparisons between the surficial hydrothermal activity to subsurface activity can thus provide information about the hydrological configuration of the system (section 5.2.2). Based on the interpreted thermal and hydrological configuration, a conceptual model of the Tompaso geothermal system has been proposed, which can be used to make suggestions on the future development of the system (sections 5.2.2, 6.2).

Identifying protoliths in geothermal areas is challenging due to the intense hydrothermal alteration. Cuttings type of sample also inhibits the interpretation of textural relationships. In this thesis, the observations have been made on the relationship between the distribution of hydrothermal minerals and rock textures (section 5.3). This observation has also included samples from Wairakei geothermal system for comparison. At Wairakei, two andesite units are present, but this thesis has only used the younger, reflecting the availability of samples (section 3.3.1). The Wairakei part of this research has utilised samples from and contributed support to a research project with GNS Science and Contact Energy. The stratigraphy of wells used in this research (WK-47, WK-48, WK-54, and WK-122) has been described by staff at GNS Science, and samples for this study have been selected based on this information.

1.5. Limitations to this research

In general, limitations and challenges experienced during this research are related to the condition and availability of Tompaso samples. One week of fieldwork has been done in Tompaso. Initially, this fieldwork aimed to cover both the surface geology and hydrothermal processes and manifestations at the field. In practise, because of the intensity of surficial weathering processes and hydrothermal alteration, fieldwork focussed on the observation of geothermal activities rather than geological features. Consequently, correlation of surface and subsurface geological units cannot be taken with confidence.

Observations of Tompaso subsurface geology have been done using a hand lens and binocular microscope. Since the samples are cuttings, collected on a 3-m interval, mixing of samples from various depths during their collection is very common. In addition, the grain size of most of the fragments ranges from <2 to rarely 5 mm. Consequently, determining lithologies from Tompaso samples is challenging. The identification of the lithologies at a particular depth is therefore based on the proportion of each lithology type present.

Ideally, this research would also have included studies on the hydrothermal mineral assemblages present in veins because the presence of veins suggests a different mechanism of formation than replacement minerals. Vein assemblages are able to give insight on the hydrothermal alteration episodes associated with hydraulic fracturing that have been experienced by the system (Utami, 2011). However, observing veins from Tompaso cuttings is difficult due to the cuttings' grain size. It is difficult not only to observe under binocular microscope, but also to select the grains for grain mount preparation.

Another challenge experienced during this research is applying SWIR analysis on Tompaso cuttings. SWIR analysis works using light reflection on the altered rock. Unlike light-coloured materials which reflect both visible and infrared wavelenghts, dark-coloured materials absorb both. The poor reflection produced by dark-colouration results in analytical noise (Simpson et al., 2006). In addition, the common presence of volcanic glass in LHD-26 samples represents another challenge. Significant amount of volcanic glass present in the samples causes issues by adding OH, H_2O and AlOH to the spectra (Zhang, 1999). Despite these challenges, SWIR analysis was still useful in characterising samples.

This thesis use SWIR instead of X-ray diffarction (XRD) analysis. XRD is widely used to investigate hydrothermal mineralogy in geothermal geology investigation as it produces more accurate results than SWIR. However, the analysis requires more time to prepare the samples. Therefore, SWIR is chosen considering the timeframe of this thesis.

The second objective of this thesis is to advance the understanding on how andesite petrology may controls hydrothermal alteration processes. To reach this objective, the andesites of Tompaso have been compared to the andesites of Wairakei geothermal system. Lahendong geothermal system, which is located 30 km apart from Tompaso, would have been an ideal comparison as its geology and geothermal characteristics are generally similar to Tompaso. However, permits of the use of samples by overseas institution from the government of Indonesia for this thesis only cover Tompaso samples. Even though Wairakei and Tompaso geothermal characteristics show some differences (section 2.1.4., 2.2.4.), the andesites petrology of the two areas are similar.

1.6. Thesis Outline

CHAPTER 1 introduces the concepts and purposes of the thesis, including the locations of where research has been taken at as well as the methods applied. It then introduces the limitations encountered during the work.

CHAPTER 2 introduces the geological settings of the Tompaso (Indonesia) and Wairakei (New Zealand) geothermal systems . The summaries of each area cover their tectonic, volcanic, and geothermal settings as well as the occurrence of andesite in the systems since the relationships of andesite textures and hydrothermal alteration distribution was studied as part of this thesis.

CHAPTER 3 summarises the analytical methods adopted in this research. The summary is presented in four categories: pre-existing data investigation, fieldwork, textural and mineralogical analyses, and 3D geological modelling using Leapfrog Geothermal software. The description of samples and sample preparation is presented under 'textural and mineralogical analyses' section.

CHAPTER 4 summarises the results of this thesis, divided into three sections. The first and second sections present both the geological and hydrothermal alteration results of Tompaso and Wairakei geothermal systems, respectively. The last section summaries all the andesite textures observed in the studied Tompaso and Wairakei samples along with the presence or absence of relationships with the distribution of secondary minerals.

CHAPTER 5 discusses the geological setting of the Tompaso area by comparing what has been known with what is shown from the results presented in chapter 4. It then discusses the characteristics of the Tompaso geothermal system. Permeability controls as well as hydrological and thermal configurations of the system are the main discussions. At the end, this chapter discusses the likelihood of andesite textures influencing the preference of hydrothermal alteration processes in both Tompaso and Wairakei samples.

CHAPTER 6 concludes the thesis by providing an evaluation on the regional geology of Tompaso area. It then concludes the characteristics of the Tompaso geothermal system by providing the conceptual model of the system as well as suggestions regarding to the future development. Finally, it concludes whether this thesis may contribute future research on the knowledge of how andesite lithologies are altered.

Several appendices are included in this thesis in electronic form.

Appendix A: Field records of the fieldwork undertaken at Tompaso area.

Appendix B: Description of Tompaso cuttings, including samples from LHD-26, LHD-27, and LHD-32, based on binocular microscopy observations.

Appendix C: List of secondary minerals presented in Tompaso and Wairakei samples based on the SWIR records.

Appendix D: Description of petrographic thin section of Tompaso and Wairakei samples.

Appendix E: Description of Tompaso and Wairakei lithologies as well as their secondary minerals composition based on the BSE-EDS imaging.

Appendix F: Short movies of the 3D models, including:

F-01: geological model.

F-02: temperature structure.

F-03: relationship of secondary epidote distribution to the present-day 240 °C profile.

F-04: relationship of secondary illite distribution to the present-day 220 °C profile.

F-05: relationship of secondary smectite distribution to the present-day 200 °C profile.

CHAPTER TWO

GEOLOGICAL SETTING

This thesis focusses on Tompaso (Indonesia) geothermal system. Additional observations have been undertaken on andesite samples from Wairakei (New Zealand), with an emphasis on understanding the role of textures in controlling the behaviour of hydrothermal alteration processes in andesite protoliths. These fields have different geological settings as well as geothermal characteristics: Tompaso is hosted within andesites of a volcanic arc. The Wairakei system is in a rifted arc setting dominated by rhyolitic volcanic products, although andesite formations (as studied here) also occur. In addition, differences in the tectonic framework of the two systems are also reflected in the geothermal characteristics, including the hydrological configuration and chemistry of hydrothermal fluids. The Wairakei geothermal system extends to the southeast, to encompass both the Wairakei and Tauhara geothermal fields[1]. However, this thesis only considers Wairakei Geothermal Field, without integrating Tauhara Geothermal Field because of the availability of samples (section 3.3.1). Thus the 'Wairakei system' discussed in this thesis refers only to the Wairakei part of the system, not to the whole Wairakei-Tauhara system as discussed in most other works (e.g. Rosenberg et al., 2009).

2.1. Tompaso Geothermal System

2.1.1. Tectonic Framework

The Tompaso system is located in the north arm of Sulawesi Island (Fig. 2.1). Two subduction zones are present: the North Sulawesi Subduction Zone to the north of Sulawesi Island (i.e., to the west of Tompaso – green box in Fig. 2.1) and the East Sangihe Subduction Zone to the east (Hall, 1996, 2009) (Fig. 2.1). The latter subduction zone is unusual in being the only example globally of an arc-arc collision zone (Morrice et al., 1983; Jaffe et al., 2004). The subduction zone located in the Molucca Sea was developed at about 25 Ma

[1] Following earlier usage (Milicich, 2013), the word 'field' is used to refer to the geothermal resource and land boundaries associated with drilling, while the word 'system' is used to refer to the geothermal natural entity.

(Late Oligocene[2]) with the subducted slab dipping to the west beneath the Sangihe Arc (Hall, 1996, 2009). At 5 Ma (Late Miocene), collision between the Sangihe on the west and Halmahera arcs on the east began, initiating an arc-arc collision with slab dipping to the west beneath the Sangihe arc and to the east beneath the Halmahera arc (Fig. 2.1) (Hall, 1996, 2009). The collision brought the two arcs into contact at about 3 Ma (Pliocene) resulting to the shortening on the Halmahera side by thrust faulting (Fig. 2.1) (Hall & Smyth, 2008). To the north of Sulawesi Island (Fig. 2.1), the North Sulawesi Subduction Zone has been active from 5 Ma, around the same time of the initiation of the East Sangihe double subduction system (Hall, 1996).

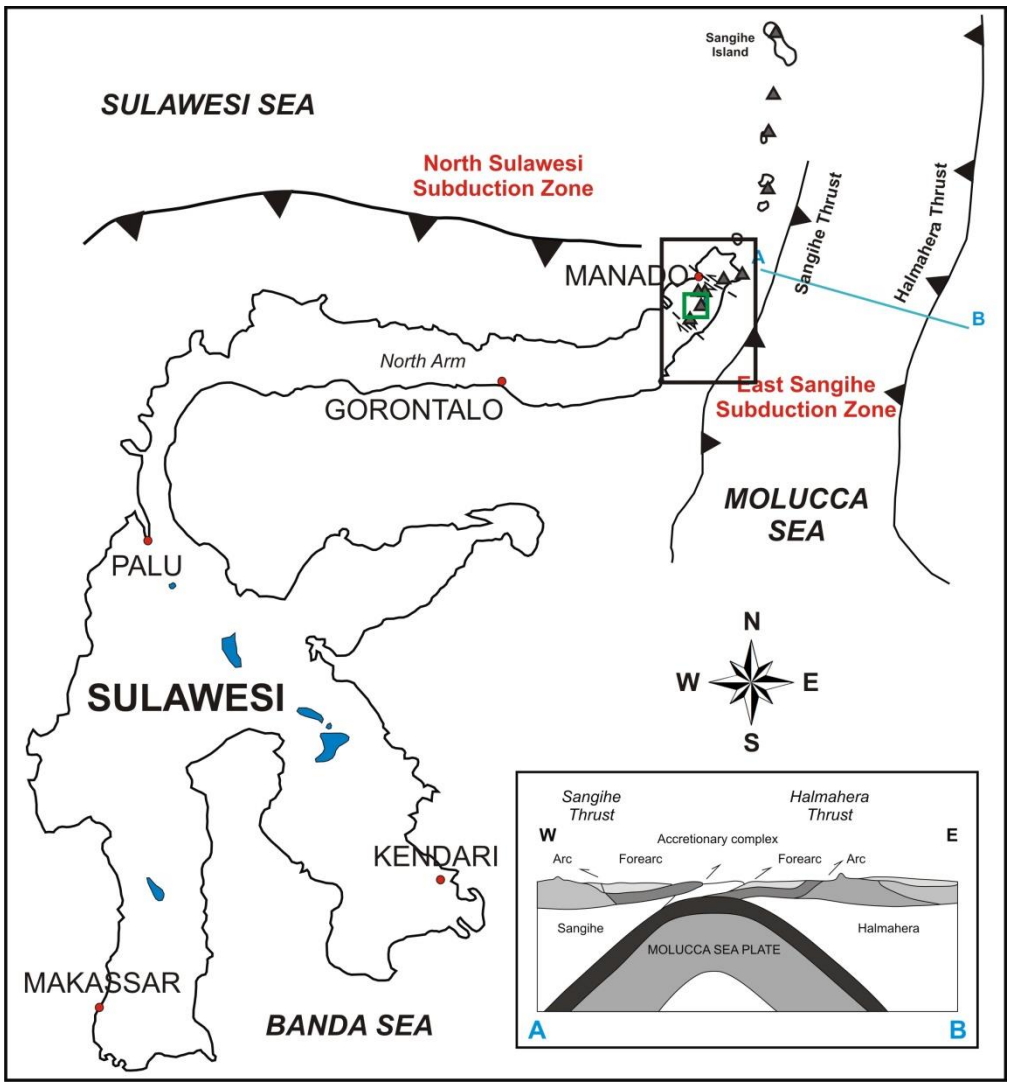

Figure 2.1. Regional setting of Sulawesi Island and the Tompaso geothermal system. The geological structures shown are only those related to the initiation of Tompaso geothermal system. The black and green outlines represented the area covered in Fig. 2.2. Inset shows the W-E cross section of the Sangihe-Halmahera thrust of the East Sangihe Subduction Zone (adapted from Jaffe et al., 2004).

[2] The ages used in this thesis are based on the 2015 International Chronostratigraphic Chart (Cohen et al., 2015)

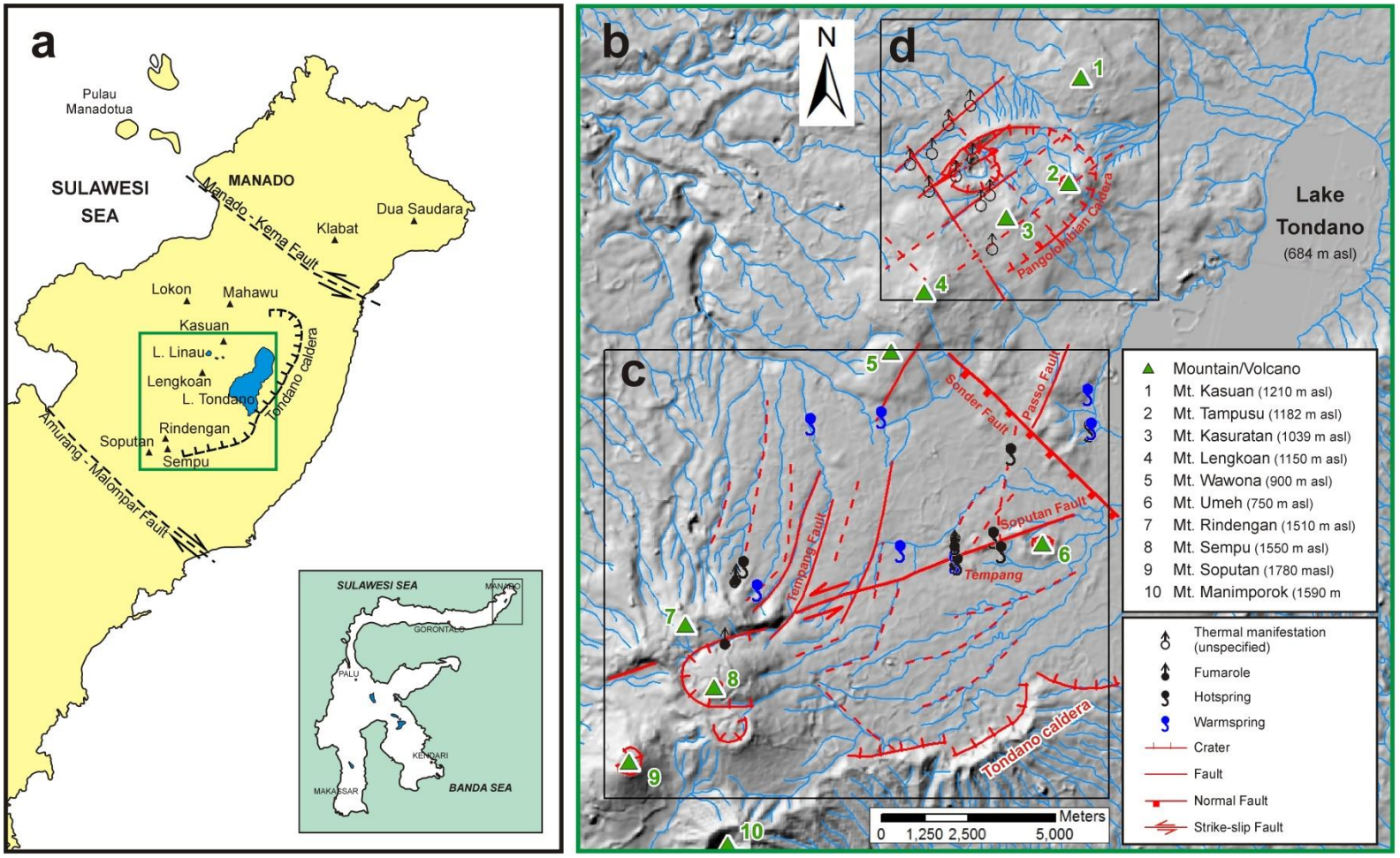

Figure 2.2. Map of the spatial relationships between volcanoes and geothermal areas at Tompaso and its vicinity: (a) The northern part of Sulawesi Island; (b) Digital terrain map of the area covered by the green box in (a); (c) Tompaso Geothermal Field; and (d) Lahendong Geothermal Field. Geological structures and positions of surficial geothermal manifestations of Tompaso are from this work and Sardiyanto et al. (2015) and those of Lahendong are taken from Utami (2011)). Thermal manifestations of Lahendong from Utami (2011) include altered ground.

The presence of both subduction zones creates a pair of parallel NW-SE striking strike-slip faults and a volcanic arc in the area around Tompaso. The strike slip faults are the dextral Amurang-Malompar Fault to the south and sinistral Manado-Kema Fault to the north (Fig. 2.2(a)) (Effendi & Bawono, 1997; Sardiyanto et al., 2015). The volcanic arc is the N-S trending Sangihe arc extending from Awu Volcano in Sangihe Island to Soputan in Sulawesi Island (Figs. 2.1 and 2.2). The arc has been initiated as a product of East Sangihe Subduction (Fig. 2.1) (Rangin & Silver, 1991; Effendi & Bawono, 1997; Handoko, 2010). The East Sangihe volcanic arc is thought to have first formed at about 7.5 Ma (Late Miocene) and may have experienced a renewal of volcanic activity, at least by the early Pliocene (Pubellier et al., 1991).

The East Sangihe Subduction Zone is responsible for the uplift and tilting of subducted slab which is inferred to have controlled the location of the Sangihe volcanic arc. The arc location is reflected by Tampusu, Kasuratan, Lengkoan, Rindengan, and Soputan volcanoes (Fig. 2.2(b)) (Handoko, 2010). Tompaso system is situated on the NE flank of Soputan Volcano, which is the southermost volcano of this arc. Soputan Volcano is inferred to lie 150 km above the Benioff zone yet its volcanic products are of chemical compositions that normally are restricted to the volcanic front, 110 km above the Benioff zone (Morrice et al., 1983).

The tectonic setting of the Tompaso Field is reflected in three major fault strikes; NE-SW, NW-SE, and NNE-SSW (Fig 2.2). Two named major faults at Tompaso are the ENE-striking sinistral strike-slip Soputan Fault (Lécuyer et al., 1997) and NW–SE striking normal Sonder Fault. The Soputan Fault controls the occurrence of most surficial geothermal manifestations, whereas the Sonder Fault is apparently unrelated to any geothermal manifestations (Fig. 2.2). Stream alignments also suggest the presence of NNE-SSW structural trends, including those referred to as the Tempang and Passo faults by previous workers (Fig. 2.2) (Sardiyanto et al., 2015). A minor number of lineaments are present in the northwest part of Tompaso.

The basement structures at Tompaso appear to be related to the growth of Soputan Volcano as geological structures in Lahendong show different trends (Fig. 2.2). Lahendong Geothermal Field is situated to the north of Tompaso and thought to have a different geothermal system from Tompaso system (Siahaan et al., 2005). At the surface, it can be seen that both geothermal fields lie within a semicircular Tondano Caldera structure (Fig. 2.2(a)). Tondano Caldera rims are visible on the E and S (Fig. 2.2(a)). The fault rims are

rectilinear and parallel to the ENE-WSW and NE-SW trends (Fig 2.2). Based on the relationship between the orientation of the rims and regional structures, the Tondano Caldera is inferred to be a result of both the East Sangihe subduction system and the ENE-striking structures (Lécuyer et al., 1997). In other words, the ENE-striking faults created a pull-apart basin, while the East Sangihe subduction system had been supplying the magma for a heat source. At the release stage of the faults, the magma was able to reach the surface generating a caldera-forming eruption. The ENE-striking structures are, however, inferred to be related to the North Sulawesi subduction system rather than the East Sangihe subduction system (Lécuyer et al., 1997).

2.1.2. Volcanic Framework of Tompaso Geothermal System

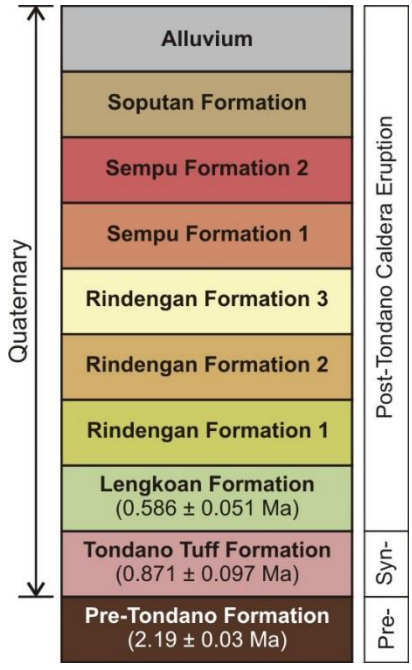

Figure 2.3. Stratigraphy of the Tompaso system (age from PT Gondwana, 1988 unpublished data cited in Utami et al., 2004)

The stratigraphy of surficial rock units in the Tompaso area can be divided into three main groups based on their ages relative to eruption of the Tondano Tuff Formation and formation of Tondano Caldera (Fig. 2.3): Pre-Tondano Formation (treated as basement rocks for the purposes of this thesis), deposits associated with the caldera-forming Tondano eruption, and post-caldera group. The Pre-Tondano Formation is characterised by thick lavas of intermediate to basaltic composition, andesite breccias, and welded tuffs with inter-bedded sedimentary layers deposited of Middle Miocene to Pliocene age (Ganda & Sunaryo, 1982; Effendi & Bawono, 1997; Siahaan et al., 2005). The volcanic products are inferred to represent an older 'Tondano volcano' that was destroyed during the formation of Tondano Caldera (Van Padang, 1951). K/Ar dating on one lava yielded an age of 2.19 ± 0.03 Ma or Late Pliocene ((PT Gondwana, 1988, unpublished data cited in Utami et al., 2004), but the full range of ages from the volcanic rocks is unknown.

Tondano volcano initially erupted basaltic andesitic compositions which then evolved to become more silicic. Eventually, a large-magnitude eruption occurred, with accompanying caldera collapse, forming a depression which now has been partly filled by water (Lake

Tondano) (Ganda & Sunaryo, 1982). Based on the inferred caldera rim (Fig. 2.2(a)), it is apparent that the area affected by the Tondano caldera-related eruption covers most of the Recent volcanic cones. Therefore, the products of the Tondano eruption are used as the time plane marker in the stratigraphy of the area. This large-magnitude eruption produced the Tondano Tuff Formation, which is composed of lapilli tuff and ignimbrite (Siahaan et al., 2005). According to Lécuyer et al. (1997), this formation consists of white rhyodacitic ignimbrites and younger, more localised grey dacitic ignimbrites. The geological report by Ganda & Sunaryo (1982) is in agreement with Lecuyer et al.'s (1997) argument that Tondano Tuff Formation has, at least, dacitic or even more silicic composition. However, other authors report that this formation has an andesitic composition (Bachri, 1977; Kavalieris et al., 1992; Effendi & Bawono, 1997). K/Ar dating suggests that the Tondano tuff was erupted at 0.871 ± 0.097 Ma (Gondwana, 1988, unpublished data cited in Utami et al., 2004) (Fig. 2.3). This unit was mentioned in the previous works as being Tertiary (Ganda & Sunaryo, 1982; Effendi & Bawono, 1997; Prasetyo et al., 2015), but according to the 2015 International Chronostratigraphy Chart (Cohen et al., 2015), its age is in the Early Pleistocene (Quaternary) range.

The formation of Tondano Caldera was followed by development of new magma pathways forming younger volcanic cones on NE-SW trends, such as Mt. Lengkoan and Mt. Sempu. After the Tondano eruption, new mafic magmas were erupted, ranging in composition from andesitic to basaltic (Ganda & Sunaryo, 1982). In the Lengkoan area, there were andesite and basaltic andesite eruptions, forming mounts Tampusu and Mahawu, and basalt eruptions from Lokon volcano (Fig. 2.2). Likewise, Sempu Volcano consists of andesite, basaltic andesite, and basalt. Andesite was also produced by Mount Rindengan, basaltic andesite by Mount Manimporok, and basalt by Soputan Volcano (Williams & McBirney, 1979; Morrice et al., 1983; Kavalieris et al., 1992; Siahaan et al., 2005). At Tompaso, the Rindengan, Sempu, and Soputan formations (Fig. 2.3), post-date the deposition of Lengkoan Formation. There is no age dating, however, for these later formations.

2.1.3. Occurrence of Andesite within Tompaso Geothermal System

This thesis includes observations of the relationships between andesite textures and the distribution of hydrothermal alteration products. This work is then limited to andesite. In the north arm of Sulawesi Island, andesite is the main volcanic lithology. Andesite can be found as a member of all formations, except for the products of the Tondano Caldera

forming eruption (Siahaan et al., 2005). Prasetyo et al. (2015) proposed that Tompaso wells penetrated down to the Pre-Tondano formation, whereas Syn-Tondano Caldera forming eruption products are encountered in the wells at approximately 800-1000 m depth. However, it is inferred in this thesis that only andesite of post-Tondano eruptions is encountered in the Tompaso boreholes (chapter 4.1.1., 5.1.).

There are 8 different formations within the Post-Tondano group, including Lengkoan Formation, three formations of Rindengan volcanic deposits, and two formations of Sempu volcanic deposits, the names indicating the inferred source volcanoes (Fig. 2.3). Among eight formations of the Post-Tondano group, the oldest is the Lengkoan Formation. According to Siahaan et al. (2005), Lengkoan Formation consists mainly of andesite lava that is observed in the western part of Pangolombian depression, and is associated with 'obsidian and tuff breccia'. The member of Lengkoan Formation found to the north of Tompaso is andesite lava. Prasetyo et al. (2015) suggested that this member could be a natural barrier between Lahendong and Tompaso Geothermal Fields at the surface.

The grouping of lithologies mentioned above is based on the physical characteristics and distribution of volcanic products at the surface. However, subsurface lithology naming done in this thesis does not follow surface lithology formations because the continuity of each formation to subsurface is difficult to trace.

2.1.4. Geothermal Setting of the Tompaso Area

There are two geothermal complexes found to the west of Tondano Caldera lake. Lokon-Mahawu area, associated with Lokon and Mahawu mountains (Fig. 2.2(a)), occurs in the northern part and Lahendong-Tompaso area in the central-southern part (Fig. 2.2(a,b)) (Prijanto et al., 1984). Plutonic activity associated with the Sangihe volcanic arc is inferred to provide heat sources for the geothermal systems. It is suspected that the currently active heat source is the magmatic system at the southwestern end of the Sangihe arc, the same system feeding Soputan Volcano (Morrice et al., 1983). Soputan is currently showing the most intense volcanic activity in the Sangihe arc, with its latest eruption in January 2016.

The Lahendong-Tompaso area covers two geothermal systems: Lahendong and Tompaso. Tompaso is situated 30 km to the southwest of Lahendong (Fig. 2.2). Both are located in Tondano volcanic depression and have indistinguishable geological, but different

geothermal characteristics. They are thought to represent two separate systems separated by an active sinistral strike-slip NE-SW fault (Siahaan et al., 2005).

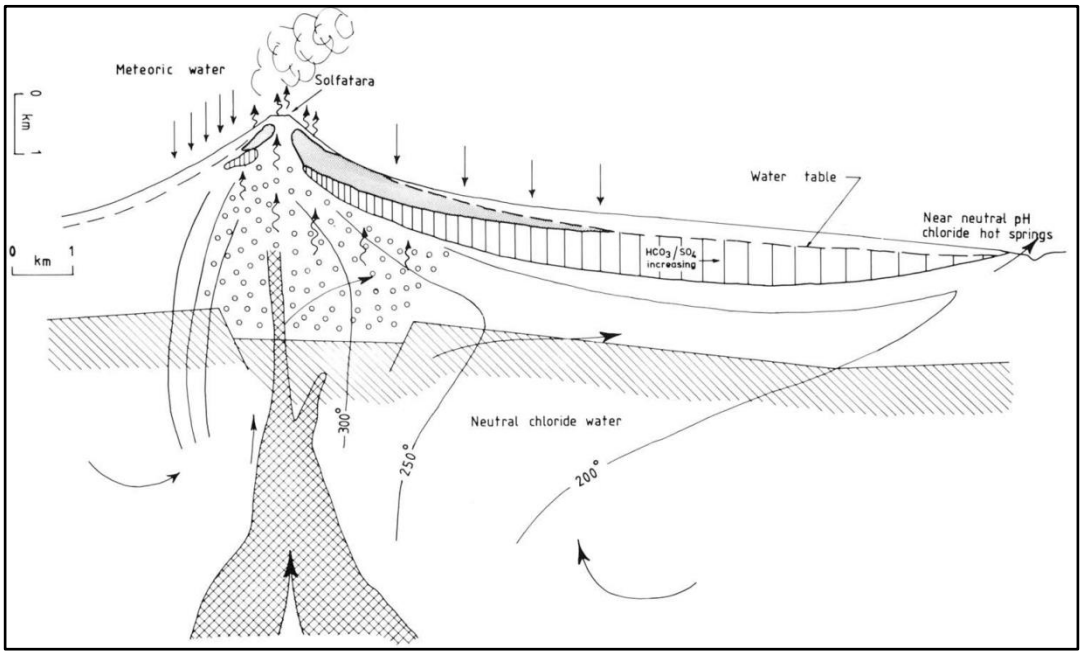

Figure 2.4. Conceptual hydrological structure of typical high relief geothermal systems. The upflow zone is characterised by fumaroles and/or solfataras and chloride waters emerge far downslope. Figure from Henley & Ellis (1983).

Tompaso system is a typical of active island-arc volcanic-hosted geothermal system, characterised by a high relief of the volcanic structures and low groundwater level (Fig. 2.4) (Henley & Ellis, 1983). The upflow zone in these systems is reflected by fumaroles and steam-heated acid sulfate waters which are sometimes associated with a perched aquifer. Steam separation from boiling processes gives rise to fumaroles, while steam-heated acid sulfate is initiated from the oxidation of the ascending H_2S steam by groundwater, and/or disproportionation of SO_2. Meanwhile, the chloride-rich water flows laterally to emerges downslope as chloride water. During this flow, chloride water matures by cooling, water-rock interaction and dilution by groundwater resulting in a high content of bicarbonate (HCO_3^-) or mixing with descending sulfate waters and steam condensates discharging chloride-sulfate waters (Henley & Ellis, 1983; Nicholson, 1993; Hochstein & Sudarman, 2015). Thus, chloride waters are commonly emerge far downslope with respect to the upflow zone in island-arc geothermal systems, such as in Tompaso.

The upflow zone of Tompaso geothermal system is associated with Soputan Volcano. The geothermal manifestations that occur on its flank indicate subsurface boiling, including fumaroles, hot pool, and steaming ground (Prijanto et al., 1984; Handoko, 2010). The distribution of many geothermal features of Tompaso follows the strike of the ENE-WSW

sinistral strike-slip Soputan Fault (Sardiyanto et al., 2015). High-temperature acidic manifestations are found at Mount Rindengan and Tempang. Bicarbonate fluids are dominant in an area close to Lake Tondano. There is also a chloride-rich hot spring observed in Tempang (Pertamina Geothermal Energy, n.d.-a; Handoko, 2010).

Tompaso geothermal system is characterised by a reservoir fracture zone (Kamah et al., 2010) where fractures are the main feature providing permeability in the reservoir. MT resistivity data of Tompaso geothermal system records that the top of the reservoir in Tempang is around 500 mbsl, while at Mount Rindengan it is at sea level. MT resistivity data indicates 750-1000 m thick of clay minerals as an altered conductive layer occur at Mount Rindengan (Handoko, 2010). Hydrothermal clay minerals have been identified and show that shallow part of the conductive layer is dominated by kaolinite, smectite, corrensite and halloysite, and the deeper part (850-950 m depth in LHD-27 and 1621 m depth in LHD-30) consists predominantly of illite and chlorite (Prasetyo et al., 2015). The distribution of hydrothermal clay minerals at depth shows an agreement with present-day temperature (Prasetyo et al., 2015) suggesting that the geothermal system has not been much modified from its initial condition.

2.2. Wairakei Geothermal System

2.2.1. Tectonic Framework

The tectonic setting of the North Island, New Zealand, is dominated by the subduction extending along the Hikurangi margin (ultimately to Tonga in the north), intra-arc rifting in the TVZ, and strike-slip faulting in the North Island Fault Shear Belt (NIFS) (Fig. 2.5) (Wallace et al., 2004; Seebeck et al., 2014a, 2014b). To the east of the North Island, the Pacific plate is subducting underneath the Australian plate, and the opposite is occurring south of the South Island. A dextral strike-slip fault system (including the Alpine Fault) occurs in the transition connecting the westward subduction system in the north to the eastward subduction system to the south (Fig. 2.5). A rapid increase of plate convergence rates occurred at about 7 Ma (Late Miocene) (Seebeck et al., 2014a). This increased the fluid flux from the slab to the mantle wedge. Increasing fluid flux to the mantle wedge reduces the mantle viscosity promoting slab bending and steepening beneath the North Island. In contrast, on the northern part of the subduction system, along Tonga-Kermadec, increasing subduction rates resulted on the movement of the subduction margin eastward. The latter process is referred as a slab rollback (Seebeck et al., 2014a).

A volcanic arc has been formed to the west of the Hikurangi subduction zone, overlying the Mesozoic greywacke basement. The greywacke basement consists of interbedded sandstone with a minor argillite (Wood, 1996; Rosenberg et al., 2009; Bignall et al., 2010). The volcanic arc within the North Island is delineated as the Taupo Volcanic Zone (TVZ) (Fig. 2.5). The TVZ is defined as an envelope drawn around all caldera structural boundaries and vent positions (Wilson et al., 1984, 1995). Since ~2 Ma (Early Pleistocene), the TVZ has been rifted (Eastwood et al., 2013) resulting in the activation of normal faults. The intensely faulted zone in the TVZ is refered as the Taupo Rift.

Slab rollback along Tonga-Kermadec and slab bending underneath North Island controls the kinematics of the Taupo Rift. In the central of North Island, the rifting is orthogonal converting into oblique rifting northward to White Island (Seebeck et al., 2014b). The obliquity of rifting is the direction of the extension relative to the rift trend. The rift is oblique if the extension direction is not perpendicular to the fault trend. Because of its obliquity, the northern part of the TVZ is rotated clockwise with respect to the rest of the TVZ (Seebeck et al., 2014b).

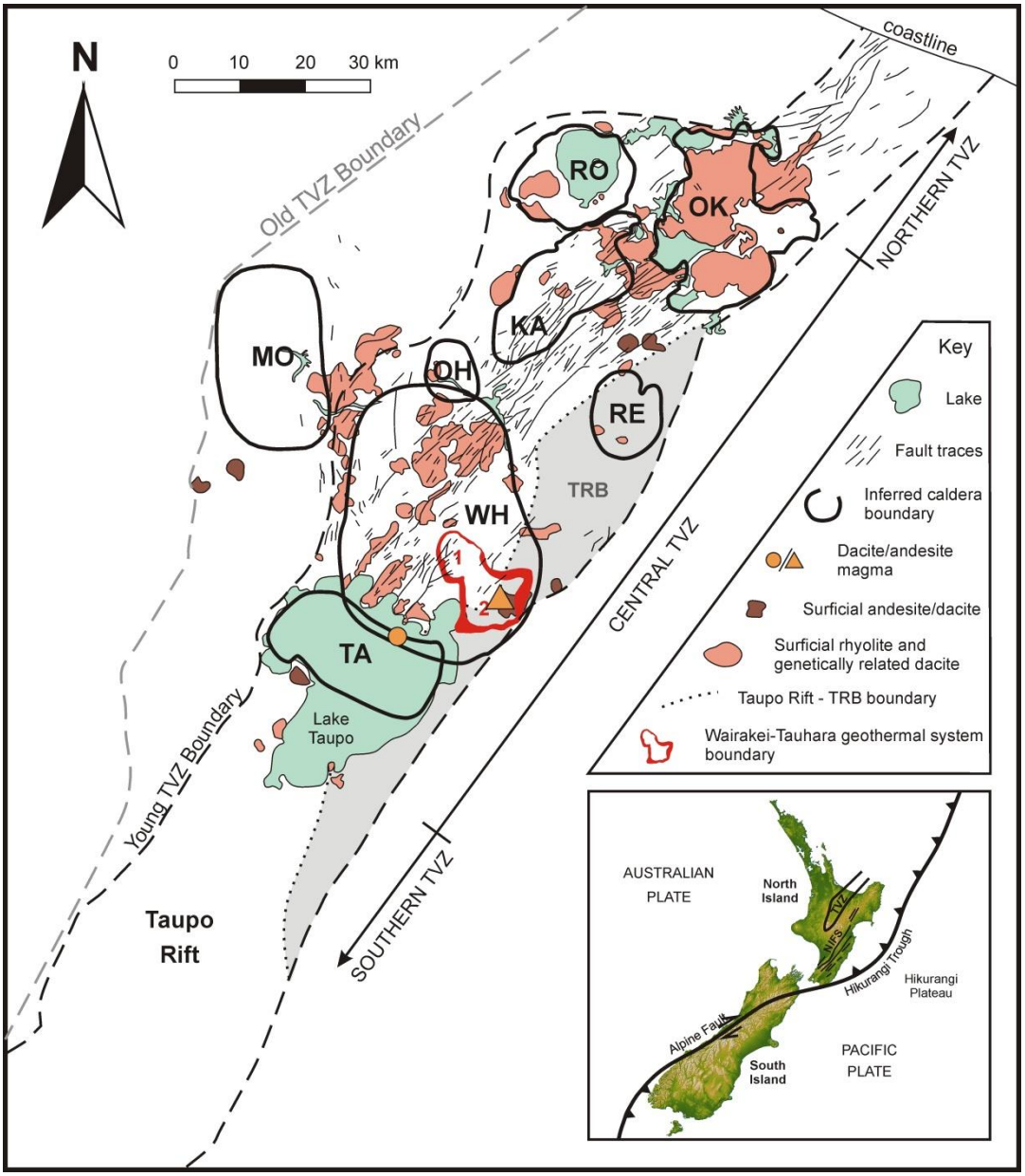

Figure 2.5. Geological features of the TVZ. Only features within the central TVZ are shown. Segmentation of the TVZ (northern, central, and southern) is based on styles, volumes, and rates of the eruptions (see explanation in the text). Regional tectonic setting of the area is shown in the inset. Old TVZ represents volcanic activity from 2-0.34 Ma; Young TVZ represents volcanic activity from 0.34 Ma to present (Wilson et al., 1995). Calderas: OK – Okataina, RO – Rotorua, KA – Kapenga, MO – Mangakino, OH – Ohakuri, RE – Reporoa, WH – Whakamaru, TA – Taupo. Figure adapted from Wilson & Rowland (2016, p. 170). Distribution of dacite/andesite vents is from Wilson et al. (1995) with only those active since 65 ka to present are shown. Surficial andesite/dacite and rhyolite-dacite represents the composition of volcanic products at the surface without referring to the composition of magma chamber (Wilson & Rowland, 2016). Taupo Rift-TRB boundary is from Wilson & Rowland (2016, p.173). The Wairakei-Tauhara geothermal system boundary is from electrical resistivity data (from Risk et al., 1984): 1 – Wairakei Geothermal Field, 2 – Tauhara Geothermal Field.

The extension rates of the northern part of TVZ are about twice those of the southern part (Villamor & Berryman, 2006). The higher extension rates on the northern part are expressed by the more developed half graben morphology (Rowland et al., 2010; Seebeck et al., 2014b). Rifting in the TVZ is inferred to be assisted by volcanism and magmatism in

the area as shown by the correspondence of the distribution of mafic and rhyolitic volcanic activity to the alignment of the rift axis (Rowland et al., 2010).

The TVZ is divided into three segments based on the styles, volumes, and rates of eruption. The northern and southern segments consist of andesitic-dacitic volcanoes, while the central segment contains rhyolitic volcanism and magmatism extending from Okataina Caldera in the north to Taupo Caldera, now occupied by Lake Taupo, in the south (Fig. 2.4) (Wilson et al., 1984; Wilson & Rowland, 2016). In the central TVZ, there are 8 major calderas so far delineated: Mangakino, Kapenga, Whakamaru, Reporoa, Rotorua, Ohakuri, Okataina, and Taupo (Fig. 2.5), respectively from the oldest to the most recent (Houghton et al., 1995; Gravley, 2004; Wilson et al., 2009).

The central TVZ consists of 2 structure belts, the Taupo Rift and Taupo Reporoa Basin (TRB), which are separated by a horst structure at the subsurface (Wilson et al., 2010). Compared to the Taupo Rift, TRB is no longer showing the fault lineaments at the surface (Fig. 2.5) due to burial by volcanic, lacustrine, and fluvial products since the formation of Reporoa Caldera (Rowland et al., 2010; Downs et al., 2014a) at 281 ± 21 ka (Downs et al., 2014a).

2.2.2. Volcanic Framework of Wairakei Geothermal System

Wairakei Geothermal Field is located within the Whakamaru Caldera depression. Even though the Torlesse greywacke is not widely found in in Wairakei, its continuity is known from the surrounding geothermal fields (e.g. Rotokawa, Ohaaki, Kawerau and Ngatamariki: (Wood, 1996; Milicich et al., 2013a, 2013b; Chambefort et al., 2014)) that it forms the regional basement of the area. Overlying the Torlesse greywacke, there is the Tahorakuri Formation. The initiation of volcanic activity in the area was indicated by the presence of andesitic volcanism associated with the Tahorakuri Formation. The Tahorakuri Formation consists of silicic ignimbrites associated with andesite that erupted at ~1.9 Ma, as soon as the intra-arc rifting was initiated (Eastwood et al., 2013; Chambefort et al., 2014). The andesitic products of this period found that are at Wairakei, referred to here as Tahorakuri andesite, are lavas which were intercepted during drilling generally below -1100 metre with respect to sea level (mRL), except for the andesite of WK-264 (Rosenberg et al., 2009; Bignall et al., 2010; Sanders et al., 2013).

The Whakamaru Group of ignimbrites overly the Tahorakuri Formation (Fig. 2.6). In the Wairakei system, the weakly to densely welded ignimbrite is the product of the

Whakamaru Caldera-forming eruption (Grindley, 1965; Houghton et al., 1995). Age dating shows that the whole Whakamaru sequence was emplaced at 349 ± 4 ka to 339 ± 5 ka (Middle Pleistocene) (Downs et al., 2014a, 2014b). The member of this group represented in the wells at Wairakei is the earliest member of a crystal-rich unit locally named Wairakei Ignimbrite (~350 ka) (Grindley, 1965; Rosenberg et al., 2009; Bignall et al., 2010).

Deposition of the Waiora Formation took place after the emplacement of the Whakamaru Group. Several volcanic centres were active during this period, such as Taupo, Okataina, Kapenga, and Rotorua (Downs et al., 2014b). This formation consists of pyroclastic and volcaniclastic rocks with interlayered sedimentary rocks. Grindley (1965) divided this formation into 5 different members based on textures and the presence/absence of quartz. Each member of the Waiora Formation in Wairakei, from bottom to top, consists of: non-welded and welded ignimbrite units (Wa_1); siltstone (Wa_2); interbedded breccia, tuff, sandstone and siltstone (Wa_3 and Wa_4); and quartz-bearing ignimbrites and associated tuffs (Wa_5) (Grindley, 1965; Rosenberg et al., 2009). This formation is widely encountered in Wairakei geothermal system (Grindley, 1965; Steiner, 1977; Rosenberg et al., 2009; Mielke et al., 2010).

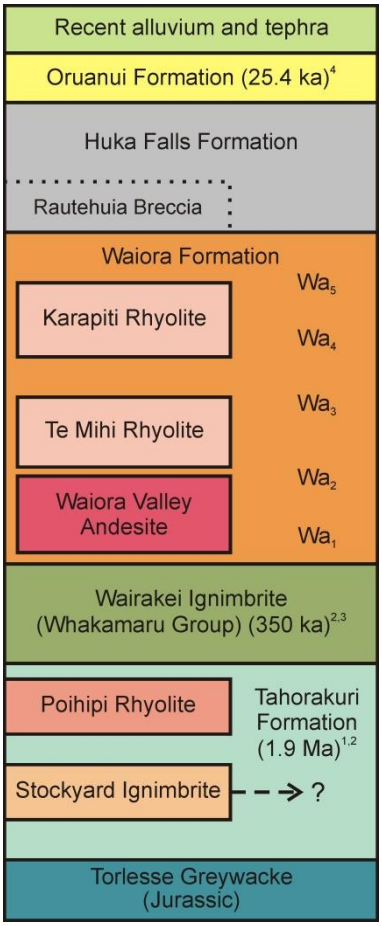

Figure 2.6. Stratigraphy of the Wairakei Field (from Bignall et al., 2010). Ages taken from: [1]Eastwood et al. (2013) [2]Chambefort et al. (2014) [3]Downs et al. (2014b) [4]Vandergoes et al. (2013).

In Wairakei wells, e.g. WK-121, WK-247, and WK-301, intercalations of andesite of Waiora Valley Andesite (WVA) and rhyolite lavas (including the Te Mihi and Karapiti rhyolites) are found within the Waiora Formation (Rosenberg et al., 2009). The WVA is up to 172 m thick in WK-48 and has a texture typical of lava (Sanders et al., 2013). Grindley (1965) observed that this formation is found either overlying a Waiora Formation member or in direct contact with the Wairakei Ignimbrite. Rosenberg et al. (2009) proposed that these lavas were extruded in at least two episodes. However, in the description of andesite distribution in Wairakei geothermal system by Sanders et al. (2013), the presence of this

separation of the WVA in Wairakei was not presented. Therefore, in this thesis, the WVA is treated as one unit of extrusive lava.

After the deposition of the Waiora Formation, the Huka Falls Formation, which consists of lacustrine sediments and volcaniclastic rocks, was emplaced in a lacustrine environment, refered as paleo-Lake Huka. Deposition occurred until interrupted by the Oruanui eruption (Wilson, 2001). Rautehuia Breccia is found at the base of Huka Falls Formation. Rosenberg et al. (2009) determined that the Rautehuia Breccia found in Wairakei consists of hydrothermal and pyroclastic breccias and may also contain debris flow breccia.

Overlying all these formations, Oruanui Formation and younger deposits respectively cover the upper part of Wairakei. The Oruanui eruption occurred at 25.4 ± 0.2 ka (Vandergoes et al., 2013). The eruption destroyed Lake Huka and formed a bigger and wider basin. A part of this basin has been filled by the modern Lake Taupo (Wilson, 2001; Cattell et al., 2015). At Wairakei, all deposits younger than the Oruanui Formation, including the products of Taupo eruption at 1.8 ka, are grouped as superficial deposits (Rosenberg et al., 2009; Bignall et al., 2010).

2.2.3. Occurrences of Andesite within Wairakei Geothermal System

The relationships between hydrothermal alteration and rock textures in Tompaso andesites have been compared to Wairakei andesites. There are two andesite units encountered in Wairakei wells. The older unit is in the Tahorakuri Formation, referred to here as Tahorakuri andesite, and the younger unit is intercalated in with the earliest (Wa_1) member of Waiora Formation (Fig. 2.6) (Grindley, 1965; Rosenberg et al., 2009; Bignall et al., 2010). The latter unit is refered as the Waiora Valley Andesite (WVA).

Sanders et al. (2013) studied both Tahorakuri and WVA andesite and found that, in general, it was hard to distinguish them from their textures yet easy to tell them apart from their chemical compositions. In their work, Sanders et al. (2013) did not separate the two episodes of the WVA andesite and treated them as a single unit of extrusive lava instead. Following their description, the WVA andesite used in this thesis is also considered as a single unit.

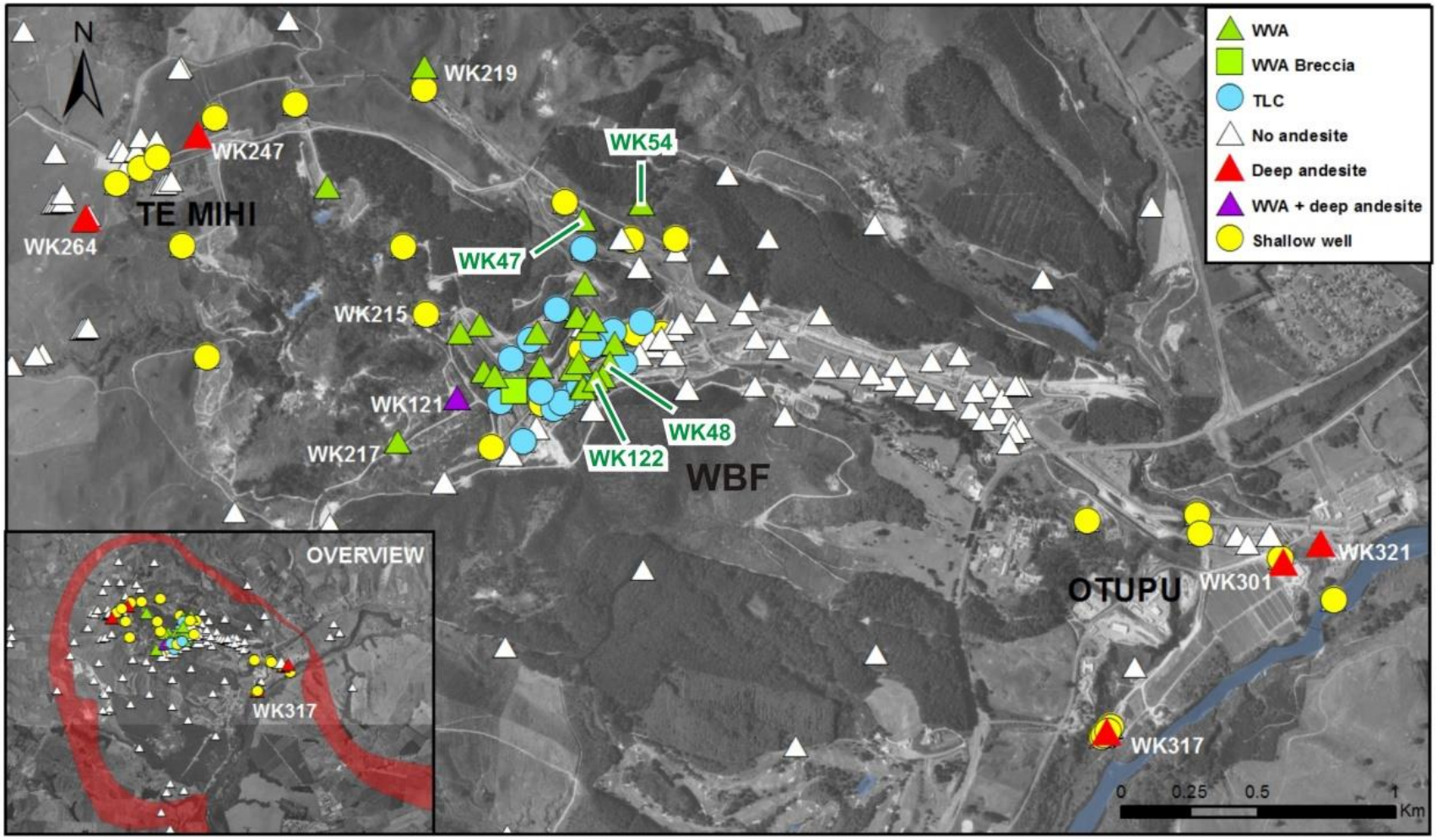

Figure 2.7. Map of the sub-surface andesite distribution in Wairakei geothermal system. Deep andesite refers to the Tahorakuri andesite. Red band in the inset shows the boundary of the geothermal system, defined from electrical resistivity measurements. WBF: Western Borefield. TLC: Total Loss Circulation. Figure taken from Sanders et al. (2013).

It is inferred that the distribution of the WVA in Wairakei is influenced by the NE-striking faults (Grindley, 1965). The NE faults have induced minor tensional NW faulting forming a pathway for extrusion of the WVA (Grindley, 1965). Therefore, the WVA is distributed along fissures at intersections of the NE-NW faults, thinning away from the intersections (Grindley, 1965). In Wairakei, the WVA is encountered widely in wells located at about the centre of the geothermal field (Fig. 2.6) (Sanders et al., 2013).

Table 2.1. Distribution of the WVA in Wairakei (Sanders et al., 2013).

Well ID	Top Depth (mRL)	Unit Thickness (m)
WK-24	-107	99
WK-26	-100	≥31
WK-26B	-100	31
WK-29	-99	107
WK-30	-154	≥30
WK-44	-170	11
WK-47*	-128	85
WK-48*	-112	172
WK-50	-131	≥28
WK-54*	-164	30
WK-56	-137	≥38
WK-57	-122	42

Well ID	Top Depth (mRL)	Unit Thickness (m)
WK-70	-97	≥30
WK-71	-117	≥105
WK-76	-122	≥86
WK-80	-133	≥136
WK-116	-143	≥18
WK-118	-143	≥23
WK-119	-155	≥20
WK-121	-119	≥43
WK-122*	-132	≥43
WK-215	-172	≥61
WK-217	-151	≥31
WK-219	-195	≥31

* Wells studied in this thesis

It can be seen in the map (Fig. 2.7) that the WVA is encountered only in wells situated at the Western Borefield (WBF). The restricted distribution pattern of the WVA suggest that this formation is a product of a small volcano which is located beneath the WBF (Rosenberg et al., 2009). In general, the WVA is at about 150-200 m depth (Table 2.1) (Sanders et al., 2013). This thesis uses the WVA samples from WK-47, WK-48, WK-54, and WK-122. WK-47 and WK-54 are located in the northern part of WBF, while WK-48 and WK-122 are in the southern part of WBF. In WK-47, the top of the WVA was reached at 128 m depth and it has a thickness of 85 m. In WK-54, the WVA is present at 164 m depth and has a thickness of 30 m. The andesite in WK-48 is encountered at 112 m depth and is >132 m thick as its base was not penetrated (Table 2.1) (Sanders et al., 2013).

2.2.4. Geothermal Setting of the Wairakei Area

The distribution of geothermal systems in the TVZ shows an agreement with the NE-striking normal faults (Rowland & Sibson, 2004). There are as many as 25 geothermal areas within the central TVZ, yet several geothermal areas have both small surface areas and low heat

outputs suggesting that these areas are either part of greater geothermal systems or remnant geothermal systems. Indications of declining geothermal activity as well as fossil systems appear in the western part but are absent in the eastern part of the TVZ (Bibby et al., 1995).

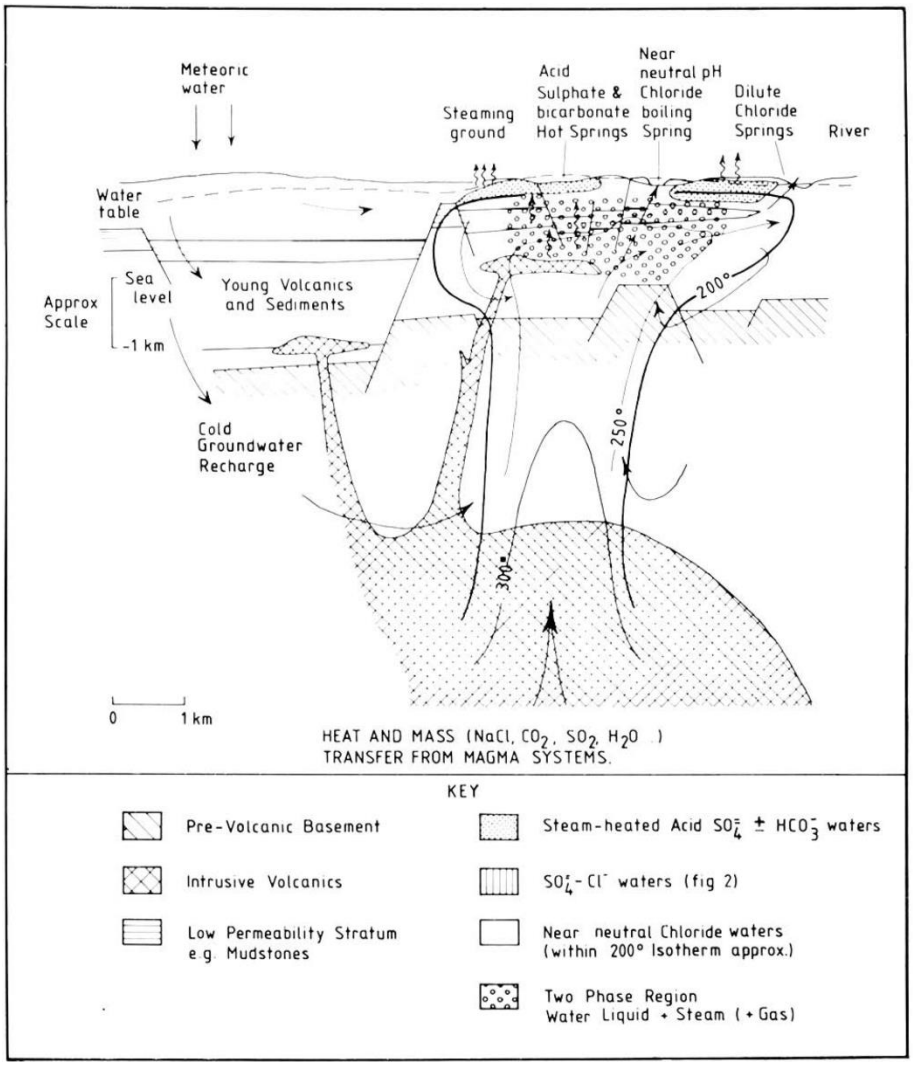

Figure 2.8. Conceptual hydrological structure of low relief typical geothermal systems. Near neutral pH chloride, dilute chloride, bicarbonate waters and acid sulfate water often occur close to one another within the upflow zone. Figure from Henley & Ellis (1983).

Wairakei Field is situated inside the Whakamaru Caldera (Fig. 2.5). From the electrical resistivity boundary, it can be seen that Wairakei Field is part of a larger geothermal system (the Wairakei-Tauhara geothermal system) extending to Tauhara Field (Mielke et al., 2010; Sepulveda et al., 2014). The Wairakei geothermal system is represented on the surface by the occurrences of hot pools, springs, geyser vents, as well as altered ground. TVZ geothermal systems are hosted by and directly linked to the large silicic volcanism, characterised by its low relief of volcanic structures. In this geothermal system, generally referred as continental-type (Fig. 2.8) (Henley & Ellis, 1983), all type of geothermal waters

(i.e. near neutral pH chloride, dilute chloride, bicarbonate and acid sulfate waters) can generally be found in the upflow zone. These waters are often emitted close to one another in continental-type geothermal systems because the distance of groundwater level to the surface is relatively small (Fig. 2.8) (Henley & Ellis, 1983; Nicholson, 1993). In Wairakei, surface manifestations of hydrothermal fluids observed are mostly chloride-rich water, some of which is located at higher elevation are slightly acidic but still containing a moderate content of chloride (Giggenbach, 1995; Bromley, 2009).

Wairakei surface features, however, have experienced some modifications in temperature, chloride content, and groundwater level partly as a result of natural processes, but mainly from electricity production during the last 60 years. The utilisation disturbed the aquifer discharge and natural recharge (Bromley, 2009; Milloy et al., 2014). The electricity production has either reduced the heat flow and chloride content in some geothermal manifestations (e.g. Geyser Valley on the NE of the Western Borefield WBF) or increase the heat flow in some other geothermal manifestations (e.g. the development of fumaroles and and hydrothermal eruptions of Craters of the Moon) (Allis, 1981; Milloy et al., 2014).

Hydrothermal alteration products show that the intensity of the processes increases with increasing depth. Low temperature minerals dominate at depths shallower than ~125 mRL, consisting of mostly smectite with calcite and pyrite. Increasing intensity from ~0 mRL is characterised by increasing K, Na, and Ca as shown by the formation of adularia, albite, calcite, illite, epidote, and wairakite (Bignall et al., 2007; Ramirez et al., 2009). The formation of these minerals is attributed to the effects of near-neutral pH fluids with maximum temperatures of >240 ^{o}C – 280 ^{o}C, as indicated by the presence of epidote and prehnite. In general this mineral association is in equilibrium with the present-day reservoir temperatures (Bignall et al., 2010).

The Wairakei geothermal system has an enhanced horizontal permeability. The layers of rhyolitic rocks of Waiora Formation provide a sub-horizontal natural permeability due to their texture (Steiner, 1977; Rosenberg et al., 2009; Mielke et al., 2010). The deep microseismic data of the system suggests a deep upflow at the NW margin of the system (Te Mihi – Fig. 2.6) (Sepulveda et al., 2014). The fluid then flows sub-horizontally through the aquifer into the Western and Eastern Borefields (Mielke et al., 2010). Apart from the inherent permeability of the Waiora Formation, the NE-striking Taupo Fault Belt also controls the fluid flow within the system. The rhyolitic lavas intercalated within the Waiora Formation (Fig. 2.6) also act as a reservoir, especially at their margins where autobreccia is

common. These permeable zones are overlain by the impermeable Huka Falls Formation which acts as the caprock of the system (Grindley, 1965; Rosenberg et al., 2009; Mielke et al., 2010; Cattell et al., 2015).

CHAPTER THREE

METHODS

The research in this thesis consists of two parts. The first part aims to understand the properties of Tompaso geothermal system since this area has not been well-studied. The geothermal characteristics here encompass the permeability as well as thermal and hydrogeological configuration of the system. The workflow to study the geothermal characteristics of the Tompaso geothermal system is shown in Fig. 3.1. Permeability of the system was assessed by comparing the variations of alteration intensity to the lithology and/or faults.

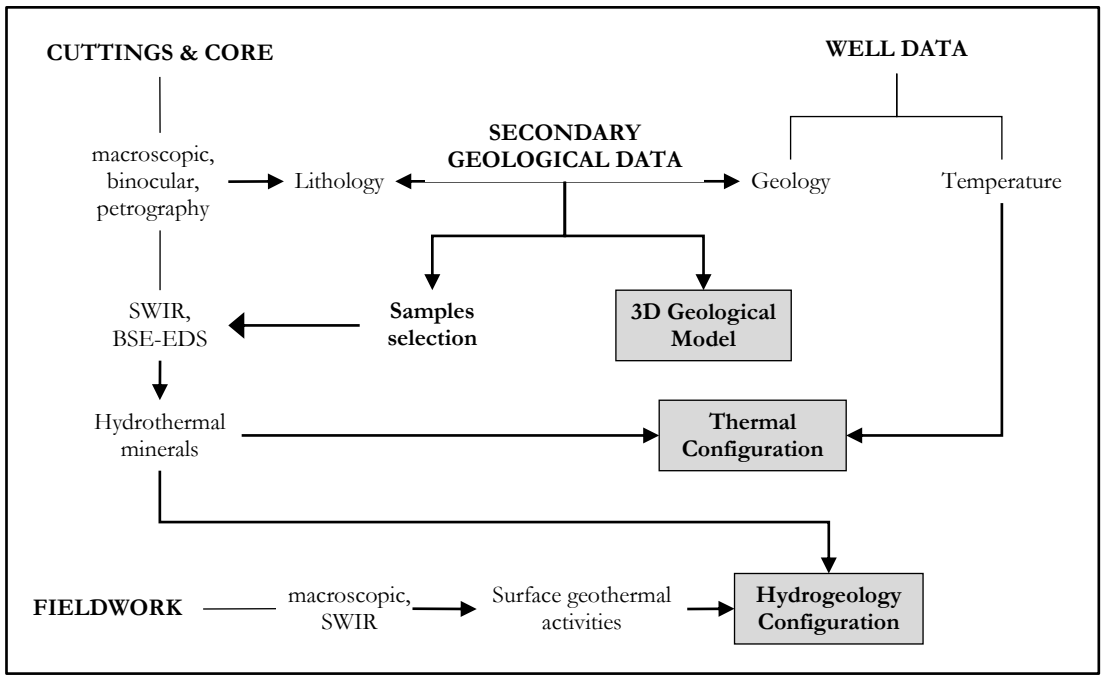

Figure 3.1. Work flow of the investigation of the Tompaso geothermal system.
Shaded boxes are the outputs of the first part of this research.

The second part of this thesis studies the relationships between andesite textures and hydrothermal alteration products. The aim is to determine whether the distribution of hydrothermal alteration minerals within the rock is a function of primary rock textures. It is expected that the second part of work could give valuable information which will be useful for future researches on identifying the original type of lithology of altered rocks. The methods used to investigate this are petrological and mineralogical observations focussing on the rock texture as well as both primary and hydrothermal mineralogy. The analyses

used include hand lens and binocular microscope observations, petrography, Short Wave Infrared (SWIR), and Back-scattered Electron (BSE) imaging combined with Energy Dispersive X-Ray Spectroscopy (BSE-EDS). The results from these investigations are then considered, based on the variation of the sample's position in geothermal system.

3.1. Pre-existing data investigation

An investigation of pre-existing data was conducted in the preliminary stage of the research and during the analysis/interpretation stage. In the preliminary stage, the investigation included studying the geological setting and the geothermal system characteristics of both Tompaso and Wairakei fields. This work led to an understanding of the characteristics of the field before collection of new data. Studying previous works on andesite, andesite textures, as well as hydrothermal alteration processes during the analysis/interpretation stage led to the confirmation and comparison of previous understanding of the behaviour of hydrothermal alteration processes linked to the rock textures.

Most of the secondary data used in this research are published public data. However, as there is little data published from the Tompaso Field, internal company data were used to study the characteristics of its system. The data available for this research are supported by PT Pertamina Geothermal Energy (PGE). PGE supplied data for all wells in Tompaso (eight wells in total) consisting of location coordinates, elevation, total depth, measured depth, and drilling direction. These properties have been used to create a 3D geological model (section 3.4). Lithology logs, as well as downhole temperatures, were also provided by PGE. The lithology logs were used to correlate the stratigraphy, while the temperature data represents the present-day conditions of the geothermal system. The present-day temperature of the system has then been compared with the past temperatures recorded by hydrothermal minerals, allowing the thermal configuration and possible natural changes of the system to be determined.

Another set of data supplied by PGE is the relative chemical compositions of surface geothermal manifestation fluids, covering chloride, bicarbonate, and sulfate content. These data combined with other surface data collected by me build the understanding of the spatial relationship of geothermal manifestations within the geothermal system.

Some data from the Wairakei Field were supplied by GNS Science and Contact Energy. Using the previously described well stratigraphy, samples for laboratory analyses have been chosen based on their stratigraphic position and compositions. As a contribution to the ongoing GNS-Contact work at the Wairakei Field, results in this thesis will support the information about hydrothermal alteration processes taken place in Wairakei geothermal system. Other data used for the research in this thesis are public data.

3.2. Fieldwork

Field observations have been conducted only at the Tompaso Field, in order to document the surface geothermal activity. Fieldwork focussed on geothermal manifestations, faults, and lithology contacts. Intense geothermal activity has altered most of Tompaso surface area, precluding a review of the geological information. No geology information has been obtained around places inferred to host faults or lithological contacts. Detailed geological observation was only possible in a few sites. Therefore, the geological observations build on existing work, including that of Ganda & Sunaryo (1982), Handoko (2010), and PGE internal unpublished data.

Twenty-nine sites were visited, with their locations decided based on the existing geological maps (Prasetyo et al., 2015), field observations, and information from local people. Observations of geothermal manifestations included defining the type, dimension, physical characteristics (such as colour, odour, and presence of bubbles), temperature and pH of the fluids if possible, and hydrothermal minerals in the immediately surrounding areas. Physical characteristics of the manifestation may give clues about the fluid chemical composition, but full chemical analyses are needed to know its chemistry. Manifestation type, together with fluid chemistry and hydrothermal mineralogy, show the position of the manifestation within the geothermal system, while its size displays the intensity of the activity which probably relates to the presence of geological structures and/or rock permeability (section 1.4). Fluid pH measurements have been done using pH universal paper and temperature measurements using an infrared thermometer IR 60. Field instruments including compass, hammer, GPS, loupe, and infrared thermometer IR60 were facilitated by the Geothermal Research Centre, Universitas Gadjah Mada, Indonesia.

Surface samples were collected from the periphery of geothermal manifestations. Most of the surface hydrothermal alteration products are clay minerals. These samples have then been analysed using SWIR to identify the specific clay minerals. Some hydrothermal alteration minerals are good indicators for acid hydrothermal alteration, while others may indicate the presence of certain elements in the fluids. There are no chemical data of the manifestation hydrothermal fluids from the surface manifestations available except relative proportion of three main compounds; chloride (Cl^-), bicarbonate (HCO_3^{2-}), and sulfate (SO_4^{2-}), supplied by PGE. Therefore, identifying the type of clay minerals from peripheral manifestations is essential to understanding the fluid chemistry.

Results of geothermal manifestation observations, as well as SWIR analysis of surface hydrothermal products, are used to give insights into the spatial relationship of each manifestation in relation to the hydrology of the Tompaso geothermal system. Comparing these results to interpretations of the spatial relationships of subsurface hydrothermal products has led to better understanding of hydrogeological configuration of the Tompaso geothermal system.

3.3. Textural and mineralogical analyses

Textural and mineralogical observations cover both primary and hydrothermal minerals. The observations on primary minerals aim to identify the origin type of the rock, while investigations of hydrothermal alteration minerals will be used as a guide to the condition of the geothermal system when the alteration took place (Browne, 1970, 1978; Reyes, 1990). Replacement and directly deposited minerals (e.g. veins) were distinguished because they yield information about different processes of alteration (Utami, 2011). Hydrothermal mineral paragenesis and vein cross-cutting relationships were observed in detail as these are important in reconstructing the hydrothermal history of the system, as shown by Utami (2011) for the Lahendong Field adjacent to Tompaso. The hydrothermal mineral paragenesis also provides an indication of changes in the geothermal system as well as the stability of the mineral. In addition, the distribution of hydrothermal alteration minerals associated to the rock textures is of particular note. By comparing Tompaso to Wairakei samples, the work aims to determine whether the distribution of hydrothermal minerals is

a function of rock texture, with the aim that the results could help in identifying the origin type or lithology of altered rocks in the future.

3.3.1. Samples and sample preparation

Data used in this thesis involved the study of core and cuttings from Tompaso and Wairakei as well as surface samples from Tompaso. The latter are altered rocks collected around the surface geothermal manifestations during fieldwork.

Tompaso core and cuttings are owned by PGE whereas Wairakei samples are under Contact Energy ownership. The usage of Tompaso samples for the research in this thesis has been approved by the Directorate General of New Energy and Renewable Energy Conservation on behalf of the Ministry of Energy and Mineral Resources of Indonesia. Samples permitted for this research cover both core and cuttings from three wells, namely LHD-26, LHD-27, and LHD-32. These wells were chosen so that each represented a different cluster – a grouping of wells based on their location. The eight wells in Tompaso are divided into three clusters, which here are labelled as LHD-26, LHD-27, and LHD-32 clusters. The LHD-26 cluster includes LHD-26 and LHD-30, the LHD-27 cluster includes LHD-27, LHD-31, LHD-33, and LHD-34, and the LHD-32 cluster includes LHD-32 and LHD-35. There are, however, only two core sections available, one from LHD-26 and one from LHD-27. Both have been prepared into polished thin sections for petrography and BSE-EDS analyses. All cuttings have been examined through binocular microscope observations, SWIR, and BSE-EDS analyses.

This thesis only used andesite from the WVA for the Wairakei Geothermal Field. Samples were taken from 4 wells: WK-47, WK-48, WK-54, and WK-122. Cuttings from WK-47, WK-48, and WK-54 were taken over certain intervals in each well. The interval of sampling depends mainly on the WVA thickness, in addition to the availability of cuttings. The selected cuttings have been utilised for SWIR and BSE-EDS. Apart from cuttings, seven previously-made thin sections (four of them polished) and one core section from WK-122 are also used. The available thin sections are WK-47, WK-54, two sections of WK-122 (both polished), and three of WK-48 (two of them polished). Polished thin sections, including a new one made from WK-122 core section, have also been used for BSE-EDS.

3.3.1.1. Grain Mounting

Grain mounts of cuttings were prepared for BSE-EDS. Grain mounts were made in two laboratories. Wairakei grain mounts were prepared at the Wairakei Research Centre, GNS Science, while Tompaso grain mounts were prepared at the thin section laboratory in School of Geography, Environment, and Earth Sciences (SGEES), Victoria University of Wellington.

Figure 3.2. Grain mounts were made containing two to four different depths.

Mount rings, vaseline, and epoxy resin and hardener were used for making the mounts. Vaseline was applied to the rings before putting samples in to make removal of the grain mount easier. Both Wairakei and Victoria labs used the same type of resin and hardener. Grain mounts were made to contain samples from two to four different depths (Fig. 3.2). The epoxy solution was poured once arranging the samples had finished. The mounts were cured at room temperature for a couple of hours before placing on the hot plate (or in the oven) at approximately 40-50^{o}C to finish the curing. Putting the mounts on the hot plate directly may cause boiling.

3.3.1.2. Lapping, Polishing and Carbon Coating

Polishing is needed to minimise topographic effects (Reed, 2005) when running BSE-EDS analysis. Lapping was carried out before polishing in order to flatten the grain mounts, using a diamond lapping machine and sandpaper. Both lapping and polishing of grain mounts were conducted in the SGEES thin section facility. Polishing has been done by the 2

ATM Saphir 560 polishing machines. In addition, all thin sections made as part of this research (i.e. not the pre-made thin sections) were polished: LHD-26/1676-1678m, LHD-27/a742-1748m, and WK-122/584.4m.

BSE-EDS require samples to be electrically conductive. Coating is needed to increase the conductivity of the samples and carbon is used as it will not contaminate the atomic number differences of the samples as BSE is strongly dependent on the average atomic number. In addition, carbon will adsorb the X-rays from the samples which is required for EDS analysis (Flegler et al., 1993). Carbon coating was done at the Electron Microscope laboratory in the School of Chemical and Physical Sciences (SCPS), Victoria University of Wellington, using a Quorum Q 150T Є coating machine.

3.3.2. Macroscopic observations of Tompaso samples

Macroscopic observations have been undertaken on Tompaso samples during fieldwork. The observations were done on two core sections of LHD-26 and LHD-27, as well as cuttings of LHD-26 and LHD-32. This work was essential to provide initial information about the stratigraphy of these wells, especially on cuttings. Cuttings are available at 3-m intervals, except at a few depths where loss of circulation occurred. Looking at the available cuttings, it is possible to observe the changing of lithologies and draw the complete sequence of stratigraphy of the wells. Results of macroscopic observation became a base to consider sample selection.

3.3.3. Detailed observation of Tompaso cuttings using binocular microscope

Due to small cuttings grainsize (<2 mm), a binocular microscope was used to observe the cuttings in more detail. The instrument used was a Wild Heerbrugg microscope at SGEES. The magnification of this microscope are 12x, 25x, and 50x.

3.3.4. Petrography

Petrography has been applied to determine the texture and mineralogy composition. The relationships between hydrothermal mineral distribution and rock texture, as well as hydrothermal minerals paragenesis, were observed. Unlike BSE imaging which produces greyscale images, colours in cross polarisation help in identifying the minerals. Mineral

identification on BSE is done by using an EDS detector. Mineral identification with EDS relies on the chemical composition. The magnification of polarised microscopy is less than the magnification available through BSE imaging. Thus, petrographic observation is limited by the grainsize of the minerals. The observation was completed using Olympus BX51 polarisation microscope. The microscope has three different magnifications (4x, 10x, and 40x) and is equipped with an Olympus DP70 camera.

3.3.5. Short Wave Infrared (SWIR) analysis

SWIR analysis is a technique to quickly identify hydrous minerals. In typical geothermal geology investigation, X-ray diffraction (XRD) is the most common technique to identify hydrous minerals, especially hydrothermal clays. However, XRD requires the clay samples to be separated from the other materials (i.e. clastic, carbonate, and sulfate rocks as well as unconsolidated materials) before they are ready to be analysed. The separation process is done through multiple treatments (Moore & Reynolds, 1989). On the other hand, SWIR only requires samples to be dry, so preparation time is quicker compared to XRD. A short running time is another advantage of this technique, even though SWIR cannot detect as many minerals as XRD (Simpson et al., 2006). Acquisition time for each sample is 3-60 seconds (AusSpec International, 2010). In this thesis, it has been set up to 10 seconds for each cycle spectra recording. The instrument used in this research is a TerraSpec 4, located at Wairakei Research Centre, GNS Science.

Using TerraSpec 4, samples are illuminated by the light source from the spectrometer causing the bending and stretching of molecular bonds in the minerals. Changes of molecular bonds create sub-molecular vibrations leading to the absorption of certain wavelengths. While certain wavelengths are absorbed by the mineral, others are being reflected. The spectrometer measures the radiation spectra reflected from the surface of the samples. The absorption features are represented as wavelengths. Wavelength positions of the absorption features express different chemical compounds and thus SWIR is useful to identify the chemistry of minerals qualitatively (Simpson et al., 2006; AusSpec International, 2010). Because this method uses light reflection, the natural colour of the rocks can influence the results. Dark rocks absorb both visible and infrared light causing a poor reflection. As a result, the spectra may show nothing but noise (Simpson et al., 2006).

Three light spectra/ranges are recorded using TerraSpec 4; visible, near infrared (NIR), and infrared. The visible and NIR absorbed spectra (less than 1200 nm) are related to sub-atomic transitions of which the majority are observed in iron; both ferric (Fe^{3+}) and ferrous (Fe^{2+}) (AusSpec International, 2010). However, the vis-NIR spectra are not taken into consideration in this thesis.

The short wave infrared spectra range from 1300 to 2500 nm. The absorption features within this SWIR range are typically related to (AusSpec International, 2010):

- Hydroxyl (OH): ~1400 nm (also ~1550 nm and ~1750-1850 nm in some minerals)
- Water (H_2O): ~1400 nm and ~1900 nm
- Al-OH: ~2160-2220 nm
- Mg-OH: ~2300-2360 nm
- Carbonate (CO_3): ~2300-2350 nm (also 1870 nm, 1990 nm, and 2155 nm in some minerals)

Based on the ability to identify the above compounds (AusSpec International, 2010), SWIR is applicable to detect the presence of the certain minerals, such as:

- Phyllosillicates (e.g. clays, chlorite, and serpentine)
- Hydroxylated silicates (e.g. epidote and amphibole)
- Sulfates (e.g. alunite, jarosite, and gypsum)
- Carbonates (e.g. calcite, dolomite, ankerite, and magnesite)

The crystallinity of the minerals, as well as the chemical composition, also influences the the mineral reflectance which can be seen on the measured spectra. Poorly crystalline minerals are characterised by rounded, broad, and poorly developed peaks. On the other hand, highly crystalline minerals display sharp and well-developed peaks (Simpson et al., 2006; AusSpec International, 2010).

This analysis method has been applied to hydrothermally-altered environments in; both active and fossil settings (e.g. Simpson et al., 2006, 2013). These works have shown that SWIR is not only able to identify crystalline minerals but is also able to distinguish clay minerals, including kaolinite, smectite, illite, and interlayered illite-smectite. These key minerals are dependant on acidity or temperature, and thus give information about the hydrothermal fluids from which they were formed (Browne, 1970, 1978; Reyes, 1990).

Compared to X-Ray Diffraction (XRD) analysis, applying SWIR takes less time, although the results may not be as accurate, especially in differentiating illite and smectite from

interlayered illite-smectite. This is due to the concentration limit that could be detected by SWIR. If the component of smectite or illite is less than ~20%, the results will plot within the smectite or illite range respectively, rather than within interlayered illite-smectite range (Simpson et al., 2013).

SWIR produces raw data in the form of a wavelength position vs reflectance chart, termed reflectance spectra. In most cases, the reflectance spectra are influenced by absorption in the infrared range resulting in the changes of wavelength range and the presence of a "reflectance hull". A reflectance hull is the curvature or the overall background shape of the spectrum which tends to distort the spectral absorption features. Therefore, correcting the spectral absorption features by removing the reflectance hull is needed before using the data. A way to remove reflectance hull is by calculating the ratio between the hull and the reflectance spectra which is known as "hull quotient" (AusSpec International, 2010). However, hull quotient processing is only required if the reflectance hull is present, as judged by the background shape of the overall spectral response. As the spectra of both Tompaso and Wairakei samples are moderately to strongly curved, a hull correction has been applied.

Hull quotient processing can be done using the same software that is used to do spectral-matching. During this research project the software used was TSG Pro 7, which contains ideal models of some certain minerals. Identification of mineral has been completed by matching the spectral absorption features measured by the TeraSpec 4 with the ideal spectral models in TSG Pro 7. The TSG Pro 7 also allows addition of new ideal spectral models into its library from other supported files.

If the absorption features of water and Al-OH (and Mg-OH) are present, calculation of mineral crystallinity is required to identify whether it is smectite, illite, or interlayered illite-smectite. Crystallinity is calculated as the ratio of H_2O/AlOH (AusSpec International, 2010; Simpson et al., 2013). Hull quotient-corrected samples having H_2O/AlOH ratios of >0.96 correspond to illite and of <0.76 to smectite. Interlayered illite-smectite will be represented by values between 0.76 and 0.96 (Simpson et al., 2013).

In addition, the common presence of volcanic glass in the samples represents another challenge. It is known that a significant amount of volcanic glass causes issues by adding OH, H_2O and AlOH to the spectra (Zhang, 1999). Fresh volcanic glass is present at shallow depth in LHD-26.

3.3.6. BSE imaging combined with EDS

A Scanning Electron Microscope (SEM) is an instrument built principally to visualise sample by sending an electron beam to the sample and using a detector to scan the reflected beam. The SEM enables taking images of samples at much greater magnifications than through light microscopy. Two options of visualisation are available; topographic and compositional contrast mode. Topographic images can be obtained using secondary electrons (SE), while compositional contrast images are obtained utilising back-scattered electrons (BSE). BSE is strongly dependent on atomic number. More BSE signal is likely to be reflected by specimens with higher mean atomic number yielding to a brighter response (Flegler et al., 1993; Reed, 2005).

Limitations arising from the size and distribution of the hydrothermal minerals control the effectiveness of defining minerals chemically rather than physically. As BSE travels in straight lines, topography can interfere with the compositional contrast requiring the surface of the specimen to be polished flat to optimise the BSE compositional imaging (Flegler et al., 1993; Reed, 2005).

Even though BSE captures contrasting chemical compositions within the rock, the map will show the differences in greyscale intensity and not the actual chemistry. Thus, X-ray measurement is used to complement SEM images to identify the chemistry of the minerals. There are two kinds of x-ray detectors. Wavelength-dispersive (WD) records one wavelength at a time, while energy-dispersive (ED) reads X-rays of all energy simultaneously. The latter is faster but has limited spectral resolution and thus is better for semi-quantitative analysis. On the other hand, WDS is good for quantitative analysis (Reed, 2005). Aside from taking a longer time for analysing, its limitation on detecting elements in a single run time is also a shortage of WDS. WDS is only able to detect a limited number of elements at once as there are commonly only a few detectors in the system. Each detector can only be set to read a single element, represented by a certain wavelength (Flegler et al., 1993). Adjusting is needed for other elements. Energy-dispersive (ED) was chosen for this research rather than wavelength-dispersive (WD) as there was no prior knowledge of what elements would present.

The BSE-EDS instrument (JEOL 6610) used in this research belongs to SCPS, Victoria University of Wellington. Both secondary electron image (SEI) and backscattered electron

image (BEI) modes are available. The instrument is equipped with energy dispersive spectroscopy (EDS) and elemental mapping capability. It is able to record data at a spatial resolution of ~5.0 nm. Magnification range of this instrument is from 10x up to 500,000x.

3.4. 3D geological modelling using Leapfrog Geothermal

3D modelling has been carried out as part of this research with a purpose to give a visualisation of the Tompaso subsurface geology as well as the thermal and hydrological configuration of the geothermal system. The work has been completed using Leapfrog Geothermal software. This software is generally used (e.g. Alcaraz et al., 2011; Milicich et al., 2014) to model subsurface geology, especially in geothermal areas. ARANZ Geo Limited (the developer of the software) facilitated a one-year licence for the purpose of this thesis.

Data needed for the modelling includes well location, properties of the well configuration (including depth, dip, and azimuth for directional drilling), subsurface geology, recent measured well temperature, and the distribution of subsurface hydrothermal minerals. Well locations, well properties, and recent well temperatures were all provided by PGE. Subsurface geology has been collected by comparing pre-existing data, such as published/public data and PGE internal unpublished data with the results obtained from detailed binocular microscope observations. The distribution of hydrothermal minerals has been obtained by petrography, SWIR, and BSE-EDS.

Two outputs have been produced, the first visualising the subsurface geology of Tompaso and the second visualising the thermal configuration of the geothermal system. The distribution of subsurface hydrothermal minerals obtained from the analyses was compared to the present day temperature of the wells, giving information on the past and present thermal configuration of the system. On the other hand, both the surface and subsurface hydrothermal alteration mineralogies are used for comparison to the subsurface geological model to draw the hydrology configuration of the Tompaso geothermal system. The thermal and hydrological configurations then were used to draw the conceptual model of Tompaso geothermal system. Results are presented in section 4.1, 5.2 and 5.3.

CHAPTER FOUR

RESULTS

The results are presented here in three parts, corresponding to the three main areas of study: Tompaso geothermal system, Wairakei geothermal system, and andesite textures. Results from the Tompaso system include those on the geology and stratigraphy, surface manifestations of geothermal activity, and hydrothermal alteration. Results from the Wairakei system only cover the hydrothermal alteration effects in the Waiora Valley Andesite formation. The last part focuses on the volcanic textures of the studied andesites.

For future reference in this thesis, an intensity of alteration (IA) term is applied to describe the degree of replacement of primary minerals/components of rock by hydrothermal minerals (Pirajno, 2009). The terms used to describe IA is subjective. In this thesis, the IA is defined by a scale of 0-1, with 0 when the rock is fresh/unaltered and 1 when the rock is completely altered. An IA of 0-0.3 (low) is categorised as weakly altered, defined by replacement of either phenocrysts(/fragments) or groundmass(/matrix) by hydrothermal minerals with the texture of the rock still preserved . A rock having IA of 0.3-0.6 (intermediate) is identified as moderately altered, shown by replacement of both phenocrysts(/fragments) and groundmass(/matrix) by hydrothermal minerals, but still preserving the texture of the rock. A strongly altered rock has an IA between 0.6 and 1 and the rock texture is no longer visible.

4.1. Tompaso Geothermal System

4.1.1. Geology and Stratigraphy

The observation of geology and stratigraphy of Tompaso was initially proposed to cover both surface and subsurface features. However, as a consequence of strong hydrothermal alteration as well as weathering at and near the surface, the primary geological surface features cannot be observed. Most of lithologies exposed have undergone strong weathering processes, reflected by a thick soil layer, and are concealed by dense vegetation

cover. In other places, particularly surrounding geothermal manifestations, the country rocks have been altered intensely to hydrothermal minerals, such as kaolinite. The strong hydrothermal alteration and weathering processes have also masked the structures, and thus there is no detail that can be observed at the surface.

Based on the description of cuttings from three wells (LHD-26, LHD-27, and LHD-32) (full description in Appendix B), the stratigraphy of Tompaso can be divided into 8 units (Fig. 4.1): Tuff B unit, Rhyolite unit, Andesite B unit, Pitchstone unit, Pyroclastic Breccia unit,Andesite A unit, Pumice unit, and Tuff A unit, respectively, from the oldest encountered unit. As volcanic products are deposited reflecting the topography, their subsurface distribution is hard to define. For this reason, in this research, subsurface formation naming does not follow surface formation naming (Fig. 4.2).

A 3D model has been created in order to visualise the subsurface geology. The extent of the model, however, only covers a small part of the Tompaso Field where subsurface data is available (Fig. 4.2).

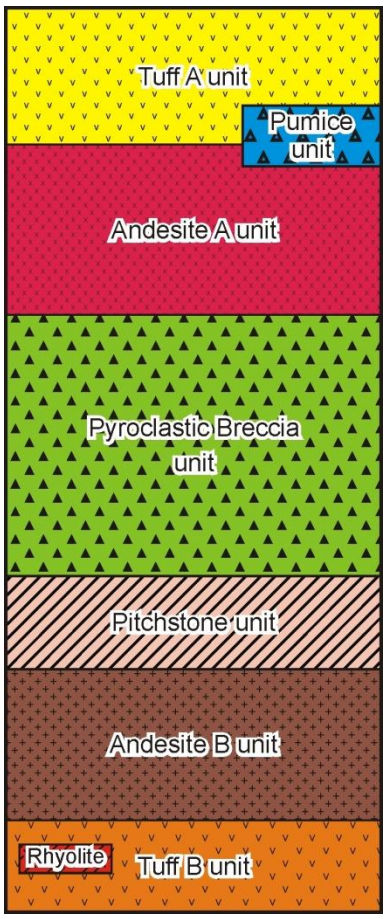

Figure 4.1. Stratigraphy of Tompaso system.

4.1.1.1. Tuff A unit

Tuff A unit is the youngest unit in Tompaso, consisting mainly of tuff and tuff breccia. This unit is thickest in LHD-26 (389 m) and thinnest in LHD-32 (132 m). Based on the distribution of lithologies on the surface (Fig. 4.2), the Tuff A unit correlates with Rindengan Formation 2 but, because there is no age dating available or undertaken in this research, the age of the Tuff A unit is unknown.

It is apparent that the rock unit contains abundant SiO_2-material as reflected by SWIR spectrum. The strong SiO_2 spectrum inhibits the detection of other components (Appendix C). Such spectrum was demonstrated to represent volcanic glass by Simpson et al. (2013).

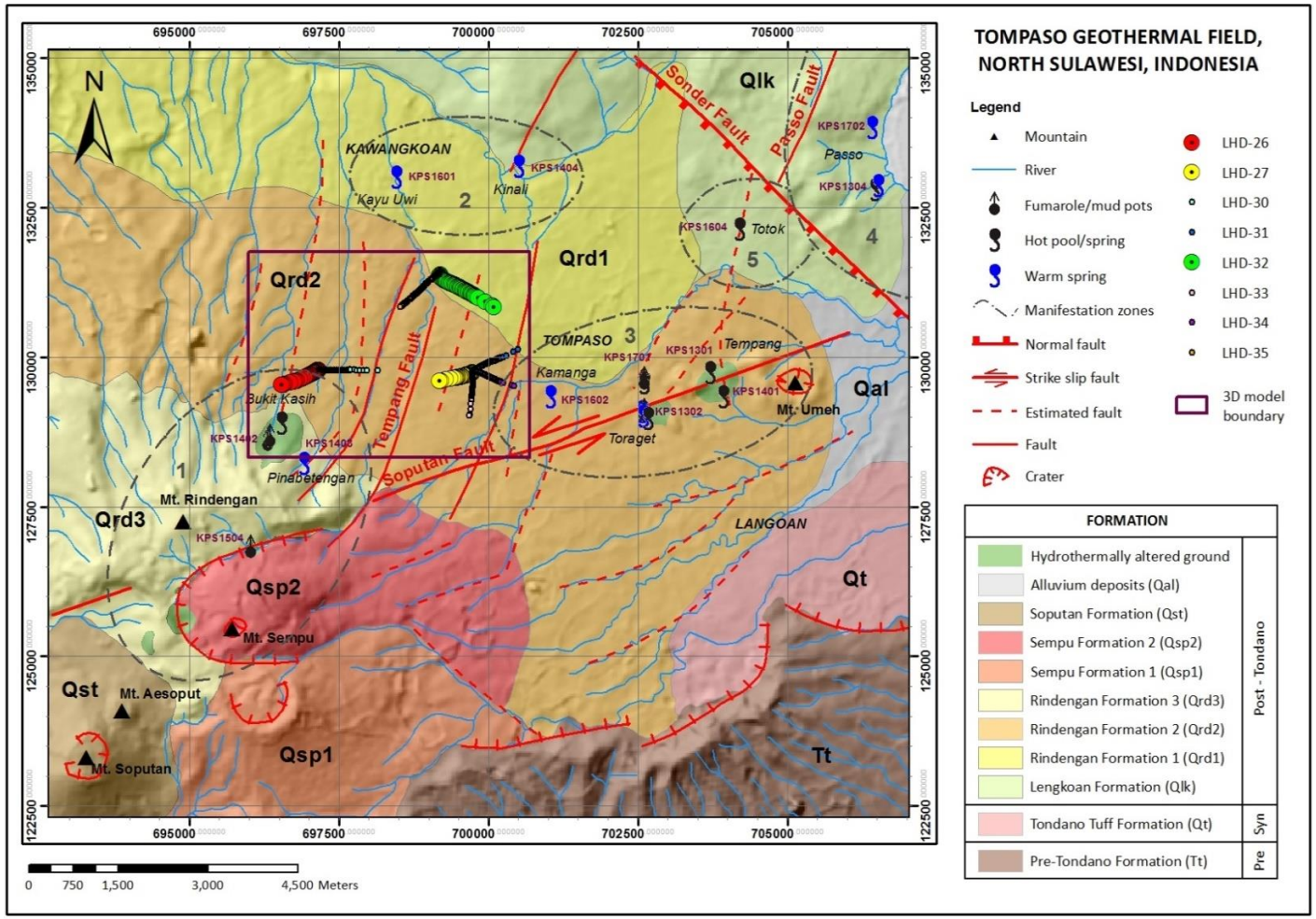

Figure 4.2. Map of the geology and distribution of the 5 geothermal manifestation zones in Tompaso. Geological units and faults are after Prasetyo et al. (2015). Numbers along the margin of the map are the UTM coordinates (the area is in 51N UTM zone). Formations are appropriate for describing surface lithologies only. Their continuity to subsurface units has not been defined either in this thesis or in any previous works. Wells used in this research are marked with bigger symbols (LHD-26, LHD-27, and LHD-32).

In LHD-26, the unit has been strongly oxidised at ~230 and 360-375 m depth. The indication of oxidation processes in this unit is absent in LHD-27 and LHD-32. Partial loss circulation occurs in LHD-32 at 93-144 m depth (Pertamina Geothermal Energy, n.d.-b), indicating a permeable zone at the contact between this unit and the underlying Andesite A unit.

4.1.1.2. Pumice unit

Underlying the Tuff A unit, a 198 m thick deposit, labelled the Pumice unit, has been encountered in LHD-27, but is absent in LHD-26 and LHD-32. Based on the discontinuous nature of the Pumice unit, LHD-27 is interpreted to have been deposited in a localised basin. This unit thins away to NW (Fig. 4.3). The source of the pumice is, however, unknown. The Pumice unit has been altered weakly at the top, but the alteration intensity increases downward. The unit overlies Andesite A unit, which is widely found in all three wells.

4.1.1.3. Andesite A unit

The thickness of the Andesite A unit ranges from 267 m in LHD-26 to 444 m in LHD-27. Andesite A unit is a lava characterised by a trachytic texture in LHD-27 (Fig. 4.4). The andesite shows a porphyritic texture with plagioclase and pyroxene phenocrysts set in a groundmass of cryptocrystalline material, plagioclase, pyroxene, and Ti-rich magnetite (here labelled as magnetite/ilmenite). The phenocryst size in LHD-26 and LHD-32 ranges from 0.3-0.7 mm, while in LHD-27 it ranges from 0.3-1.5 mm with 1 mm being the dominant size of phenocryst. The grainsize of the microlites groundmass ranges from 20-100 µm. Glomerocrysts of plagioclase+pyroxene are present. Sieved-plagioclase is only found in LHD-26.

This unit is the least altered unit in the Tompaso Geothermal Field. However, the middle part, at about 500-600 m depth, of LHD-27 is strongly altered (IA = 0.6-1). This depth coincides with the occurrence of a tuff lens (Appendix B), but the scale of the tuff is too small to be shown in the 3D model (Fig. 4.3).

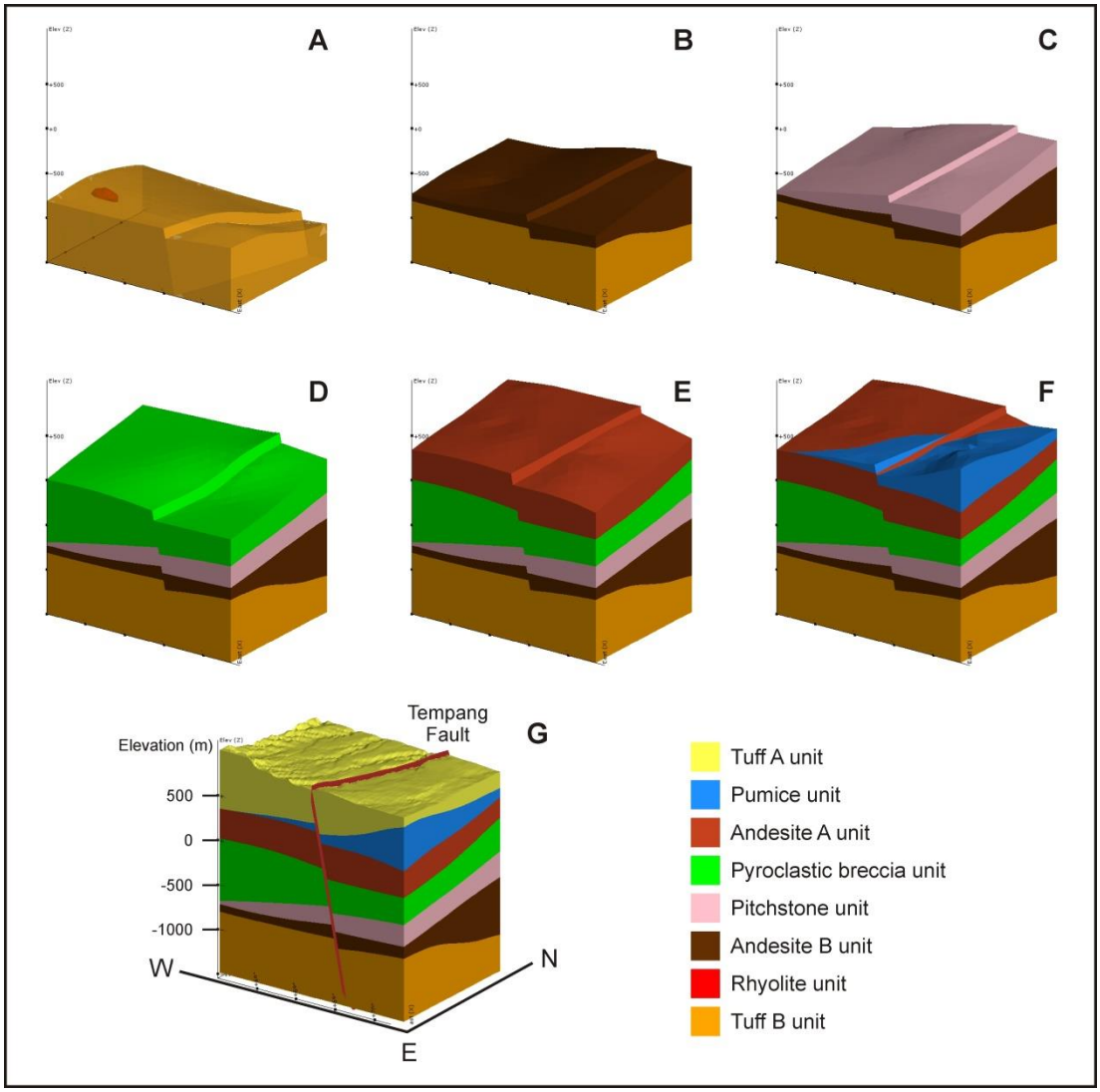

Figure 4.3. Geological succession of Tompaso geothermal system in 3D unit-per-unit model (from A to G) generated using Leapfrog Geothermal software. The location of area covered in this model relative to the rest of Tompaso Geothermal Field is shown in Fig. 4.2.

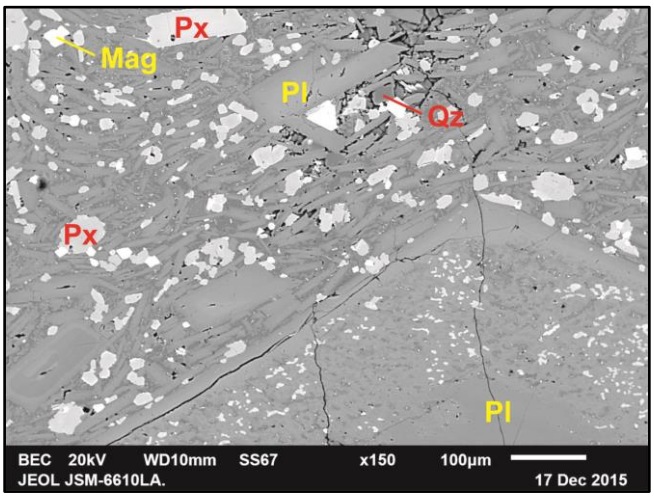

Figure 4.4. BSE image of an andesite showing trachytic texture in LHD-27/501 m. The rock consists of plagioclase (Pl), pyroxene (Px), and magnetite(/ilmenite) (Mag) set in groundmass of plagioclase and glassy cryptocrystalline material (dark grey). The biggest plagioclase phenocryst, at the bottom of image, shows a sieve texture with magnetite and glass inclusion. Plagioclase phenocrysts show clear zoning. Some plagioclase phenocrysts have been altered to quartz (Qz)

4.1.1.4. Pyroclastic Breccia unit

The Andesite A unit is underlain by the Pyroclastic Breccia unit, consisting of andesite breccia, andesitic tuff breccia, andesite lava, and andesitic tuff (Appendix B). In LHD-26, this unit has a thickness of 825 m containing abundant andesitic pumice fragments (Fig. 4.5). In LHD-27 and LHD-32, the unit is only 375 and 560 m thick, respectively. Pumice is minor in these wells.

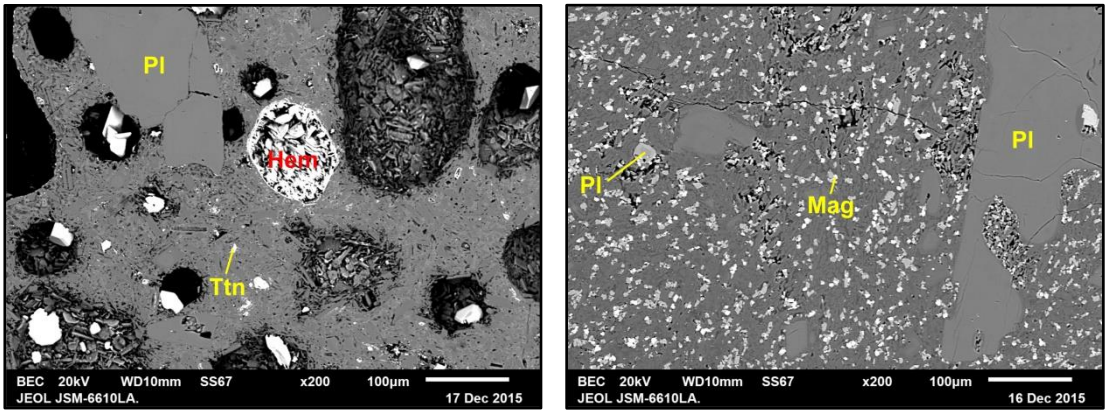

Figure 4.5. BSE image of Pyroclastic Breccia unit. **Left-hand panel:** pumice fragment of LHD-26/833-836 m consisting of plagioclase (Pl) and pyroxene which has been altered to titanite (Ttn) set in groundmass of plagioclase, magnetite/ilmenite (rare – not present in the photograph), and glassy cryptocrystalline material (dark grey – altered to hematite and quartz). Some vesicles have been filled by hematite (Hem) and titanite. Most of vesicles remain open. **Right-hand panel:** embayed plagioclase (Pl) at LHD32/891-894 m. The rock consists of plagioclase (Pl), pyroxene (Px), magnetite(/ilmenite) (Mag), apatite (rare – not present in the photograph) and cryptocrystalline groundmass.

The andesite rock fragments of this breccia unit show a trachytic porphyritic texture consisting of plagioclase and pyroxene phenocrysts set in a groundmass of plagioclase ±pyroxene and cryptocrystalline material. In addition to the abundance of pumice, this rock unit also differs from the other units by having large embayed plagioclase crystals (phenocrysts) (Fig. 4.4) and swallowtail fine plagioclase crystals (groundmass). The Pyroclastic Breccia unit has a finer grained groundmass when compared to the Andesite A unit, with crystals ranging from 20-40 µm.

The IA of this unit is generally high, except in LHD-32. At depth of less than 700 m (about 250 m from the top of the unit), the IA is low to intermediate. In LHD-26, intensive oxidation processes have altered the primary component to hematite at depths of 800-830 and 1280- 1300 m. Loss of circulation in this unit occurs in LHD-26 at 689-899 m depth (Pertamina Geothermal Energy, n.d.-c).

4.1.1.5. Pitchstone unit

Pitchstone is a massive rock consisting predominantly of dark-coloured glass (Best, 2003). It has a similar appearance to obsidian, only its lustre is resinous rather than glossy. In Tompaso, the pitchstone contains a minor (<15%) number of plagioclase, pyroxene, quartz, and magnetite/ilmenite microlites. The pyroxene is only about 2-5% of the rock volume. The size of the microlites is 0.03-0.5 mm. Volcanic glass can either have an andesitic or silicic composition. Results from BSE-EDS show that the composition of the groundmass is SiO_2-rich, consisting mainly of wispy glass shards (Fig. 4.6), suggesting that it may have a silicic composition.

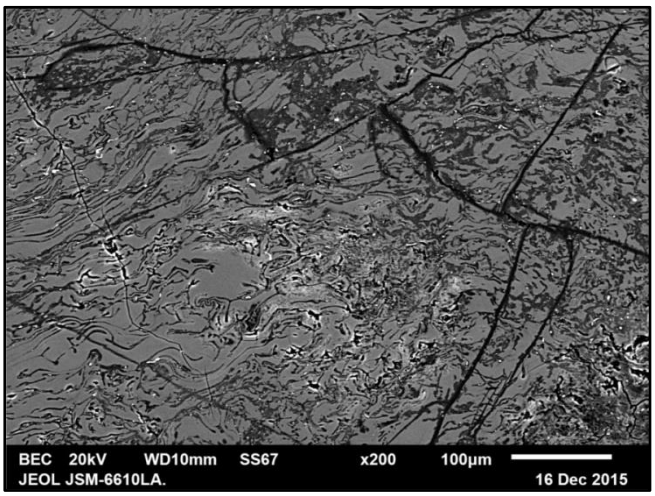

Figure 4.6. BSE image of wispy glass shards of LHD-32/1224-1227 m pitchstone.

In addition, a reconnaissance chemical analysis has been undertaken to the pitchstone using Electron Probe Microanalysis (EPMA) in order to know the general composition of the rock. The instrument was set to use a defocused beam of 20 µm and was standardized as for rhyolitic volcanic glass. The results show that the pitchstone has SiO_2 content as much as 73-78 wt% (normalized) confirming that the rock is rhyolitic. Typical rhyolitic rocks contain >68 wt% SiO_2, while andesitic and dacitic rocks commonly have ~57-62 and ~62-68 wt% SiO_2, respectively (Sigurdsson et al., 2000). The EPMA results also show totals of 85-93 wt% suggesting that the samples are strongly hydrated. This is in agreement with the characteristics of pitchstone which generally contains 6-10 wt% water absorbed at near atmospheric conditions (Best, 2003). In addition, the proportion of Ca to Ca+Na+K in the plagioclase phenocrysts in the Pitchstone unit suggest a low An values (An_{47} – An_{55}). This An value is similar to the An values of the plagioclase crystals in silicic post-Oruanui rhyolites in Taupo, New Zealand (Barker, et al., 2015).

According to the map of Prasetyo et al. (2015), their Lengkoan Formation is the only rock unit containing obsidian. K/Ar dating on basalt lava within the Lengkoan Formation yielded an age of 0.586 ± 0.051 Ma (PT Gondwana, 1988, unpublished data cited in Utami, 2011). However, a correlation between the Pitchstone unit inferred in this thesis and Lengkoan Formation cannot be determined as there is no age dating in this research.

The Pitchstone unit underlies the Pyroclastic Breccia unit. In the three studied wells, layers of pitchstone lava are found only in LHD-32, while in LHD-26 and LHD-27, pitchstone is present mainly as rock fragments in tuff or andesite breccia. In addition, lithologies of LHD-26 and LHD-27 are strongly altered, so it is difficult to identify this unit in these well. The identification was based on the presence of pitchstone chips, which represent less than ~10% of the cuttings. The Pitchstone unit has a thickness of 129 and 343 m in LHD-26 and LHD-32, respectively. This is the deepest unit reached in LHD-27 so that the exact thickness of the Pitchstone unit in LHD-27 is unknown. The thickness penetrated in LHD-27 is 142 m.

In addition to the intense alteration in LHD-26, the lithology at 1508-1514 m in this well has been intensely oxidised. The primary component of the rock has been replaced entirely by hematite. Unlike in LHD-26 and LHD-27, the Pitchstone unit in LHD-32 is weakly altered. The groundmass is generally still fresh, slightly altered to quartz. Another andesite succession, referred to here as the Andesite B unit, is encountered underlying the Pitchstone unit in LHD-26 and LHD-32. In LHD-26, a loss of circulation occurs (Pertamina Geothermal Energy, n.d.-c) corresponding to the contact between the Pitchstone and Andesite B units.

4.1.1.6. Andesite B unit

The Andesite B unit is characterised by its triangular-shaped plagioclase phenocrysts (Fig. 4.7) which can be seen under back-scattered electron (BSE) imaging. However, instead of a product of the emplacement processes, the triangular shape of the plagioclase more likely shows that the grainmount/sample cuts truncate the alignment direction of the crystals which suggest that the distribution of plagioclase has a certaion orientation/alignment. It is, thus, likely that this unit is lava. In addition, the Andesite B succession found in LHD-32 consists of swallowtail plagioclase groundmass. Glass shards are found at the upper part of the succession in LHD-26 down to 1676 m depth. The lava presents a trachytic texture. The andesite rock consists of 0.1-0.7 mm plagioclase, pyroxene, and magnetite/ilmenite set in a groundmass of 20-80 µm plagioclase, pyroxene, magnetite/ilmenite, and cryptocrystalline

material. The size of swallowtail plagioclase groundmass is up to 0.1 mm. Glomerocrysts of plagioclase+pyroxene are present.

In LHD-26, this unit has been moderately altered, whereas in LHD-32, the alteration intensity is very high, particularly below 1600 m from the surface in LHD-32. The Andesite B unit is the deepest unit penetrated in the LHD-32 borehole, with a minimum thickness proven of 850 m. In contrast, the Andesite B unit thickness in LHD-26 is only 144 m.

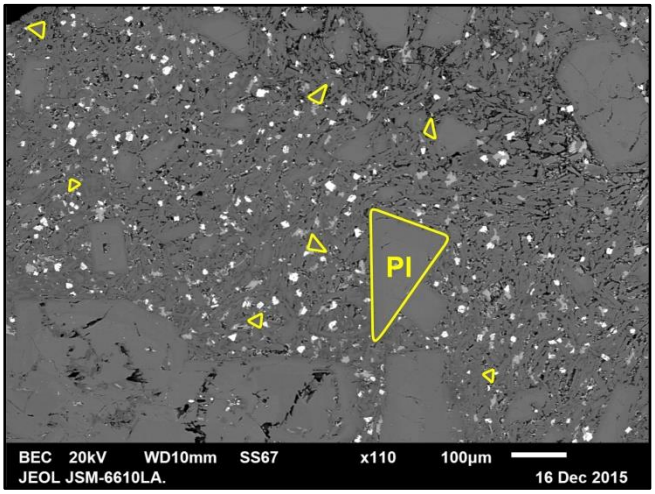

Figure 4.7. BSE image of Andesite B unit. This rock unit is characterised by the presence of triangular-shaped plagioclase (Pl) phenocrysts. Groundmass of the rock consists of plagioclase (mid grey), pyroxene (light grey), magnetite/ilmenite (white) and glassy cryptocrystalline material (dark grey). Sample: LHD-32/1410-1413 m.

4.1.1.7. Tuff B unit

The deepest unit encountered in LHD-26 is another tuff referred as the Tuff B unit. Pumice is found in minor amounts (<10%) in this unit, compared to the Tuff A unit. The IA of this unit is intermediate (IA = 0.3-0.6).

4.1.1.8. Rhyolite unit

An 84 -m-thick Rhyolite unit penetrates the Tuff B unit. The lithology shows a porphyritic texture with plagioclase, pyroxene, and magnetite/ilmenite set in a groundmass of plagioclase, quartz, and cryptocrystalline material (Fig. 4.8). The size of the phenocrysts ranges from 0.1-0.5 mm and the groundmass ranges from 20-60 µm. The percentage of quartz in the rock is 35%, while pyroxene is only 2%. With this abundance of quartz, it is apparent that this rock unit has a higher SiO_2 content than the andesitic units. The Rhyolite

unit occurs interbedded in pumice-bearing tuff, the Tuff B unit (Fig. 4.3), so that the Rhyolite unit is inferred to be a lava. This rock unit has been moderately altered, showing IA of 0.3-0.6.

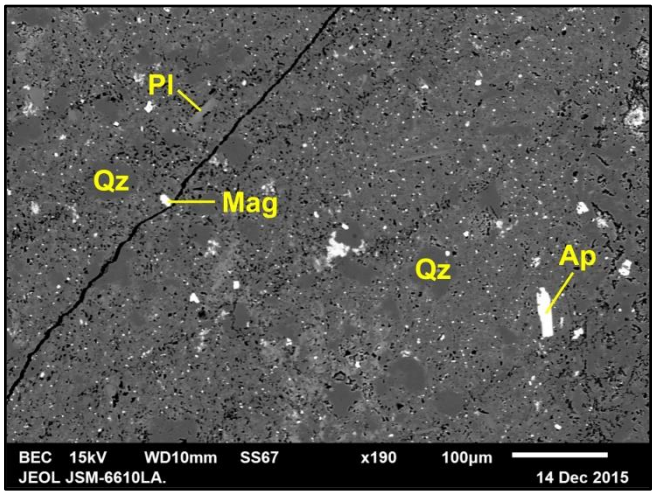

Figure 4.8. BSE image of the Rhyolite unit. The rock consists of quartz (Qz), plagioclase (Pl) magnetite(/ilmenite) (Mag), apatite (Ap), pyroxene (rare – not seen in the figure), and glassy cryptocrystalline materials. Sample of LHD-26/1841-1844 m.

4.1.1.9. Tempang Fault

There are a number of structures in Tompaso Field (Prasetyo et al., 2015), including Soputan Fault (sinistral strike slip), Sonder Fault (normal), Passo Fault, and Tempang Fault (Fig. 4.2). As the 3D model extent is limited to the location of drilled wells, only the Tempang Fault is able to be shown in the model (Fig. 4.2). There was no indication found of this fault at the surface during fieldwork and its presence is inferred from published works (e.g. Prasetyo et al., 2015; Sardiyanto et al., 2015).

The NNE-SSW Tempang Fault is drawn as a normal fault in the 3D geological model (Fig. 4.3), following the previous model by Prasetyo et al. (2015). The fault intersects LHD-27 at 1550 m depth and LHD-32 at 1400 m depth, but its presence is not clearly reflected in the samples. The Tempang Fault is estimated to intersect LHD-27 at ~1550 m depth, while total loss of circulation occurs from 1400-1750 m depth although it is unclear whether the total loss of circulation that occurs in LHD-27 correlates to the fault. In LHD-32, hematite is present at 1500 m depth coinciding with the estimated depth of the Tempang Fault. However, since the occurrence of hematite is not continuous, the formation of hematite in this well cannot be correlated to the fault. Yet, the Andesite unit at the depth below the estimated depth of Tempang Fault shows high alteration intensity (IA) unlike the rest of the

unit. Although it is uncertain, the intense alteration intensity may be related to the presence of the Tempang Fault. However, the presence of the Tempang Fault in both wells, LHD-32 and LHD-27, is reflected in the temperature configuration model of the geothermal setting. It is apparent from the model that the eastern fault block is hotter. The temperature profile of LHD-27 illustrates that the present-day temperature decreases below 1500 m depth at where the borehole is cutting through the western fault block (Fig. 4.9).

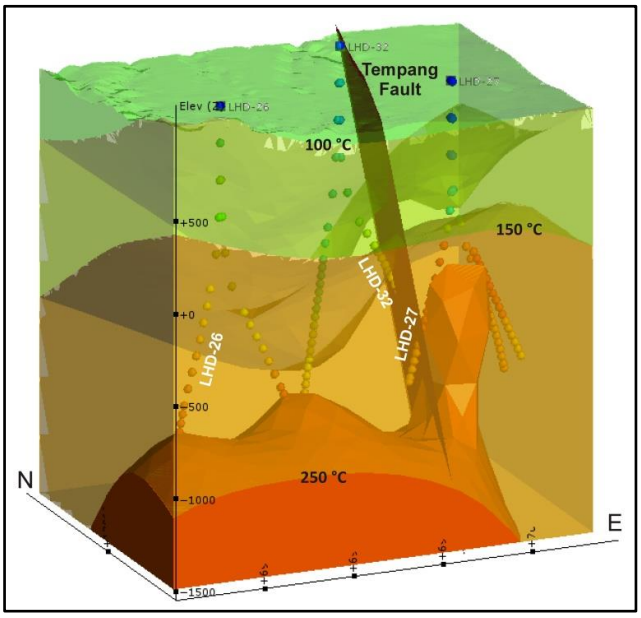

Figure 4.9. 3D model of the present-day temperature structure of Tompaso geothermal system. Isotherms are 100, 150, and 250 °C, generated by interpolating boreholes measured temperatures using Leapfrog Geothermal software.

4.1.2. Surface Manifestations

Fourteen geothermal features/complexes were observed during fieldwork. These geothermal manifestations are distributed into four different locations, referred to here as "manifestation zones" (detailed descriptions of each stop site in Appendix A). Geothermal manifestations present in Tompaso include hot springs, hot pools, warm springs, mud pots, fumaroles, and steaming ground. In this research, hot springs are defined as those where temperatures are higher than 60 ^{o}C.

Hydrothermal alteration processes, especially near-surface alteration in Tompaso, include leaching which is caused by a very reactive (i.e. acid) hydrothermal fluid. Acid fluid dissolves primary components of the country rocks. It is common that leaching processes are strong enough to dissolve minerals leaving crystal-shaped cavities in the rocks. The occurrence of these crystal-shaped cavities is used in this thesis as an indication of leaching.

4.1.2.1. Manifestation zone 1

Manifestation zone 1 is located on the flank of Mt. Rindengan (Fig. 4.2), and is dominated by fumaroles (sites KPS 1402 and KPS 1504). Fumaroles (Fig. 4.10) are characterised by high vapour content. The type of geothermal manifestations present in zone 1 suggests that the manifestations are occurring above the groundwater level, from where liquids will flow to the margin of the system and thus only vapour can move upward and be emitted on the surface. At Bukit Kasih (KPS 1402), fumaroles, hot springs, hot pools, a warm spring, and steaming ground are present. Indications of acid fluids are shown by the main replacement of country rocks by kaolinite and by the abundance of crystal-shaped cavities. Measured pH of the emitted fluids is 1 (Table 4.1) which also shows that the surface fluids are extremely acidic. Sulfur is common in this zone and is not present in other zones. All of the geothermal manifestations of this zone exceed 90 ^{o}C, except for the Pinabetengan warm springs (KPS 1403) which have a temperature of <50 ^{o}C.

Figure 4.10. Characteristics of manifestation zone 1. Left: high vapour content and abundant sulfur deposit (yellow minerals surrounding the vents). Right: indications of leaching shown by crystal-shaped cavities.

4.1.2.2. Manifestation zone 2

Manifestation zone 2 includes surficial geothermal features located around Kawangkoan (Fig. 4.2), including Kinali (KPS 1404) and Kayu Uwi (KPS 1601) warm springs, which have temperatures of 50 ^{o}C and 37 ^{o}C, respectively (Table 4.1). Both warm springs are slightly acid. The pH of Kinali fluids is 6, whereas for Kayu Uwi fluids it is 5.5 (Table 4.1). Both geothermal manifestations occur on the banks of rivers (Fig. 4.11), and the surrounding area is covered by dense vegetation. It is highly likely that the hydrothermal fluids have been mixed with meteoric water. There is a lack of other geothermal features in the areas surrounding these springs. No mineral deposition is observed. In addition, the host rock lithology seems to be strongly weathered rather than hydrothermally altered.

Figure 4.11. Characteristics of manifestation zone 2: discharged at the edge of rivers and surrounded by a dense vegetation cover. Left: Kinali warm spring (KPS 1404). Right: Kayu Uwi warm spring (KPS 1601).

4.1.2.3. Manifestation zone 3

Manifestation zone 3 is located at Tempang and in the vicinity of Mt. Umeh crater (Fig. 4.2). Many discharges are present in Zone 3; five of them have been observed during fieldwork. These five features include Tempang hot springs (KPS 1301) (Fig. 4.12), Toraget hot pools and mud pots complex (KPS 1302), Karumenga hot spring (KPS 1401), Kamanga hot spring (KPS 1602), and Tompaso mud pots and hot springs complex (KPS 1701). Looking at the distribution of geothermal manifestations within Zone 3, it is apparent that the occurrence of these features is closely coincident with the mapped surface trace of the Soputan Fault (Fig. 4.2). Geothermal manifestations of this zone are characterised by the wide extent of altered areas, high temperatures, and high discharge rates. The temperature range in this zone is from 40 to 80.8 ^{o}C with only 25% of the discharges at temperatures of <60 ^{o}C (Table 4.1). The results of pH measurement of hydrothermal fluids from this zone suggests that the fluids are mainly near-neutral pH fluids even though acid fluids are also present at the Toraget complex of hot pools and mud pots (Fig. 4.12) (KPS 1302) (Table 4.1).

Figure 4.12. Geothermal features at zone 3. Left: Tempang hot spring (KPS 1301). Right: Toraget mud pot (KPS 1302). Mud pots are only present at zone 3.

Table 4.1. Summary of the geothermal activity at the Tompaso geothermal manifestations. Detailed descriptions of each stop site are in Appendix A. Hydrothermal minerals are from field observation and SWIR results (Appendix C).

Manifestation Zone	Stop Sites	Feature(s)	T (°C)	pH	Indications of Leaching on Country Rocks	Hydrothermal Minerals
1	Bukit Kasih fumarole (KPS 1402)	fumaroles, hot pool, steaming ground	94	1	present	kaolinite, sulfur, alunogen, hematite, silica sinter (opal), smectite, opal, alunite, gibbsite
	Pinabetengan warm spring (KPS 1403)	warm spring	48.7	5.5	-	smectite
	Sempu fumarole (KPS 1504)	fumaroles	90.3	-	present	kaolinite, sulfur, silica (opal), smectite, opal, gypsum
2	Kinali warm springs (KPS 1404)	warm springs	50.4	6	-	smectite
	Kayu Uwi warm spring (KPS 1601)	warm spring	37	5.5	-	smectite
3	Tempang hot spring (KPS 1301)	hot springs, steaming ground	77.7	7.5	-	kaolinite, hematite, alunogen, silica sinter, smectite
	Toraget manifestation complex (KPS 1302)	warm springs; hot spring; mud pots	40-50 (warm spring); 73.3 (hot pool); 78 (mud pots)	3-4	-	kaolinite, smectite, opal
	Karumenga hot spring (KPS 1401)	hot spring	69	6	-	
	Kamanga warm spring (KPS 1602)	warm spring	43	6	-	
	Tempang manifestation complex (KPS 1701)	hot springs, mud pots (active and extinct), steaming ground	74.5-80	4	-	kaolinite
4	Passo hot spring (KPS 1304)	hot spring	63.3	7	-	
	Passo warm spring 1 (KPS 1305)	warm spring	60	6	-	
	Passo warm spring 2 (KPS 1702)	warm spring	39.6	6	-	
5	Totok hot spring (KPS 1604)	hot spring, steaming ground	73.6	5.5	-	kaolinite, sulfur, hematite

4.1.2.4. Manifestation zone 4

At the northeast end of Tompaso (Fig. 4.2), hot springs and warm springs occur that are grouped as Manifestation zone 4. These geothermal features are situated at the edge of Lake Tondano (KPS 1304, KPS 1305, and KPS 1702) suggesting that the hydrothermal fluids emitted in these geothermal manifestations are likely to have mixed with meteoric water. The temperatures range from <40 ^{o}C to about 60 ^{o}C and acidity measurement of the fluids shows a near-neutral pH type of fluids (Table 4.1). Geothermal features at zone 4 do not contain steam-fed zones (Fig. 4.13) reflecting that the topography of the area is at the groundwater level. Similar to zone 2, there is a lack of other geothermal features in the surroundings of these springs (Fig. 4.13). The country rock lithologies have been strongly weathered rather than hydrothermally altered.

Figure 4.13. No-steam features at zone 4. Left: hot spring (~60 °C) emitted inside one of the houses. Right: warm spring occurs in the middle of a paddy field.

4.1.2.5. Manifestation zone 5

All geothermal manifestations included in zones 1 to 4 have been mapped in previous works (Pertamina Geothermal Energy, n.d.-a; Handoko, 2010). However, there is an additional geothermal manifestation, here labelled zone 5, which is not recorded on any pre-existing map. This manifestation is represented by Totok hot spring (KPS 1604), situated between zones 3 and 4 (Fig. 4.2). The hot spring is slightly acid with pH value of 5.5 and a temperature of >70 ^{o}C (Table 4.1). The spring has a low discharge rate giving the appearance of a pool. Steaming ground as well as altered ground is present on the edge of the pool (Fig. 4.14). Replacement minerals are mainly kaolinite and hematite (Table 4.1). This manifestation has similar characteristics to geothermal features in zone 3 (Fig 4.7) yet its location suggests that Totok hot spring should not be included in zone 3. Instead of being along the Soputan Fault, Totok hot spring occurs closer to the NNE-striking fault, a

second order of the Soputan Fault (Fig. 4.2), although there is no evidence that the siting of this hot spring has been controlled by the fault.

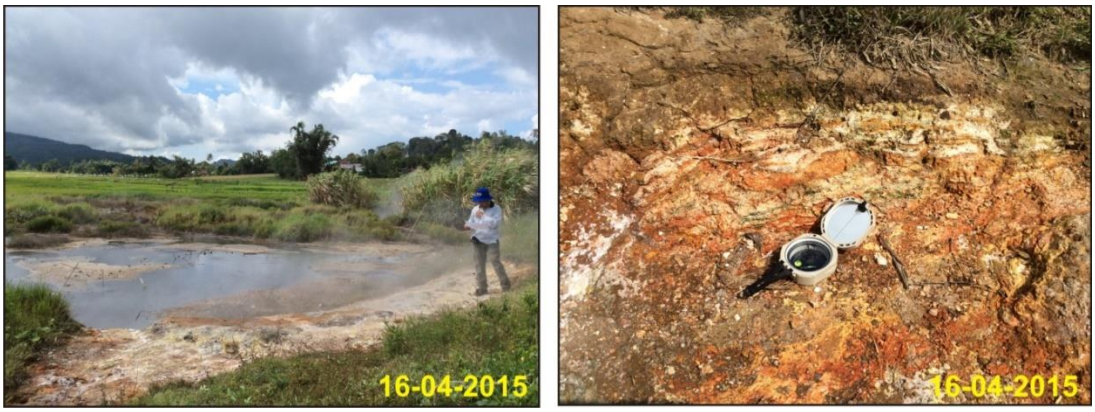

Figure 4.14. The only geothermal feature in zone 5. Picture on the right is a zoomed-in of the altered ground at the edge of the pool on the left-hand panel (see explanations in the text).

4.1.3. Hydrothermal Alteration

Hydrothermal alteration products have been studied in this thesis through binocular microscopy, short-wave infrared (SWIR) analysis, petrography, and back-scattered electron (BSE) imaging combined with energy dispersive spectroscopy (EDS). The observations cover both replacement and vein filling minerals. Replacement minerals that could be identified are clay minerals, chlorite, calcite, epidote, pyrite, Fe-oxide, and quartz. Identification of clay mineral species has been done using SWIR and BSE-EDS. Hydrochloric acid (HCl) was used to support the identification of calcite. Iron oxides (Fe-oxides) identified in this work are mostly hematite. Other minerals that rarely present as replacement minerals are sulfur, chalcedony, and sulfide minerals (e.g. pyrite).

Other indications of hydrothermal processes being observed are the occurrence of veins and their filling minerals, as well as indications of leaching processes. However, only limited amounts of core were available and observing veins from cuttings is not easy. Indications of leaching processes can be easily recognised by the occurrence of cavities in the rocks, and hydrothermal minerals that are stable under acidic conditions, such as kaolinite. Vesicles originally present in the rocks due to explosive eruption processes have a different shape to leached cavities. The latter normally follow the shape of the pre-existing minerals

4.1.3.1. *Surface hydrothermal alteration*

Hydrothermal minerals formed at the surface in the Tompaso area are generally indicators of acid steam-heated conditions including kaolinite, gibbsite, jarosite, and alunite (Table 4.1). In addition to these minerals, opal is also present in a number of samples (Table 4.1). The deposition of opal indicates an acid condition, even though not directly, where the acid hydrothermal fluids take all the other chemical components away from primary minerals leaving silica behind in the rocks. Kaolinite and opal are present widely at almost all stop sites. Meanwhile, alunite, jarosite, and gibbsite are present only at KPS 1402 and KPS 1604 (Table 4.1) suggesting that the hydrothermal fluids that occurred at these places are strongly acid. A small amount of gypsum occurs at KPS 1504.

Figure 4.15. Alunogen formed at KPS 1301.

In addition to altered rock samples, from SWIR results, silica residue is present at KPS 1301 and KPS 1402 (Appendix A). Silica residue is deposited mostly at the edge of hot pools. At these two sites, alunogen (Fig. 4.15) is also present. Alunogen is sulfate efflorescence mineral, formed in an acid environment in which kaolinite was decomposed by acid steam at low temperature (steaming ground). The reverse reaction may take place if alunogen reacts with silica saturated fluids with higher pH (Lawless et al., 1997; Martin et al., 1999, 2000). Alunogen is only stable under a hot and dry or humid (but not wet) environment as aqueous fluids will dissolve the mineral (Martin et al., 2000).

4.1.3.2. *Subsurface hydrothermal alteration*

Results from binocular microscopy (Appendix B), SWIR (Appendix C), microscopic petrography (Appendix D), and SEM-EDS (Appendix E) have been used to infer subsurface hydrothermal alteration patterns in cuttings samples from Tompaso. Microscopic petrography has been done only on LHD-26/1676-1678 m and LHD-27/1742-1748 m due to the limited availability of suitable material (core). SWIR analysis on Tompaso andesite (subsurface samples/cuttings) was not as effective as it was on surface samples. This is due

to the low alteration intensity at most depths leading to unrecognisable spectra due to the dark rock colouration as well as the abundance of volcanic glass at shallow depth in LHD-26 (see Chapter 3). In other words, the detection ability of SWIR depends on the alteration intensity of the rock in andesite. In this research, the alteration intensity of andesite in LHD-27 is generally high (with abundant less dark chlorite and clays) so that the natural colouration is not a problem for this well.

Replacement minerals

Replacement minerals present at Tompaso (Fig. 4.16, 4.17, 4.18) are kaolinite, smectite, interlayered clays, illite, chlorite, calcite, chalcedony, epidote, anhydrite, jarosite, leucoxene, adularia, iron oxides, pyrite, and quartz. In addition, but not drawn in the logs, albite, titanite, and magnesite are also found as a replacement minerals in Tompaso (detail description in Appendix E). Chalcedony, anhydrite, leucoxene, and adularia are only present in LHD-26. Meanwhile, jarosite is only found in LHD-27. Iron oxides in the Tompaso rocks are mostly hematite.

Kaolinite – $Al_2Si_2O_5(OH)_4$

Tompaso samples at shallow depths consist mostly of kaolinite. In LHD-26 and LHD-27, kaolinite is present down to ~300 m depth (~500 m above sea level (masl)), while it is found down to 500 m (267 masl) in LHD-32. Kaolinite is identified in this thesis through SWIR and BSE-EDS analyses. Kaolinite is formed in acidic environment at temperature of <200 °C in active geothermal fields in Philippines (Reyes, 1990), in agreement with present-day temperatures 40-100 °C in Tompaso (Pertamina Geothermal Energy, n.d.-d). The formation of kaolinite suggests that acidic hydrothermal fluids dominate the shallow part of Tompaso geothermal system.

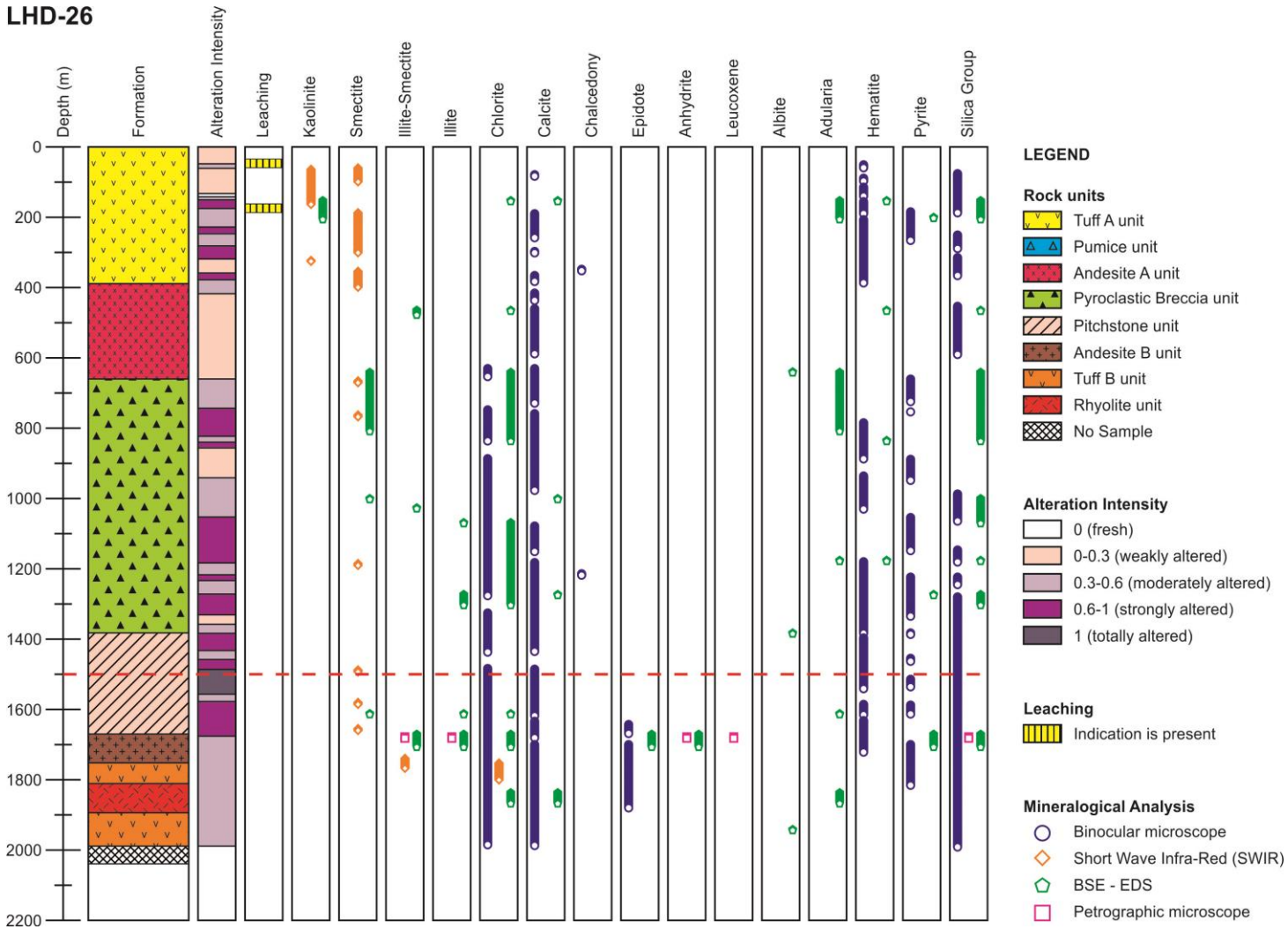

Figure 4.16. Log lithology and hydrothermal mineralogy of LHD-26. The explanation of the alteration intensity is in Appendix B. Red dashed lines is the estimated depth of A-A' fault.

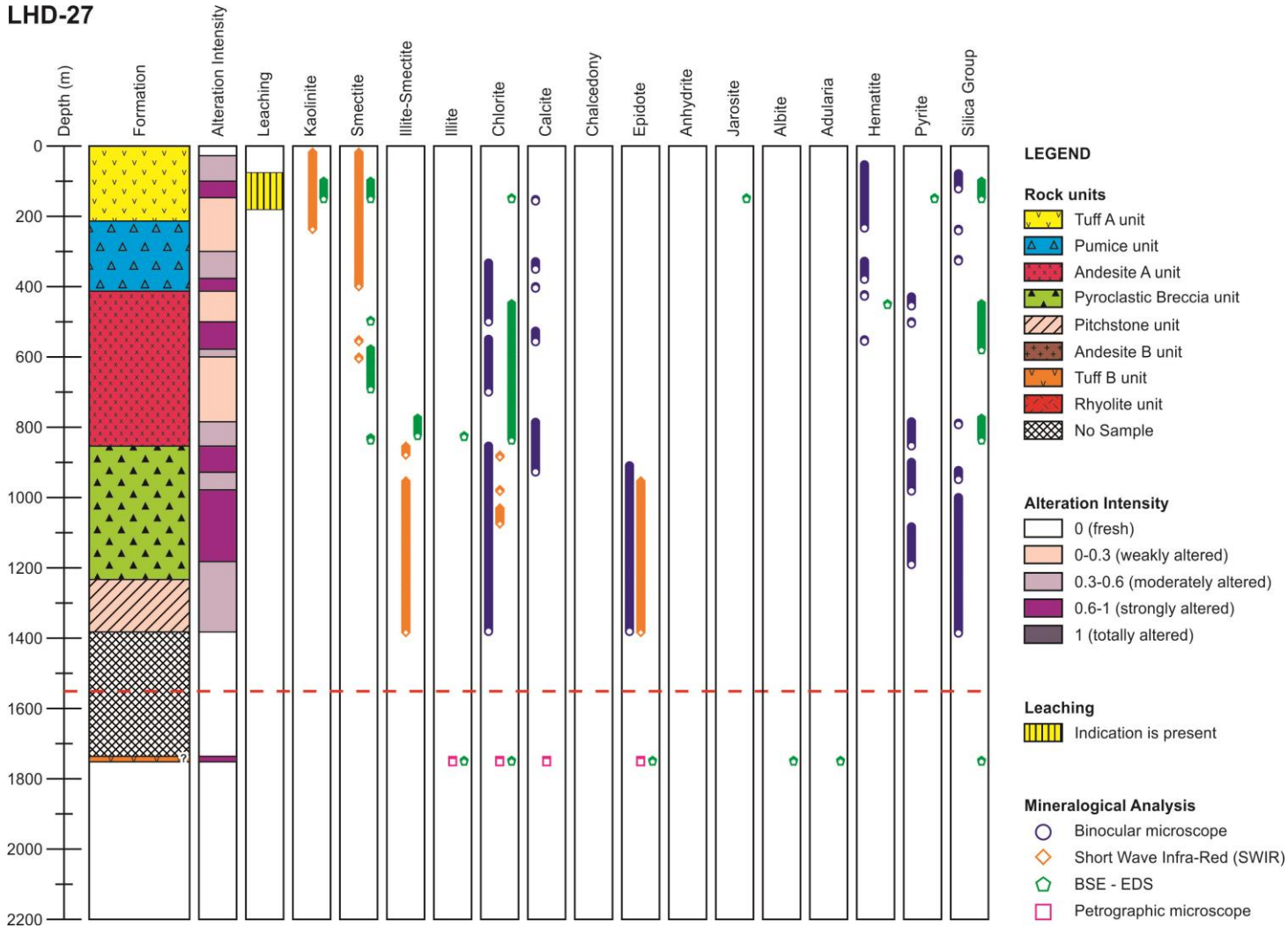

Figure 4.17. Log lithology and hydrothermal mineralogy of LHD-27. The explanation of the alteration intensity is in Appendix B. Red dashed lines is the estimated depth of Tempang Fault.

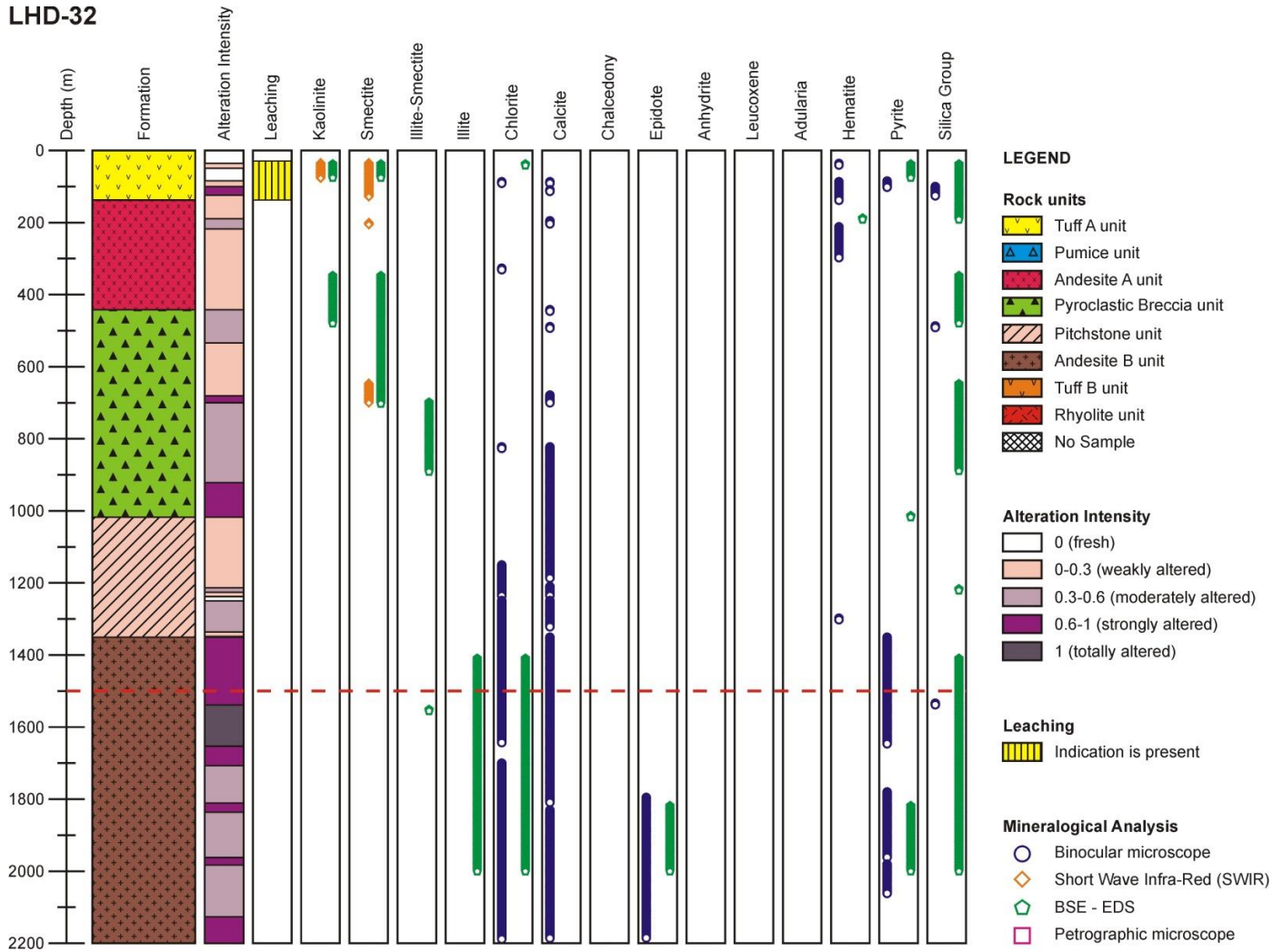

Figure 4.18. Log lithology and hydrothermal mineralogy of LHD-32. The explanation of the alteration intensity is in Appendix B. Red dashed lines is the estimated depth of Tempang Fault.

Smectite – $(Ca,Na)_{0.3}(Al, Mg, Fe, Zn)_{2-3}[(Si,Al)_4O_{10}](OH)_2.nH_2O$

Smectite in this work is identified through SWIR and BSE-EDS. The formation of this mineral is controlled by temperature. Smectite is assumed to be formed at temperature below 180-200 °C in active geothermal fields in Philippines (Reyes, 1990). Therefore, the deepest occurrence of smectite in a geothermal system can be used to mark the <200 °C isotherm. The deepest formation of smectite in Tompaso geothermal system occurs at 1613 m (~660 mbsl), 825 m (~23 mbsl), and 700 m (~70 masl) at LHD-26, LHD-27, and LHD-32, respectively.

The deepest occurrence of smectite in LHD-26 coincides with a slightly higher temperature than 200 °C. The present-day temperature at this depth is 227 °C (Pertamina Geothermal Energy, n.d.-d). The deepest occurrence of smectite in LHD-27 is within the 800-900 m zone of abrupt temperature increase from 128-254 °C (Pertamina Geothermal Energy, n.d.-d) suggesting that it is likely that the measured temperature at 825 m matches the formation temperature of smectite. On the other hand, the deepest occurrence of smectite in LHD-32 show a temperature of 70 °C; lower present-day temperature. It is apparent that LHD-32 has experienced cooling since the formation of smectite.

Interlayered clays

Interlayered clays found in Tompaso geothermal system are mainly illite-smectite. Interlayered illite-smectite is found widely in LHD-27 and LHD-32, but rarely in LHD-26 (Fig. 4.16, 4.17, 4.18). It is found at 1700-1900 m (750-950 mbsl) in LHD-26, 750-1400 m (90 masl – 510 mbsl) in LHD-27, and 700-900 m depth (75 masl – 100 mbsl) in LHD-32. In addition, interlayered illite-smectite is also found in LHD-32/1554-1557 m as detected by BSE-EDS. These depths are below the formation of smectite, in agreement with the formation temperature of interlayered illite-smectite which is higher than that of smectite. Reyes (1990) considered the formation of interlayered illite-smectite occurs between 180 and 260 °C. These interlayered clays are present at the measured temperature of 233-255 °C, 70-260 °C, and 70-165 °C in LHD-26, LHD-27, and LHD-32, respectively (Pertamina Geothermal Energy, n.d.-d).

In addition, interlayered chlorite-illite is also present in LHD-26 and LHD-32 (Appendix E). Interlayer of chlorite-smectite was reported previously by Moore & Reynolds (1989).

However, it is inferred that the chlorite-clay interlayered phases found in this study are chlorite-illite based on the presence of potassium (K) in the mineral as detected using BSE-EDS. Chlorite-illite is also present in active geothermal systems in New Zealand (Ji & Browne, 2000). Due to the overall rarity of an interlayered chlorite-illite phase in Tompaso, this phase is not used in any interpretation of the Tompaso geothermal system.

Illite – $K_{0.65}(Al,Fe,Mg)_{2.0}[Al_{0.65}Si_{3.35}]O_{10}(OH,F)_2$

Illite is formed at temperatures of over 220 °C, as demonstrated at Ngawha geothermal field in New Zealand and some active geothermal fields in Philippines (Reyes, 1990; Cox & Browne, 1998). However, Ji & Browne (2000) suggested that illite may also form at a lower temperature. Using samples from Ohaaki-Broadlands and Waiotapu, they inferred that illite is formed at temperature of >160 °C. In their work, they also demonstrated that the formation temperature of illite can be evaluated using its crystallinity. However, there is no illite crystallinity investigation taken in this thesis and thus the formation temperature of illite in Tompaso cannot be estimated.

Illite is present sporadically at 1100-1700 m depth (1050-1550 mbsl) in LHD-26. Meanwhile, illite is detected through BSE-EDS at 825 m depth (23 mbsl) and 1745 m depth (800 mbsl) in LHD-27. Illite is present continuously in LHD-32 from 1400-2000 m depth (435-855 mbsl). Temperature range of these depths is 153-233 °C (Pertamina Geothermal Energy, n.d.-d).

Chlorite – $(Mg,Fe^{2+},Fe^{3+},Mn,Al)_{12}[(Si,Al)_8O_{20}](OH)_{16}$

Chlorite is the most common mineral throughout the Tompaso geothermal system, replacing plagioclase, pyroxene, and groundmass (Fig. 4.19). Chlorite is easily identified in all analyses conducted in this work. The shallowest occurrence of chlorite in LHD-26 is 625 m depth (165 masl) where the measured temperature is ~100 °C (Pertamina Geothermal Energy, n.d.-d). Chlorite is most abundant in LHD-27 at 350 -1400 m depth (490 masl – 500 mbsl) in LHD-27, coexisting with calcite. Present-day temperature at this depth are ~40-260 °C (Pertamina Geothermal Energy, n.d.-d).

In LHD-32, chlorite is most abundant from 1300 m depth (370 mbsl) where the present-day temperature is >138 °C (Pertamina Geothermal Energy, n.d.-d). The occurrence of chlorite

in LHD-32 coexists with the occurrence of epidote. It is apparent that chlorite in Tompaso is stable over a wide range of temperatures, especially in LHD-27. Lawless et al. (1997) considered that the formation temperature of chlorite depends on its chemical composition. Quantitative chemical analysis was not undertaken in this work. Chlorite cannot therefore be used as a thermometer but is a good indicator of near neutral pH hydrothermal fluid conditions.

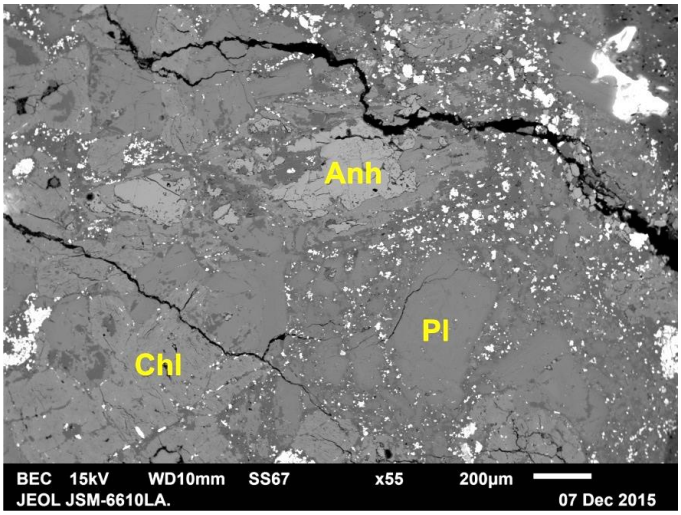

Figure 4.19. Sample of LHD-26/1676-1678 m. Chlorite (Chl) and anhydrite (Anh) has replaced pyroxene. Plagioclase (Pl) is generally still fresh.

Calcite – $CaCO_3$

Calcite is most abundant in LHD-26 and almost present in all depths throughout the well as identified under binocular microscope combined with acid test using hydrochloric acid (HCl). However, BSE-EDS results show that calcite is most abundant at depth of 1800-1900 m, coexisting with interlayered illite-smectite, chlorite, and adularia. This depth also coincides with the depth of the Rhyolite unit. The temperature measured at this depth is ~250 °C (Pertamina Geothermal Energy, n.d.-d).

Unlike in LHD-26, the presence of calcite in LHD-27 and LHD-32 cuttings was only detected under binocular microscope which was confirmed by the acid test using HCl. BSE-EDS results do not show any replacement of primary minerals by calcite. Calcite is found sporadically in LHD-27 from 300 to 900 m depth or 500 masl to 60 mbsl, where the measured temperatures are 50-255 °C (Pertamina Geothermal Energy, n.d.-d). In LHD-32, calcite is most abundant at depth below 800 m or 20 mbsl, coexisting with present-day temperature of >77 °C (Pertamina Geothermal Energy, n.d.-d).

Epidote – $Ca_2Al_2O(Al,Fe^{3+})OH[Si_2O_7][SiO_4]$

Epidote is a common temperature indicator mineral in geothermal systems. In active geothermal systems in Philippines and New Zealand, epidote is stable at temperature of >240 °C (Reyes, 1990; Cox & Browne, 1998). Epidote is thought to have formed by neutral pH alkali chloride water with low dissolved CO_2 (Browne & Ellis, 1970).

The shallowest occurrence of epidote in LHD-26 is 1650 m depth or about 696 mbsl according to binocular microscope observations and BSE-EDS analyses. This depth was measured to have a temperature of 230 °C (Pertamina Geothermal Energy, n.d.-d). BSE-EDS results of LHD-32 cuttings start showing epidote from 1800 m depth or 760 mbsl showing a present-day temperature of 193°C (Pertamina Geothermal Energy, n.d.-d).

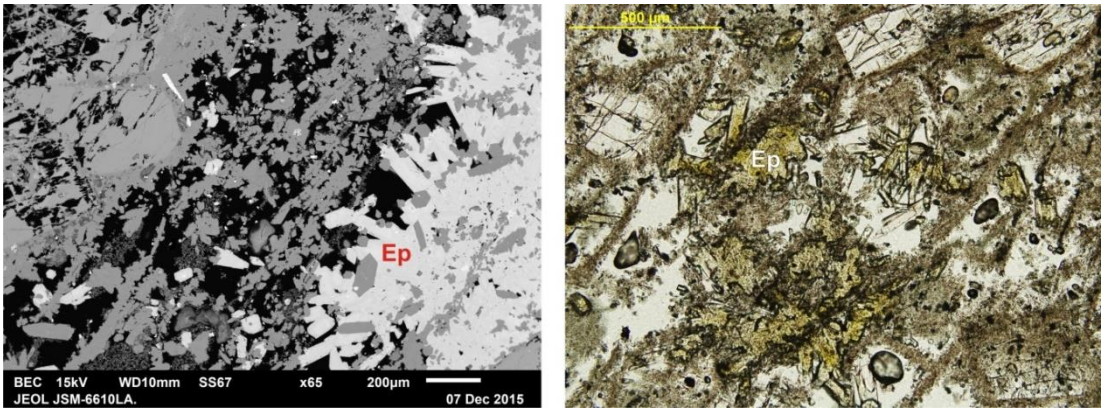

Figure 4.20. Acicular epidote along with quartz (Ep) in LHD-27/1742-1748 m. Left: BSE image. Right: plane polarised thin section image.

The shallowest replacement by epidote in LHD-27 is identified to have formed at 900 m depth (87 mbsl) according to binocular observation. This depth coincides with present-day 254 °C (Pertamina Geothermal Energy, n.d.-d). From the shallowest depth of epidote in three observed wells, it is apparent that LHD-27 has not experienced much change in its temperature, while LHD-26 and LHD-32 have experienced cooling, particularly in LHD-32.

Epidote occurs in Tompaso predominantly as a replacement mineral of pyroxene. However, the sample LHD-32/2000 m shows a replacement of plagioclase by epidote. In addition, epidote is also present in LHD-27/1742-1748 m as a replacement mineral of tuff fiamme (Fig. 4.20). In this sample, epidote shows a perfect acicular shape. However, there is a reversal temperature in LHD-27 and present-day temperature at the depth where acicular epidote present is 208 °C (Pertamina Geothermal Energy, n.d.-d).

Anhydrite – $CaSO_4$

Anhydrite is formed in geothermal systems at the point where the neutralisation of the acid fluids occurs. In Alto Peak system (Philippines), anhydrite is stable at 220-500 °C with that generated at >400°C formed by magmatic-hydrothermal processes (Reyes et al., 1993), while at other geothermal systems in Philippines, anhydrite is present from a temperature of 180 °C (Reyes, 1990). In Tompaso geothermal system, anhydrite is only present in LHD-26. Through petrography and BSE-EDS microscopy, anhydrite is identified at 1675 m depth (720 mbsl). These depths show present-day temperatures of 230°C (Pertamina Geothermal Energy, n.d.-d).

Jarosite – $KFe^{3+}_3(SO_4)_2(OH)_6$

Jarosite is an iron-rich member of the alunite group. This mineral is a product of hydrothermal alteration processes by acid hydrothermal fluids (pH<3) with low sulfate activity (Reyes, 1990; Lawless et al., 1997). Jarosite is active at temperature ranging 30 -120 °C in active geothermal systems in Philippines (Reyes, 1990). In Tompaso, jarosite is only present in LHD-27 at 140 m or 860 masl. The measured temperature at this depth is 28 °C (Pertamina Geothermal Energy, n.d.-d).

Hematite – Fe_2O_3

Hematite is formed by an oxidation of country rocks. The occurrence of hematite in magmatic-hydrothermal geothermal systems indicates that the altering hydrothermal fluids consist mainly of meteoric water. Meteoric water delivers oxygen, which is effectively absent in magmatic water, from the surface to the depth of the hematite formation. Hematite is only present from the near-surface in LHD-27 down to 550 m depth or 240 masl. In LHD-32, hematite is present at from the near-surface down to 300 m depth (470 masl) and at ~1300 m depth (~365 mbsl). The latter depth shows a present-day temperature of 138 °C (Pertamina Geothermal Energy, n.d.-d. On the other hand, hematite is present sparsely throughout LHD-26, with its deepest occurrence at 1710 m depth or ~750 mbsl where the measured temperature is 235 °C (Pertamina Geothermal Energy, n.d.-d). At depths of 800-830 m, 1280-1300 m, and 1508-1514 m, hematite has totally replaced

the primary components of the country rocks. The deepest intense hematite replacement occurs at ~1500 m depth (~560 mbsl) (Appendix B) shows a measured temperature of 216 °C (Pertamina Geothermal Energy, n.d.-d).

Adularia – $KAlSi_3O_8$

Adularia is an alkali feldspar which forms in production zones of geothermal systems with high permeability (Browne, 1970, 1978). BSE-EDS results show that adularia is found sporadically as a replacement mineral in LHD-26. Its occurrence at ~200 m depth (~600 masl) in this well coexisting with kaolinite. This coexistence may show a change in thermal regime because adularia and kaolinite cannot present in equilibrium (discuss further in section 5.2.3). Adularia is also found in LHD-27 at 1750 m or ~790 mbsl depth as identified under petrographic microscope. Adularia is absent in LHD-32.

Chalcedony – SiO_2

The formation of chalcedony in active geothermal systems occurs at low temperature (~180 °C; Fournier, 1985). In Tompaso, chalcedony is only present in LHD-26 with its deepest occurrence at 1200 m depth or ~300 mbsl, where the present-day temperature is 180 °C (Pertamina Geothermal Energy, n.d.-d). This measured temperature matches with the formation temperature of chalcedony reported in published works.

Silica group – SiO_2

Silica group minerals are the most common hydrothermal products in active geothermal systems. They form in both neutral pH and acidic environments. Silica group minerals also form under a wide range of temperature. Silica-saturated hydrothermal fluids are likely to form quartz at temperature above 190 °C (Reyes, 1990) and chalcedony or other silica at temperature below 190 °C. Amorphous silica (i.e. opal-A) is normally present at near the surface as it forms ar around room temperatures. Opal-A is common in geothermal maifestations where the fluids are acid. Acid fluids tend to remove other elements from the country rocks and leave the silica behind (i.e. amorphous silica). Amorphous silica and

quartz are often difficult to distinguish because they have a similar appearance, especially in fine-sized cuttings as relied on in samples used in this work.

Comparing the results of binocular observation and BSE-EDS analysis, it is apparent that BSE-EDS quartz is mostly a product of devitrification or recrystallization of volcanic glass groundmass of the rocks (detailed description in Appendix E). In binocular observation results of LHD-26, silica is present at 2 main depths; <400 m (316 masl) and >1000 m depth (140 mbsl). The measured temperatures at these depths are <111 °C and >165 °C, respectively. It is likely that the shallow silica is amorphous silica and the deep silica is quartz.

Two silica zones are also identified in LHD-27 from binocular observation. The shallow zone occurs at <300 m depth (520 masl), while the shallow boundary of the deep zone occurs at between 800 and 900 m (5-85 mbsl). The latter depth is where a rapid temperature increase occurs from 128 °C at 800 m depth to 254 °C at 900 m. In binocular observation results of LHD-32, silica is identified at 100, 500, and 1500 m depth, corresponding to measured temperatures of 40, 55, and 162 °C, respectively (Pertamina Geothermal Energy, n.d.-d).

Pyrite – FeS_2

Pyrite is one of sulfide minerals present in Tompaso geothermal system. Pyrite is present sporadically in LHD-26, LHD-27, and LHD-32 from near surface down to near the deepest depth penetrated by the wells. Pyrite is not a good indicator for temperature as it is stable in a wide range of temperature from 20 to >340 °C (Reyes, 1990).

Other minerals

In addition to the replacement minerals mentioned previously, these minerals are also present replacing the primary lithologies in Tompaso geothermal system: titanite, albite, chalcopyrite, prehnite, magnesite, and sulfur. Titanite, albite, and prehnite are present only in LHD-26. Detailed descriptions of these minerals are in Appendix B and E. Titanite and albite are present sporadically in LHD-26. Titanite has been reported to be stable at >150 °C (Cox & Browne, 1998), but this temperature is not applicable for this research since

titanite is also present in near-surface samples. Prehnite is present in LHD-26 at ~1300 m depth or 400 mbsl where the measured temperature is 193 °C (Pertamina Geothermal Energy, n.d.-d). This temperature is lower than its formation temperature in active geothermal systems in Philippines and New Zealand, (240-350 °C: Reyes, 1990; Cox & Browne, 1998). Magnesite is present at 1000 m depth (150 mbsl) in LHD-26 and at 1550 m depth (545 mbsl) in LHD-32.

Direct deposited minerals

Veins are commonly present in Tompaso samples. The presence of veins as well as their filling minerals is mostly observed through petrography and BSE-EDS imagery. It is challenging to identify veins from cuttings as the size of Tompaso cuttings is mostly <2 mm. However, chips of quartz and quartz+chlorite are present in cuttings and thus only these two veins can be identified through binocular microscope imagery. As the size of cuttings is very small, it is rare to find two or more veins in a cutting chip. Consequently, the cross cutting relationships between all the veins cannot be determined. Two core cuts are available: LHD-26/1676-1678 m and LHD-27/1742-1748 m. Thin sections were made from these samples. Under petrography microscope, the second sample shows only quartz-filled veins. The first sample shows only anhydrite-filled (Fig. 4.21) and titanite-filled veins, but no cross-cutting relationships are present between these veins.

The summary of the vein- and vesicle-filling minerals in the Tompaso geothermal system is presented in Table 4.2. In general, seven different vein associations are present in Tompaso: zeolite, titanite, clays (illite/smectite), chalcedony, anhydrite ± (quartz ± pyrite ± pyroxene), hematite, and quartz ± chlorite ± (pyrite/chalcopyrite) ± calcite ± hematite. Titanite-filled veins are only present in LHD-27 at 576 m (215 masl) and 1745 m (800 mbsl) depth, respectively. Clay-filled veins are rare, with two different clays found: smectite at 576 m depth (215 masl) in LHD-27 and illite at 1700 m depth (750 mbsl) in LHD-26.

Chalcedony is present as a vein filling mineral in the upper part of LHD-26 down to 1000 m (150 mbsl). Anhydrite has filled veins in LHD-26 samples below 1274 m (385 mbsl). At 1700 m depth (750 mbsl), anhydrite has partly been deposited with quartz, pyrite, and pyroxene. The shallowest occurrence of anhydrite-filled veins coincides with the deepest occurrence of hematite-filled veins. Hematite is present as vein filling mineral only in LHD-26 from near surface down to 1274 m (385 mbsl).

Table 4.2. Vein and/or vesicles filling minerals in Tompaso (from Appendix B, D, and E).

Well	Depth (m)	Vein (or vesicles) fillings
LHD-26	60-70	Quartz, hematite
	150-170	Hematite, chalcedony
	203-221	Hematite
	365-383	Quartz+chlorite
	401-410	Quartz+pyrite
	455-593	Quartz±chlorite±hematite
	464-467	Wairakite
	797-818	Clay, chlorite
	803-806	Quartz+pyroxene
	833-860	Quartz
	833-836	Hematite, titanite
	947-983	Quartz±titanite
	983-1031	Chalcedony
	1076-1145	Quartz±chlorite
	1178-1181	Adularia, quartz±chlorite±pyrite
	1181-1202	Quartz
	1211-1220	Quartz
	1226-1268	Quartz±chlorite±pyrite
	1268-1271	Quartz
	1274-1277	Quartz±hematite, anhydrite
	1277-1286	Quartz
	1289-1310	Quartz±chlorite±calcite
	1325-1433	Quartz±chlorite
	1490-1544	Quartz (drusy)±chlorite
	1580-1598	Quartz+pyrite
	1628-1670	Quartz+pyrite
	1676-1678	Anhydrite±(quartz+pyroxene+pyrite), illite
	1766-1850	Quartz+chlorite±pyrite

Well	Depth (m)	Vein (or vesicles) fillings
LHD-27	126	Quartz
	327-351	Quartz
	426-474	Quartz
	576	Smectite
	600	Quartz+chlorite
	876	Quartz+chlorite
	900	Quartz
	999	Quartz+chlorite
	1050	Quartz+chlorite
	1101	Quartz
	1125	Quartz
	1742-1748	Quartz, titanite
LHD-32	483-519	Quartz, clay
	645-648	Quartz
	891-894	Quartz (drusy)
	1074-1215	Quartz±chlorite±chalcopyrite
	1224-1230	Quartz+chlorite
	1350-1704	Quartz±chlorite
	1773-1806	Quartz+chlorite
	1974-2130	Quartz±chlorite

The most common vein association is quartz ± chlorite ± (pyrite/chalcopyrite) ± calcite ± hematite. The main composition of this association is quartz ± chlorite, whereas pyrite/chalcopyrite, calcite, and hematite are minor (Table 4.2). In LHD-26, the distribution of quartz only and quartz ± chlorite is random. On the other hand, quartz ± chlorite is present in LHD-27 within the range of 600-1050 m (190 masl – 213 mbsl) depth. Quartz(only)-filled veins are present above and below these depths. In LHD-32, quartz is present as monomineralic filling vein in the upper part of the well, down to 1000 m or 170 mbsl. Quartz±chlorite is present downward from this depth. At some particular depths, this association shows a drusy texture on the quartz (Table 4.2).

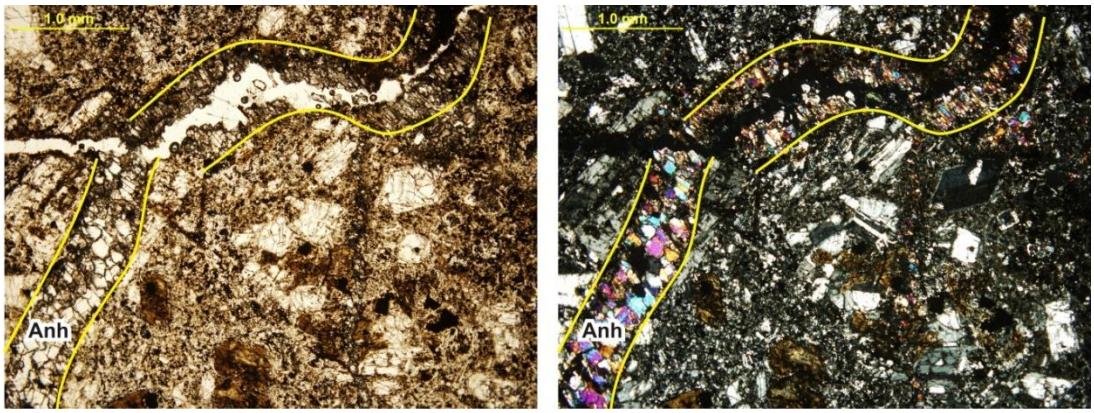

Figure 4.21. Petrographic images of anhydrite±(quartz±pyrite±pyroxene) vein in LHD-26/1676-1678 m. Left-hand panel is the plane polarised of the right-hand panel. Petrographic microscopy can only identify anhydrite (Anh) in the vein. Identification of quartz, pyrite, and pyrite has been done through BSE-EDS. The vein shows mosaic texture of filling. The open crack was formed after the anhydrite-filled vein resulting in brecciation of the upper part of the anhydrite-filled vein.

4.2. Wairakei Geothermal System

4.2.1. Petrography of the Waiora Valley Andesite (WVA)

The part of this research on the Wairakei geothermal system is confined to the Waiora Valley Andesite (WVA), as sampled in boreholes WK-47, WK-48, WK-54, and WK-122. The WVA is characterised by a porphyritic texture which is still clearly visible under the petrographic microscope (Appendix D). The phenocryst assemblage in WVA samples consist predominantly of plagioclase with a minor amount of pyroxene. Hornblende, magnetite, and apatite are present as accessory minerals. Glomerocrysts of plagioclase and plagioclase+pyroxene are also present (Fig. 4.22). These characteristics are consistent with the description of WVA by Sanders et al. (2013). A type of coarse sieve-textured plagioclase (Fig. 4.23), which is pointed out by Sanders et al. (2013) as one of the characteristic features of the WVA, is also present in WK-54 and WK-122 samples (Appendix D).

The andesite sample from WK-122 shows a strongly-developed flow banding texture (Fig. 4.23). Similarly, WK-47 andesite shows a trachytic texture at 628 m depth, which is taken as indicating that the rock represents a lava flow (MacKenzie et al., 1982). The characteristics of the WVA shown by the samples are consistent with Sanders et al.'s (2013) interpretation of the origin of the WVA as a lava body.

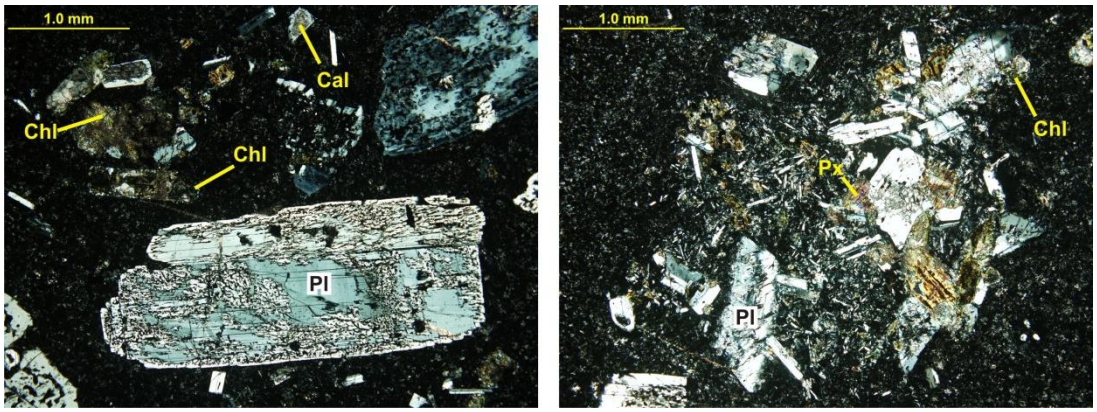

Figure 4.22. Characteristics of the WVA. Left-hand panel: coarse plagioclase crystals (Pl) with strongly-developed sieve texture. Smaller plagioclase has been replaced by calcite (Cal). Chlorite (Chl) has replaced pyroxene. Right-hand panel: glomerocrysts of plagioclase (Pl) + pyroxene (Px). The pyroxene has been partially replaced by chlorite (Chl).

Figure 4.23. Flow banding texture of andesite at WK-122/584 m.

4.2.2. Hydrothermal Alteration of the WVA

Petrographic, SWIR and BSE-EDS analyses have been done on Wairakei samples (detailed descriptions in Appendix C, D, and E). Most of the samples used in this thesis were taken in a certain interval depending on the thickness of the WVA succession in each well (Table 4.3, 4.4, 4.5, and 4.6), except where thin sections or polished thin sections were provided by GNS Science.

The shallow part of the WVA succession in WK-47, 570-622 m, was replaced by smectite, interlayered illite-smectite, and chlorite (Table 4.3). At a greater depth, WK-47/628 m shows a replacement by chlorite, quartz, calcite, wairakite, albite, adularia, Fe-oxide, natrolite(?), interlayered illite-smectite under petrographic and BSE-EDS examination. Below 628 m depth, quartz and titanite are present as replacement minerals (Table 4.3).

Table 4.3. Hydrothermal minerals found in the WVA of WK-47: results from SWIR (Appendix C), petrographic observation (Appendix D), and BSE-EDS (Appendix E). Results are reported at 9-m-intervals, except marked.

Depth (m)	Replacement minerals	Vein- (or vesicle-) fillings
570*	smectite	-
576	smectite	-
585	interlayered illite-smectite	-
594	chlorite, interlayered illite-smectite	-
613	chlorite, interlayered illite-smectite	-
622	chlorite, interlayered illite-smectite	-
628**	chlorite, quartz, calcite, wairakite, albite, adularia, Fe-oxide, natrolite(?), interlayered illite-smectite	calcite and clay minerals
631	chlorite, quartz, interlayered illite-smectite, titanite	-
640	chlorite, interlayered illite-smectite	-
649	chlorite, quartz, interlayered illite-smectite, titanite	-
658	chlorite, quartz, interlayered illite-smectite, titanite	-

* top of the succession

** polished thin section is available

Compared to WK-47, replacement minerals of WK-48 are more varied (Table 4.4). The WVA succession encountered in the latter well has been mainly altered to interlayered illite-smectite, illite, chlorite, calcite, quartz, and titanite. Epidote is present at 582 and 608 m depth, coexisting with leucoxene. Adularia occurs at 573 and 608 m depths. Albite is also found replacing the WVA at 518, and 608 m. Pyrite is present at 555, 582, and 608 m depths in WK-48. The only sample showing zeolite replacement in WK-48 is the sample at 582 m depth.

Table 4.4. Hydrothermal minerals found in the WVA of WK-48: results from SWIR (Appendix C), petrographic observation (Appendix D), and BSE-EDS (Appendix E). Results are reported at 18-m-intervals, except marked.

Depth (m)	Replacement minerals	Vein- (or vesicle-) fillings
515*	smectite	-
518	illite, quartz, chlorite, titanite, albite	-
536	chlorite, interlayered illite-smectite	-
555	illite, quartz, chlorite, titanite, albite, pyrite	-
573	chlorite, interlayered illite-smectite, quartz, adularia, titanite	-
582**	chlorite, clay minerals, epidote, calcite, zeolite, pyrite , leucoxene	calcite
591	chlorite, illite, quartz	-
608**	calcite, interlayered illite-smectite, chlorite , adularia, epidote, albite, leucoxene, pyrite, titanite	wairakite , calcite, wairakite+chlorite
610***	calcite, clay minerals, chlorite, quartz	calcite, quartz+clay minerals, wairakite
628	chlorite, illite, quartz, calcite, interlayered illite-chlorite, titanite	calcite
646	chlorite, illite, quartz, calcite, interlayered illite-chlorite, titanite	-
664	chlorite, illite	-
683	chlorite, illite, quartz, albite, titanite	quartz+calcite+chlorite

* top of the succession

** thin section is available

*** polished thin section is available

It is apparent that the hydrothermal alteration processes undergone by WVA samples in WK-54 are homogenous based on the petrographic mineralogical identification, SWIR, and BSE-EDS analyses (Table 4.5). The replacement minerals present at each depth are almost identical. The WVA of WK-54 has been replaced mainly by chlorite and interlayered illite-smectite. Quartz, titanite, calcite, and pyrite are present in samples at 600 m, 610 m, 619 m, and 628 m depths in WK-54. Samples at these four depths have been investigated using petrography, SWIR, and BSE-EDS analysis, while samples from the other depths have been passed only through SWIR. SWIR is not able to detect as many minerals as petrography and BSE-EDS. Thus, it is possible that quartz, titanite, calcite, and pyrite may also be present at other depths, but are not detected due to the limitations of the methods.

Table 4.5. Hydrothermal minerals found in the WVA of WK-54: results from SWIR (Appendix C), petrographic observation (Appendix D), and BSE-EDS (Appendix E). Results are reported at 3-m-intervals.

Depth (m)	Replacement minerals	Vein- (or vesicle-) fillings
597	chlorite, interlayered illite-smectite	-
600	chlorite, illite, quartz, pyrophillite(?), titanite	quartz
604	chlorite, interlayered illite-smectite	-
607	chlorite, interlayered illite-smectite	-
610	illite, calcite, quartz, chlorite, titanite, pyrite, hematite, prehnite	-
613	chlorite, interlayered illite-smectite	-
616	chlorite, interlayered illite-smectite	-
619	chlorite, illite, quartz, calcite, titanite	-
622	chlorite, interlayered illite-smectite	-
625	chlorite, interlayered illite-smectite	-
628	chlorite, illite, quartz, calcite, titanite, pyrite	-
631	chlorite, interlayered illite-smectite	-

There were only three samples available from WK-122 for this work. The first sample is WK-122/580.5 m, showing a replacement assemblage of clay minerals, chlorite, calcite, albite, and epidote. Beneath this depth, WK-122/584.1 m has been altered to calcite, clay minerals, albite, and epidote with the absence of chlorite. The deepest sample of WK-122 is the core cut at 584.4 m. Petrography and BSE-EDS results show that the host rock in this sample has been replaced by illite, calcite, chlorite, quartz, and titanite.

Table 4.6. Hydrothermal minerals found in the WVA of WK-122: results from petrographic observation (Appendix D), and BSE-EDS (Appendix E).

Depth (m)	Replacement minerals	Vein- (or vesicle-) fillings
580.5	clay minerals, chlorite, calcite, albite, epidote	quartz±calcite±chlorite±pyrite
584.1	calcite, clay minerals, chlorite, adularia	quartz, calcite
584.4	illite, calcite, chlorite, quartz, titanite	calcite

Comparing all the mineralogical identification results from WK-47, WK-48, WK-54, and WK-122, it is apparent that all the WVA samples studied in this research show a number of

veins and vesicles (Table 4.3, 4.4, 4.5, and 4.6). Most of these open spaces have been filled by hydrothermal minerals. In general, the vein fillings minerals in the WVA can be grouped into four associations. The first association or 'event' is abundant calcite which is present in all the samples, except WK-54. The second association is wairakite±chlorite (Fig. 4.24). This association is only found in samples from WK-48 (Table 4.4). The third association is quartz±clay minerals, found in WK-48/610 m, WK-54/600, and WK-122/584.1 m. Clay-filled veins present in WK-47/628 m may also be part of the third association. The last association is quartz ± calcite ± chlorite ± pyrite veins, found in WK-48/683 m and WK-122/580.5 m. There are no cross-cutting relationships visible between these associations in the samples examined and therefore, the sequence of hydrothermal alteration episodes is difficult to establish. The shape of the quartz ± calcite ± chlorite ± pyrite veins show that the veins were formed by hydraulic fracturing processes (Fig. 4.24D).

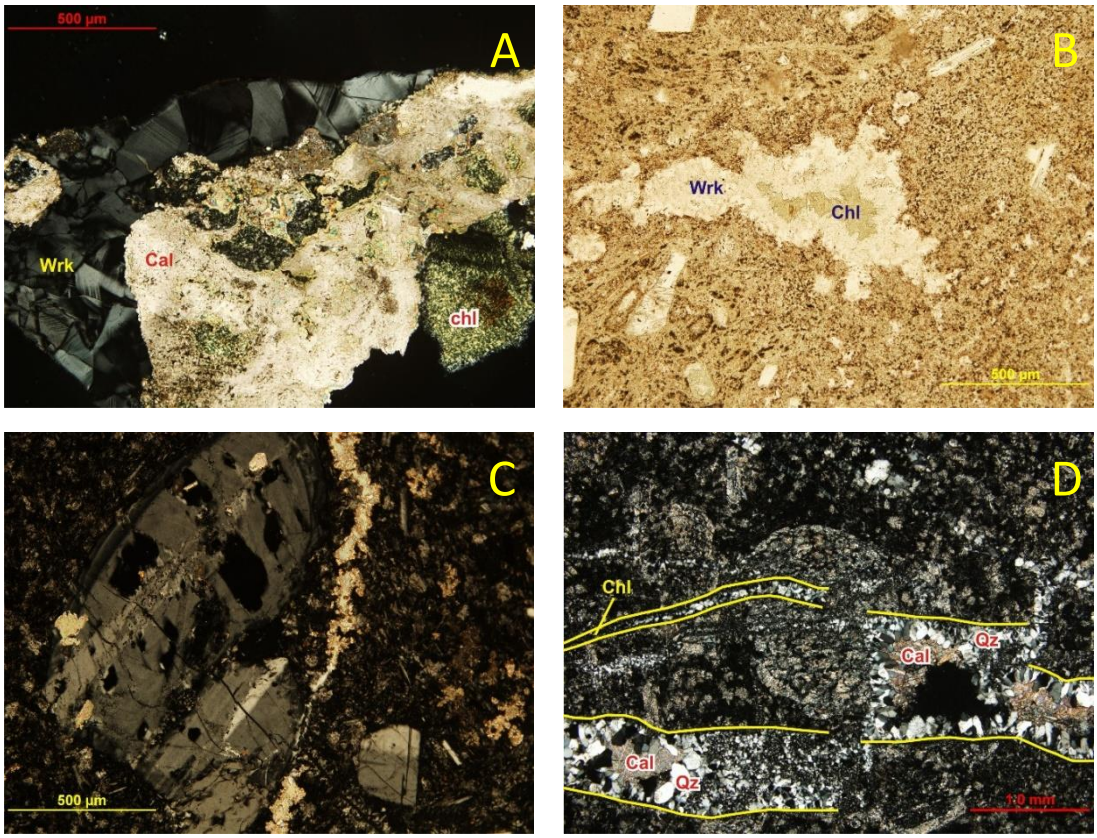

Figure 4.24. Vein (or vesicle) filling minerals in the WVA: wairakite at WK-48/610 m (A), wairakite+chlorite at WK-48/608 m (B), calcite at WK-48/582 m (C), and quartz±calcite±chlorite at WK-122/580 m (D). Wrk: wairakite; Cal: calcite; Chl: chlorite, Qz: quartz.

4.3. Andesite Textures

One of the purposes of this thesis is to understand the role of rock textures on controlling the processes of hydrothermal alteration, with a specific case of andesite lithologies. Petrological analyses of the samples have been done through binocular observation, petrography, and BSE-EDS. It is known from the analyses that all the andesitic volcanic rocks studied in this research show a porphyritic texture. The phenocrysts are mostly plagioclase, pyroxene, hornblende (only in Wairakei samples), and magnetite (or Ti-rich magnetite in Tompaso samples). In general, plagioclase is less altered when compared to ferromagnesian minerals, including pyroxene and hornblende (Fig. 4.25). Except for cryptocrystalline material, the groundmass consists of generally the same minerals as the phenocrysts but in smaller size.

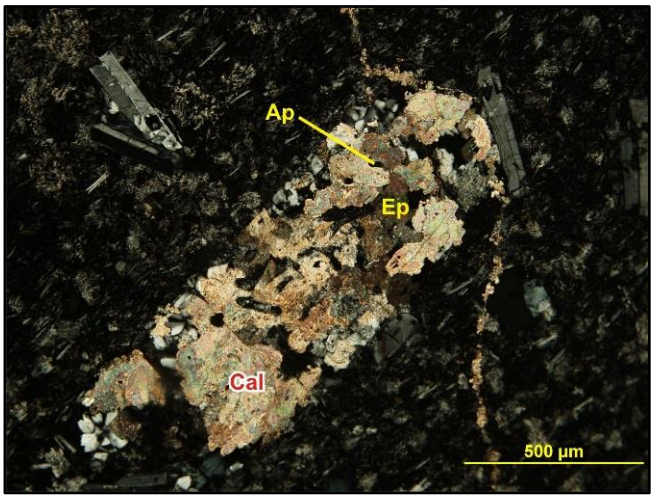

Figure 4.25. Pyroxene has been altered more intensely than plagioclase (upper left). Pyroxene, showing apatite (Ap) inclusion, has been replaced by calcite (Cal) and epidote (Ep). Sample of WK-48/582-583 m.

Chemical composition appears to determine the preferences of hydrothermal alteration processes. However, there is an inconsistency shown by zoned plagioclase. Zoning in plagioclase is formed by changes in composition from core to rim (MacKenzie et al., 1982). A few samples show that zoning in plagioclase results in the zoning of alteration. For example, in WK-47/628 m, the zoned plagioclase is fresh at the rim and altered to chlorite at the core (Fig. 4.26). The WK-122/584.4 m sample also shows that the inner zone of the zoned plagioclase has been altered to calcite and quartz whilst the outer zone remains fresh (Fig.4.26). In contrast, zoned plagioclase in WK-54/610 m is still fresh when other plagioclase has been partially replaced by calcite (Fig.4.26). It is unclear if the cause of the fresh plagioclase minerals is they are present as a monomineralic glomerocryst or other factors. This sample is available in non-polished this section and therefore a qualitative

chemical analysis (EDS) cannot be performed to confirm the composition of the zoned plagioclase.

Crystal size does not affect the preferences, where phenocrysts can be less altered than groundmass in some samples and the opposite at other samples. The phenocrysts are commonly more altered than groundmass since they have been fractured, although not always. There are other textural features found in the samples, including sieve textures in plagioclase and glomerocrysts. In addition, flow-banding and trachytic textures are also present in some samples. All of these components, except the trachytic texture, are observed to affect the pattern of hydrothermal alteration in certain ways which is discussed later in the text.

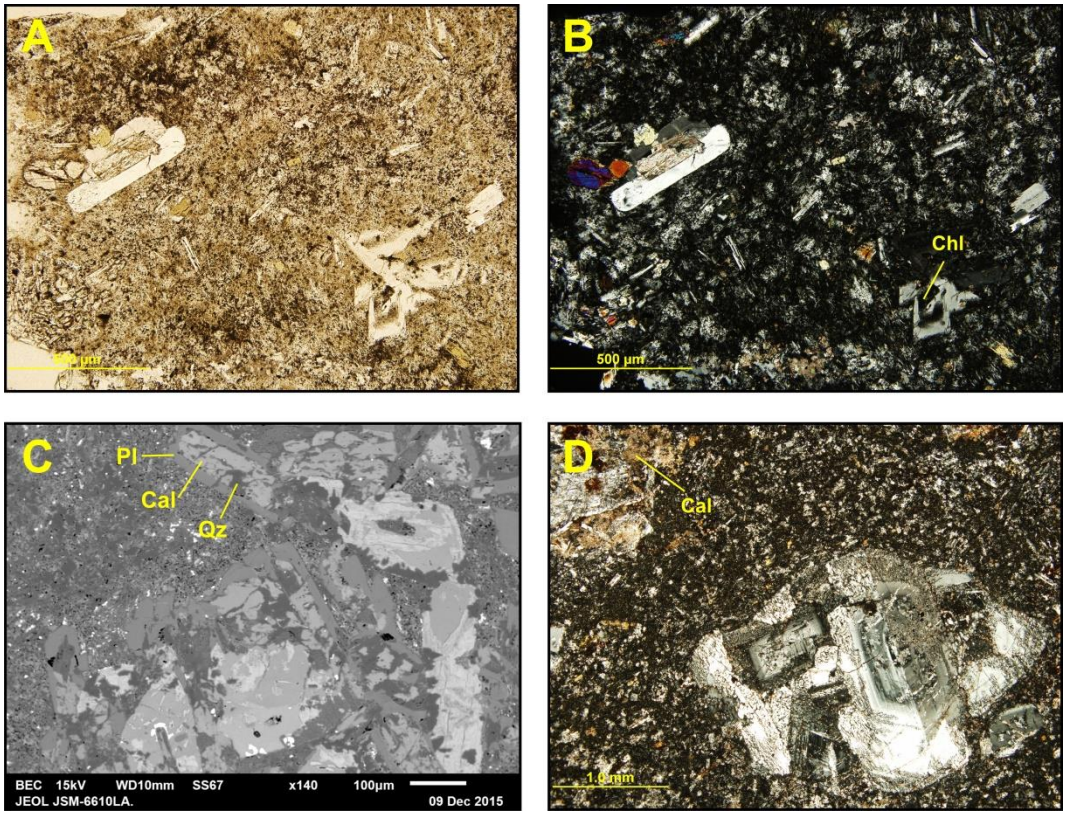

Figure 4.26. A (PPL) and B (XPL): chlorite (Chl) replacement of the inner zoned-plagioclase in WK-47/628 m sample. C (BSE-EDS): replacement of the inner zoned plagioclase by calcite (Cal) and quartz (Qz). D (XPL): zoned plagioclase minerals do not show variation of hydrothermal alteration to the zoning, while the other plagioclase has been partially replaced by calcite (Cal).

4.3.1. Sieved-plagioclase

Sieved-plagioclase is common in Wairakei samples and found in some Tompaso samples (Table 4.7). Sieve-textured plagioclase differs from other plagioclase by containing

abundant small, interconnected, box-shaped glass inclusions. The presence of glass inclusions gives a porous appearance of the plagioclase (MacKenzie et al., 1982). The texture may be formed due to mineral instability during magma mixing, rapid decompression of magma, or both (Nelson & Montana, 1992). Observations on sieved-plagioclases show that the zones rich in glass inclusions are general more altered than the rest of the crystal.

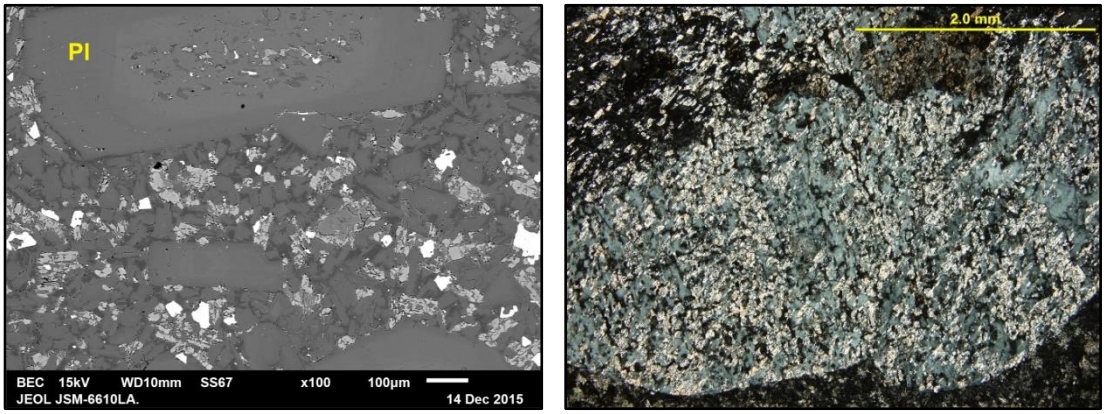

Figure 4.27. Sieved-texture on plagioclase (Pl) shown by the presence of glass inclusions creating a broken appearance. Sieved-plagioclase shows higher alteration intensity than non-sieved-plagioclase. Left: BSE image of LHD-26/1064, where glass inclusions have been replaced by chlorite. Right: crossed polarised image of WK-122/580.1 m, glass inclusions have been replaced by calcite.

Table 4.7. The occurrence of sieved-plagioclase in Wairakei and Tompaso samples (from Appendix D and E).

No.	Well ID/depth
1.	LHD-26/1064-1067 m
2.	LHD-26/1841-1844 m
3.	LHD-32/351-354 m
4.	LHD-32/483-486 m
5.	LHD-32/693-696 m
6.	LHD-32/1410-1413 m
7.	LHD-32/2000 m
8.	WK-47/628 m
9.	WK-48/582-583 m

No.	Well ID/depth
10.	WK-48/608-609 m
11.	WK-48/610 m
12.	WK-48/628 m
13.	WK-48/646 m
14.	WK-54/610-613 m
15.	WK-122/580.5 m
16.	WK-122/584.1 m
17.	WK-122/584.4 m

In LHD26/1064 for example, the sieved-texture has been replaced by chlorite while the rest of the crystal remains fresh. Another example is WK-122/580.1 m where the sieved-texture has been altered to calcite while the rest of the crystal is still fresh (Fig. 4.27) (detail description in Appendix E). Since glass inclusions react more quickly, the presence of these inclusions increase the surface for chemical exchange of the sieved plagioclase. Increasing the intensity of glass inclusions (i.e. increasing the intensity of sieve texture) corresponds to the increase of hydrothermal alteration precipitation within the sieved plagioclase.

4.3.2. Glomerocrysts

A glomerocryst is an aggregate of phenocrysts. Some petrologists use the term glomerocryst to refer a monomineralic aggregate only and use the term cumulocryst to refer a polymineralic aggregate (MacKenzie et al., 1982). However, both monomineralic and polymineralic aggregates of phenocrysts are labelled as glomerocrysts in this thesis. Three kinds of glomerocrysts are observed in Tompaso and Wairakei samples. There are glomerocrysts of plagioclase, [plagioclase+pyroxene (Pl+Px)], and [plagioclase+pyroxene +magnetite/ilmenite (Pl+Px+Mag/Ilm)] (Table 4.8).

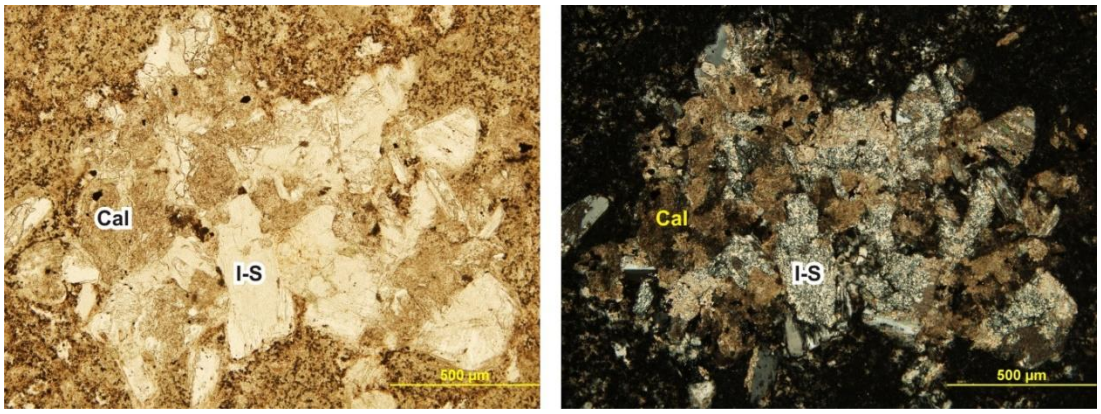

Figure 4.28. A glomerocryst of plagioclase and pyroxene (WK-48/608-609 m). Plagioclase has been replaced by clays, probably interlayered illite-smectite (I-S). Pyroxene has been replaced by calcite (Cal).

Table 4.8. The type of glomerocrysts present in Wairakei and Tompaso samples (from Appendix D and E).

No.	Well ID/depth	Minerals
1.	LHD-26/635-638 m	Pl
2.	LHD-32/525-528 m	Pl+Px+Mag/Ilm
3.	WK-47/628 m	Pl+Px
4.	WK-47/631 m	Pl+Px
5.	WK-47/649 m	Pl+Px
6.	WK-47/658 m	Pl+Px
7.	WK-48/582-583 m	Pl+Px

No.	Well ID/depth	Minerals
8.	WK-48/608-609 m	Pl ; Pl+Px
9.	WK-48/610 m	Pl+Px
10.	WK-54/610-613 m	Pl ; Pl+Px
11.	WK-122/580.5 m	Pl ; Pl+Px
12.	WK-122/584.1 m	Pl
13.	WK-122/584.4 m	Pl ; Pl+Px

In the same sample, plagioclase glomerocrysts show a similar IA as plagioclase single minerals. On the other hand, glomerocrysts of [Pl+Px] appear to have a higher IA than their constituent minerals where isolated (Fig. 4.28) (detail descriptions in Appendix D and E). The difference of IA is not much significant in pyroxene, though pyroxene in the [Pl+Px] glomerocrysts is slightly more altered. In contrast, plagioclase often remains fresh as a single mineral while it is altered in [Pl+Px] glomerocrysts. The same alteration patterns of plagioclase and pyroxene occur with [Pl+Px+Mag/Ilm] glomerocrysts where magnetite/ilmenite remains fresh. It is apparent that interlocking/aggregation with pyroxene makes the plagioclase become less stable and easier to be replaced.

4.3.3. Flow-banding

Flow-banding texture is present in WK-122/584.4 m andesite lava. The arrangement of mineral composition and/or size in this sample does not represent a function of the flow-banding. Instead, the banding is likely created by shearing processes during the lava emplacement. The distribution of replacement minerals in this rock corresponds to the flow-banding as it can be seen from the cut core (Fig. 4.24). However, the banding is not visible in BSE-EDS imaging.

4.3.4. Trachytic texture

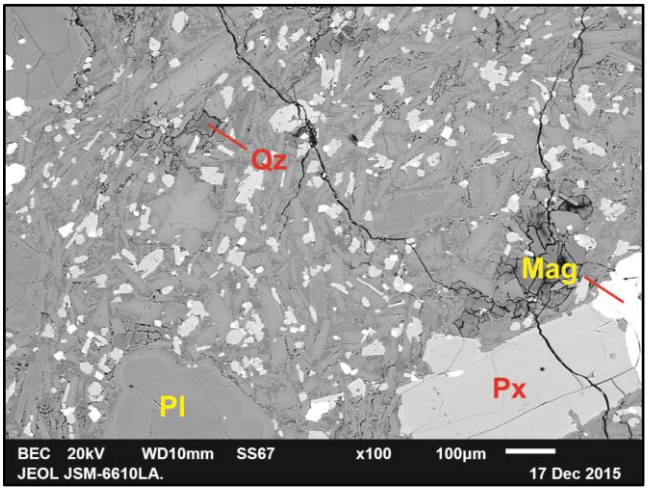

Figure 4.29. Trachytic texture of LHD-27/501 m. Plagioclase (Pl), pyroxene (Px), and magnetite/ilmenite (Mag) are generally still fresh. Groundmass has been partially replaced by quartz (Qz).

Table 4.9. The occurrence of trachytic texture in Wairakei and Tompaso samples (from Appendix D and E).

No.	Well ID/depth
1.	LHD-27/464-467 m
2.	LHD-27/450 m
3.	LHD-27/501 m
4.	LHD-27/675 m
5.	LHD-27/774 m
6.	LHD-27/825 m
7.	LHD-32/891-894 m

No.	Well ID/depth
8.	WK-47/628 m
9.	WK-47/631 m
10.	WK-48/582-583 m
11.	WK-48/591 m
12.	WK-48/613 m
13.	WK-48/646 m
14.	WK-54/600 m

Trachytic texture is characterized by a subparallel arrangement of microcrystalline plagioclase laths in the groundmass (MacKenzie et al., 1982). This texture is typical of lava. In Tompaso and Wairakei, trachytic texture is common (Table 4.9). However, in terms of distribution of hydrothermal alteration products, it is apparent that this texture does not control the hydrothermal alteration processes. The distribution of hydrothermal alteration minerals is patchy showing no correlation with the trachytic texture (Fig. 4.29).

4.3.5. *Welded texture*

Welded texture is present in LHD-27/1742-1748 m. The rock is an andesite breccia containing abundant fiamme (Fig. 4.30). Fiamme are glassy lenses with flame-like shapes in welded pyroclastic deposits; the alignment of fiamme defines the foliation in welded pyroclastic deposits (McPhie et al., 1993). Volcanic glass is likely to be the least resistant volcanic product to hydrothermal alteration processes and likely to be the first component to be replaced, as shown by the andesite breccia sample. In this sample, fiamme have been altered more intensely than the rest of the rock. As the fiamme are aligned in a long dimension in the rock, it seems that the hydrothermal alteration processes follow the rock texture. Even though this texture is present in pyroclastic breccia (i.e. not related to the focus of the study – which is andesite lithologies) and also the relationship between this rock and the rest of the LHD-27 succession is unknown because there is no sample available due to loss of circulation, this sample also demonstrates that texture influences the distribution of hydrothermal minerals in the rock.

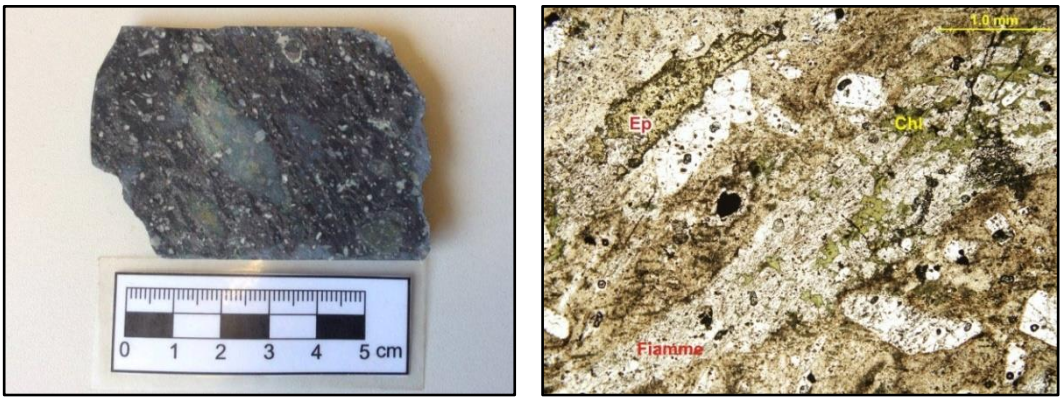

Figure 4.30. Welded texture at 1742-1748 m depth: hand sample (left) plan polarised thin section (right).

CHAPTER FIVE

DISCUSSION

This chapter discusses in three different sections the results presented in chapter 4. The first section revises the geological setting of Tompaso area, by comparing what has been known from previous works to what is observed from this work. The second section discusses the permeability control, the hydrological, and the thermal setting of the Tompaso geothermal system. The last section discusses the distribution of hydrothermal alteration products with respect to andesite textural characteristics.

5.1. Update on Geological Setting of Tompaso Area

The subsurface geology of the Tompaso area consists of Tuff B unit, Rhyolite unit, Andesite B unit, Pitchstone unit, Pyroclastic Breccia unit,Andesite A unit, Pumice unit, and Tuff A unit (section 4.1.1). Considering the regional geology of the area (section 2.1.2), the basement rock of Tompaso area is a succession of intermediate to basaltic composition lavas, andesite breccia, and welded tuff with inter-bedded sedimentary layers, labelled as Pre-Tondano Formation. Prasetyo et al. (2015) suggested that the lithology of Tompaso from about sea level down to the deepest lithology penetrated in the wells is Pre-Tondano Formation. However, in this work, this depth correlates to Pyroclastic Breccia, Pitchstone, Andesite B, and Tuff B unit (section 4.1.1) (Fig. 5.1). The Andesite B unit is a succession of andesite lava. Welded tuff is found only at 1750 m depth in LHD-27, within the Tuff B unit. Inter-bedded sedimentary layers are not present in any of these units. As there is not enough evidence, the correlation of the Tuff B – Andesite B – Pitchstone – Pyroclastic Breccia units to the Pre-Tondano Formation is unknown.

Regional geology of Tompaso area appears to be predominantly influenced by the products of Tondano Caldera forming eruption, labelled as Tondano Tuff Formation. Therefore, these products have been used as an age marker for the stratigraphy of the area (section 2.1.2). Tondano Tuff Formation has been widely accepted to cover the most of northern part of North Sulawesi. However, there has not been age dating or chemical analysis on the

composition of this formation. Lecuyer et al. (1997) mentioned that this formation consists of two members: white rhyodacitic ignimbrites and the younger, more localised grey dacitic ignimbrites. Ganda & Sunaryo (1982) agreed that Tondano Tuff Formation has, at least, dacitic composition or even more silicic. In contrast, some other workers argued that this formation has an andesitic composition (Bachri, 1977; Kavalieris et al., 1992; Effendi & Bawono, 1997).

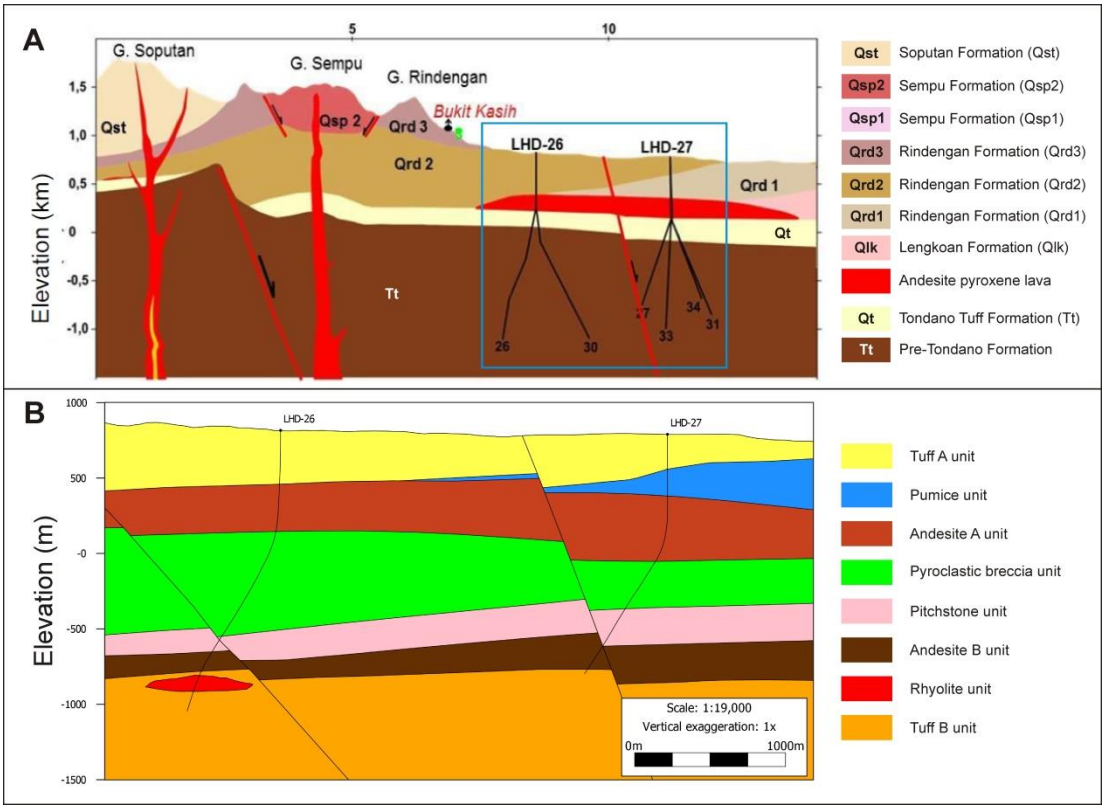

Figure 5.1. (A) Cross section of Tompaso subsurface geology inferred by Prasetyo et al. (2015), following surface formation naming (Fig. 5.2). Basement rock is Pre-Tondano Formation. (B) Cross section of Tompaso subsurface geology inferred in this thesis. The extent of cross section B is marked in blue outline in cross section A. Location of the cross section to the rest of model is in Fig. 5.2.

In the subsurface geological model by Prasetyo et al. (2015), Tondano Tuff Formation overlies Pre-Tondano Formation. However, Prasetyo et al. (2015) did not mentioned the composition of the formation, i.e., whether it is dacitic, andesitic, or something else. Considering caldera-forming eruptions are normally silicic in composition, there is no indication of this formation present in the cuttings from three studied wells.The only silicic volcanic lithology found in this thesis is Pitchstone unit. However, this unit is more comparable to Lengkoan Formation than Tondano Tuff Formation (section 5.1.1).

The Tondano Tuff in the Prasetyo et al. (2015) model is overlain by an andesite pyroxene lava unit (Fig. 5.1(A)). This lava unit is at the same depth as Andesite A unit inferred in this thesis. The Andesite A unit consists of andesite pyroxene lava with magnetite/ilmenite

accessory mineral. It is apparent that the andesite pyroxene lava in Prasetyo et al. (2015) has the same mineralogy as the Andesite A unit in this thesis. However, age dating needs to be done for future research to understand the relationships of this unit to the rest of the regional stratigraphy. The andesite pyroxene lava in Prasetyo et al. (2015) is older than Lengkoan Formation. On the other hand, if the Pitchstone unit inferred in this thesis correlates to the Lengkoan Formation, the andesite pyroxene lava should be younger than Lengkoan Formation.

Near the surface, the distribution of Pumice and Tuff A units in this work are similar to Rindengan Formation 1 and Rindengan Formation 2 in the Prasetyo et al. (2015) model, respectively. However, the correlation cannot be made because the age of the Pumice and Tuff A units are unknown. As no age dating has been undertaken in this thesis, the subsurface stratigraphy from this work is not compared to the formation division at the surface, even though the distribution of some units agrees with the regional geology at the surface.

The Tompaso area is controlled by predominantly NE-SW and NNE-SSW fault trends (section 2.1.1) (Fig. 5.2). Due to availability of subsurface data, the 3D model built in this thesis only covers the area in the vicinity of LHD-26, LHD-27, and LHD-32. One of the NE-SW faults able to be included in the 3D model is the Tempang Fault (Fig. 5.2) which has also been discussed by Prasetyo et al. (2015). Even though this fault has been accepted to exist, it is not represented in the wells studied (section 5.2.1). Besides the Tempang Fault, there is another fault proposed in this work (labelled as A-A' fault) (section 5.1.2)

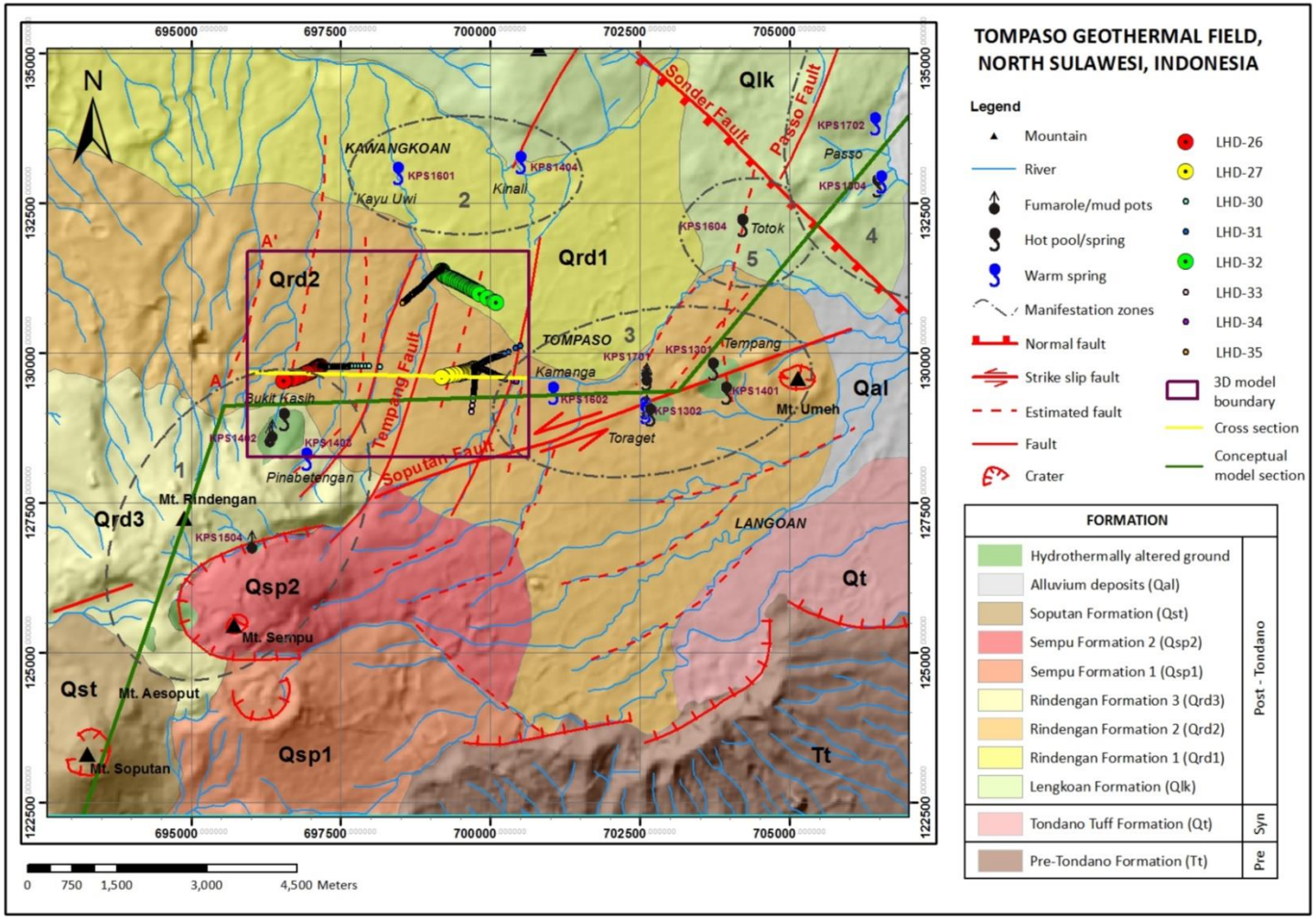

Figure 5.2. The extent of the subsurface geological model (Fig. 4.3; Fig. 5.3) is restricted to the availability of samples (drilling wells – purple outline). The proposed A-A' fault is the western end fault within the model boundary. Yellow line represents the cross section in Fig. 5.1(B). Green line represents the conceptual model section in Fig. 5.7.

5.1.1. Pitchstone occurrences and silicic volcanic activity in Tompaso

Pitchstone unit in Tompaso system consists of pitchstone lava (only present in LHD-32) and pitchstone-rich pyroclastic breccia (section 4.1.1.5). This unit is thickest in LHD-32 and thinnest in LHD-26. Due to the constraint of availability of the samples, the distribution of this unit outside of the modelled area is unknown. However, as the lithology of this unit in LHD-32 has the characteristics of a lava, it is likely that the Pitchstone unit is a lava dome with its centre located at around LHD-32.

The BSE-EDS results show that the rock consists predominantly of volcanic glass with minor crystals. Pitchstone differs from obsidian by its lustre. However, both rocks are formed of volcanic glass. Glassy volcanic rocks (i.e. obsidian/pitchstone) are mostly of rhyolitic composition (McPhie et al., 1993; Sigurdsson et al., 2000). In agreement with that, the EPMA results show that the SiO_2 content of the Pitchstone unit is in the range of rhyolitic composition (section 4.1.1.5). Therefore, the occurrence of pitchstone in Tompaso is unusual since Tompaso is generally an andesitic volcanic setting. In Tompaso regional geology, Lengkoan Formation is the most similar lithology to the Pitchstone unit, but their correlation cannot be confirmed without age dating.

Another silicic unit present in Tompaso is the Rhyolite unit (section 4.1.1.8). Even though this unit is only present in LHD-26 with only 85-m thick, the occurrence of this unit is in agreement with the Pitchstone unit showing that there is a rhyolitic activity in Tompaso area. The Tompaso area has been inferred to lie on the Tondano Caldera depression. However, the dimension of the Pitchstone and Rhyolite units do not represent sufficient vollumes of rhyolitic magma to have supplied the Tondano Caldera forming eruptions.

Both Pitchstone and Rhyolite units are inferred to be lavas (sections 4.1.1.5, 4.1.1.8). Thus, the source of the magma should be directly below where the units are present. Considering the dimension of both rock units, it is likely that the source is a shallow magma chamber. In volcanic arc system such as Tompaso, the volcanic activity is generally driven by andesitic magma systems which commonly initiate at a great depth. Consequently, the coalescence of magma is not always able to reach the surface and, instead, would be accumulated in shallow magma chambers in which fractionation crystallization and differentiation take place. As a result, the shallow magma chamber contains relatively more evolved magma (i.e. more silicic composition) compared to the deep andesitic magma chamber. The Pitchstone and Rhyolite units are thought to form by this mechanism. This is only one

possible paragenesis of the Pitchstone and Rhyolite units. More data, especially from the extended modelled area, is needed to understand the rhyolitic volcanic activity in Tompaso.

5.1.2. A-A' fault

The presence of the A-A' fault has been inferred from the hydrothermal mineralogy present in LHD-26. This work does not propose a new fault, but a subsurface continuation of the existing surface lineament (Fig. 5.2) and its possible role in the hydrology of Tompaso geothermal system.

Hydrothermal mineralogy present in LHD-26 which includes hematite and anhydrite suggests the possibility of a fault. In this well, hematite is found sparsely down to 1700 m depth, but the deepest intense hematite-replacement occurs at 1500 m depth (Appendix B). The formation of hematite in LHD-26 suggests there is a circulation of oxydising water in the upper part of LHD-26. Hematite could also be formed by weathering process as well as oxidation of lava during its emplacement due to reaction with meteoric water. In LHD-36, hematite is present in various lithologies, including pyroclastic rocks. In addition, there is no paleosol found in LHD-26 samples. Therefore, it is considered that hematite was not formed by either oxidation of lava or weathering processes. It may, thus, suggest that cooler oxidising water is present in this part of the geothermal system.

The deepest occurrence of hematite coincides with the shallowest occurrence of anhydrite (section 4.1.3.2). Anhydrite has been formed abundantly at 1675 m depth (Appendix D and E). In geothermal systems, anhydrite is an indicator mineral of a neutralisation process of acid fluids because of its reverse solubility with respect to temperature. There are three mechanisms likely to form anhydrite in geothermal systems. The first mechanism occurs at near surface where acid sulfate waters percolate rapidly downward and then mix with more neutral pH fluids or become neutralised through reactions with country rocks. The second mechanism involves an introduction of rising SO_2-rich magmatic fluids, which is observed in Philippines geothermal systems and also at Karaha-Telaga Bodas geothermal system in Indonesia (Reyes et al., 1993; Moore et al., 2002). The third mechanism is an oxidation process of deep degassing H_2S to form anhydrite at depth as mainly observed in New Zealand geothermal systems (Robinson, 1985; Marini et al., 2011). The only way to truly identify the origin of the anhydrite is via sulfur isotope analyses (Robinson, 1985; Marini et al., 2011). However, in this study, the presence of anhydrite justaposed with

hematite in LHD-26 favours downward circulating slighty acidic sulfate water at 1675 m depth.

The present-day temperature recorded in LHD-35 shows that the meteoric water-dominated zone extends to the east and likely ends to the west of Tempang Fault. It is likely that there is a structure controlling the circulation of cooler oxidising water in this part of the system. This observation leads to a hypothesis of a fault being present, here is named as the A-A' fault. This fault may act as an aquifer for cooler oxidising slighty acid sulfate-rich fluid resulting in the precipitation of a hematite-anhydrite front.

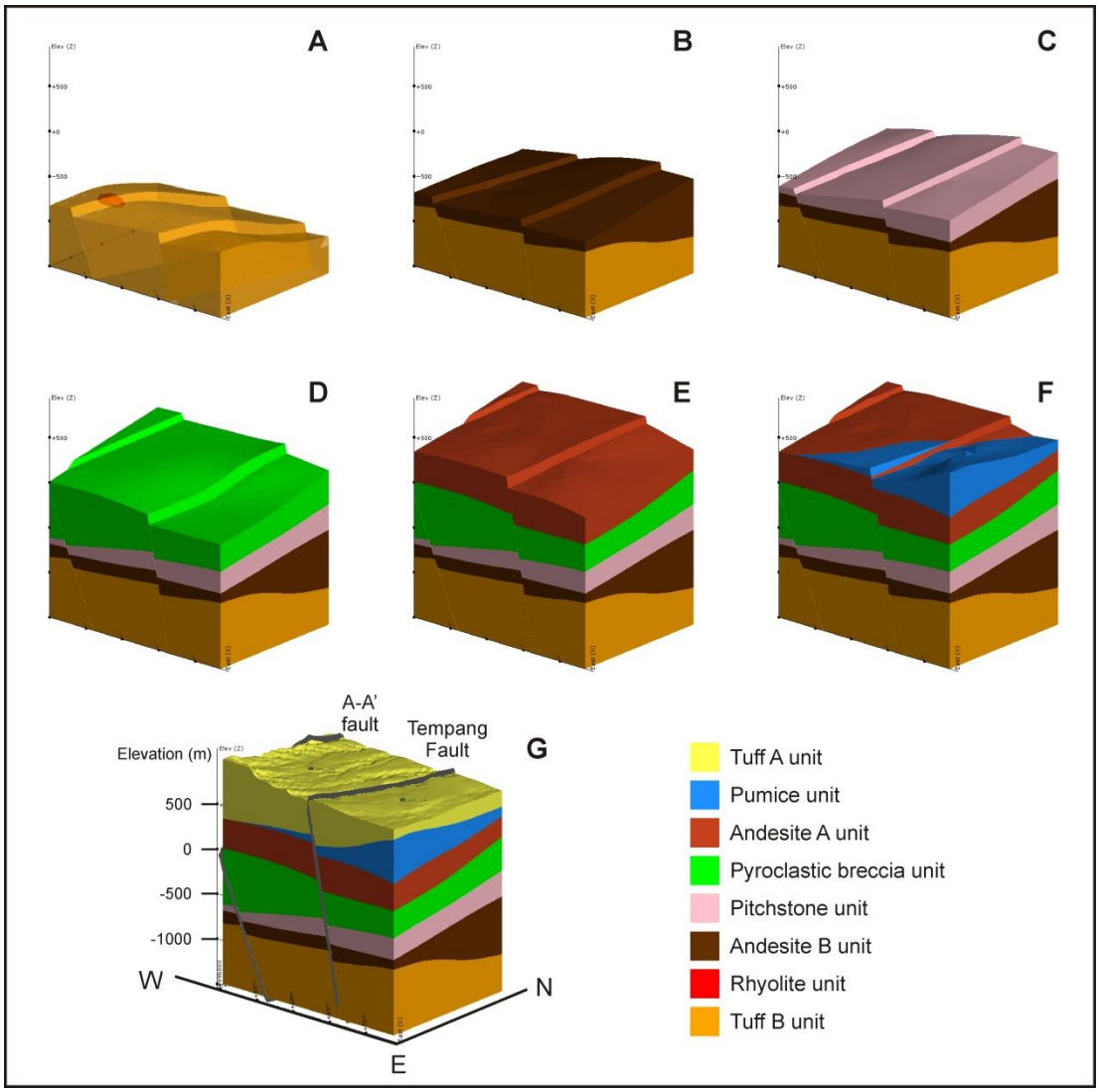

Figure 5.3. 3D geological model with the inferred A-A' fault generated using Leapfrog Geothermal software. (See electronic appendix F-01 for the 3D 360°-rotated visualisation of the model).

In addition to the hematite-anhydrite front, the predicted depth of the A-A' fault coincides with high IA of the Pitchstone unit at ~1500 m depth in LHD-26 (Fig. 4.16). The Pitchstone unit is weakly to moderately altered except at ~1500 m depth which may also suggest the

presence of the A-A' fault. Because the A-A' fault is parallel to the Tempang Fault, the dip angle of Tempang Fault is considered to interpolate the dip angle of fault A-A'. With the presence of fault A-A', the distribution of geological units in the subsurface should be affected. The updated geological model of Tompaso is illustrated in Fig. 5.3. Further investigation needs to be done to confirm existence of the A-A' fault.

5.2. Tompaso Geothermal System

5.2.1. Permeability controls of Tompaso system

Permeability is a key component in geothermal systems. Faults are the common permeable structures in volcanic-hydrothermal systems as most of these systems are situated in tectonically active areas. Kamah et al. (2010) inferred that the reservoir of the Tompaso geothermal system is strongly fractured. These fractures are essential in providing permeability within the reservoir. The circulation of hydrothermal fluids within Tompaso geothermal system (section 5.2.2.) are in agreement with the previous study showing that the permeability of the system is mostly controled by faults/fractures.

At the surface, the distribution of geothermal features within manifestation zone 3 demonstrates that the outflow of the system is controlled by the NE-SW Soputan Fault (Fig. 5.2). Observations in this study are in agreement with NNE-SSW faults determining the movement of hydrothermal fluids within the Tompaso system. The A-A' fault intersects LHD-26 at ~1500 m depth. The hydrothermal mineralogy suggests that this fault acts as a channel transporting meteoric water to depth from surface (section 5.1.2). The third fault is Tempang Fault, intersecting LHD-27 and LHD-32. This fault is predicted to have been hydrothermally sealed (section 5.2.2). Thus the Tempang Fault acts as a barrier confining the uprising hot hydrothermal fluids to the east from the circulating shallow surface water to the west. The role of the A-A' and Tempang Faults to the hydrological setting of Tompaso geothermal system is discussed in the next section (section 5.2.2).

5.2.2. Hydrological setting of Tompaso system

The type and distribution of surficial geothermal manifestation are controlled by the hydrological setting of a geothermal system. In Tompaso, the surficial geothermal features are distributed into 5 manifestation zones (Fig. 5.2), each of which has different characteristics. Detailed description of each manifestation zone and the map of their locations are presented in section 4.1.2.

The upflow of Tompaso geothermal system is located around Bukit Kasih on the northern flank of Soputan-Sempu-Rindengan volcano complex as indicated by manifestation zone 1 (Fig. 5.2). This manifestation zone is dominated by fumaroles and steaming ground, associated with acid hot springs, acid hydrothermal minerals (e.g. kaolinite), and rock leaching. The high acidity of hydrothermal fluids in this zone is proven by its high levels of sulfate in the fluid (Pertamina Geothermal Energy, n.d.-a). Intense fumarolic activity in this zone suggests that there could be a magmatic water influx at depth. Magmatic water consists of water, CO_2, HCl, SO_2 and H_2S. Magmatic SO_2 can experience disproportionation, while mixing with H_2O, producing H_2S acid gas and H_2SO_4 acid water. The H_2S then gives rise to fumaroles (and acid hot springs) in this zone (Henley & Ellis, 1983; Giggenbach, 1992; Shinohara et al., 1993).

The Soputan Fault is presumed to control the outflow of the Tompaso geothermal system, indicated by the presence of manifestation zone 3 (Fig. 5.2). This zone shows the most intense surficial geothermal activity which can be seen from the number of geothermal features, extent of the hydrothermally altered area, and temperature of the water (up to 80 °C). Compared to the other zones, manifestation zone 3 shows the most extensive geothermal activity, with the largest number of features located close one to another. The zone is characterised by hot springs and mud pots, having temperature of mostly 70-80 ^{o}C (section 4.1.2.3). Chemical analysis of hydrothermal water in manifestation zone 3 indicates discharge of four types of geothermal water: chloride, chloride-sulfate, chloride-bicarbonate, and sulfate-bicarbonate waters (Pertamina Geothermal Energy, n.d.-a).

One of the possible scenarios for the discharge of these hydrothermal fluids at the same zone is that, at depth, geothermal fluids undergo boiling processes due to adiabatic decompression during their travel upward. Boiling processes separate acid steam, which is mostly H_2S, from water. Near surface, oxidation of H_2S occurs due to the steam adsorption by meteoric water. Oxygen in the meteoric water reacts with the sulfuric acid gas producing

steam-heated acid sulfate waters by releasing H^+ and SO_4^{2-} (Henley & Ellis, 1983; Nicholson, 1993). Bicarbonate contents on the hydrothermal fluids are supplied by meteoric waters. Meanwhile, the Soputan Fault acts as an opening structure and allows chloride-rich hydrothermal waters to rise quickly to the surface without undergoing boiling.

It can be seen from the map (Fig. 5.2) that the surficial geothermal features of manifestation zone 3 are distributed along the Soputan Fault. It is likely that the Soputan Fault accommodates the flow of hydrothermal fluids from the upflow zone, around Bukit Kasih, to the NE towards Tempang. The second order structure of Soputan Fault may facilitate the formation of manifestation zone 5, as this zone has similar characteristics to manifestation zone 3 (section 4.1.2.5).

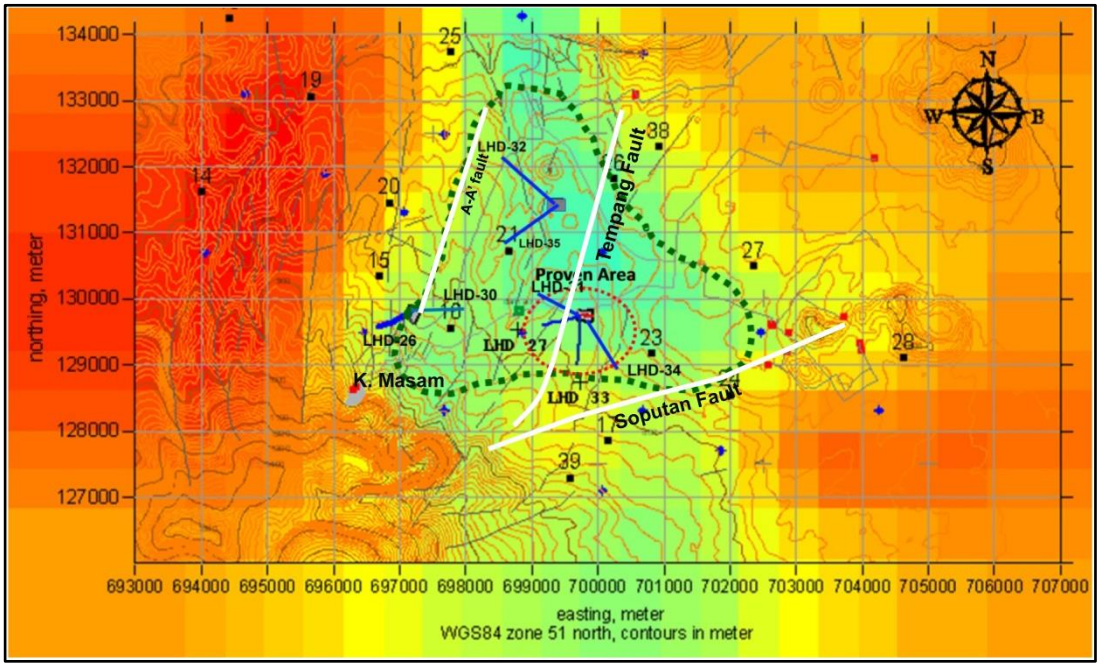

Figure 5.4. MT resistivity map of Tompaso area at 2000 m depth (~1000 mbsl) (modified from Handoko et al., 2010). Dotted line is the boundary of Tompaso geothermal system. The projected direction of LHD-31 and LHD-32 are wrong, see Fig. 5.2 for the correct direction. White lines are fault planes at 1000 mbsl. Soputan Fault is assumed to have a vertical fault plane.

The margin of Tompaso geothermal activity at the surface is marked by the occurrence of manifestation zone 4. Even though some features show a temperature of ~60 ^oC (section 4.1.2.4), the hydrothermal water chemistry is rich in bicarbonate (HCO_3^-) in agreement with cooler temperature and more mature waters (Pertamina Geothermal Energy, n.d.-a). This manifestation zone is formed by the same mechanism as manifestation zone 3. However, high content of bicarbonate suggests that the proportion of cold meteoric water is higher than those composing fluids at zone 2. Lake Tondano is likely responsible for introducing cold meteoric water, as this manifestation zone is located at the edge of the lake. Following

Henley and Ellis's (1983) model, the margin of geothermal systems typical of active island-arc volcanoes is characterised by near neutral pH chloride hot spring. The low content of chloride in this manifestation zone suggests that this zone is still located within the steam-heated zone and the margin of the system is somewhere further to the E-NE.

Even though the surficial hydrothermal activity extends from the flank of Soputan Volcano (SW) to the edge of Lake Tondano (NE), MT resistivity data shows that the potentially productive area of Tompaso geothermal system, projected at the subsurface, is restricted to the vicinity of the existing wells (Fig. 5.4) (Handoko, 2010; Raharjo, 2012). Increasing depth associated with decreasing pore space resulted in reducing the bore fluid effects which lead to the increase in resistivity (Ussher et al., 2000; Chave & Jones, 2012). In addition, hotter hydrothermal fluids form low conductivity alteration products (e.g. illite and chlorite) (Árnason et al., 2000; Ussher et al., 2000) On top of this low conductivity prospected zone, there is an impermeable conductive clay cap (Fig. 5.5). The colder outer margin of the geothermal system is marked by the conductive (low resistivity) zone (Fig. 5.4) (Árnason et al., 2000; Chave & Jones, 2012). The MT resistivity map of Tompaso geothermal system at 2000 m depth (Handoko, 2010; Raharjo, 2012) suggests that LHD-26 cluster[3] is located at the margin, while LHD-27 and LHD-32 clusters are in the middle of Tompaso potential productive area (Fig. 5.4).

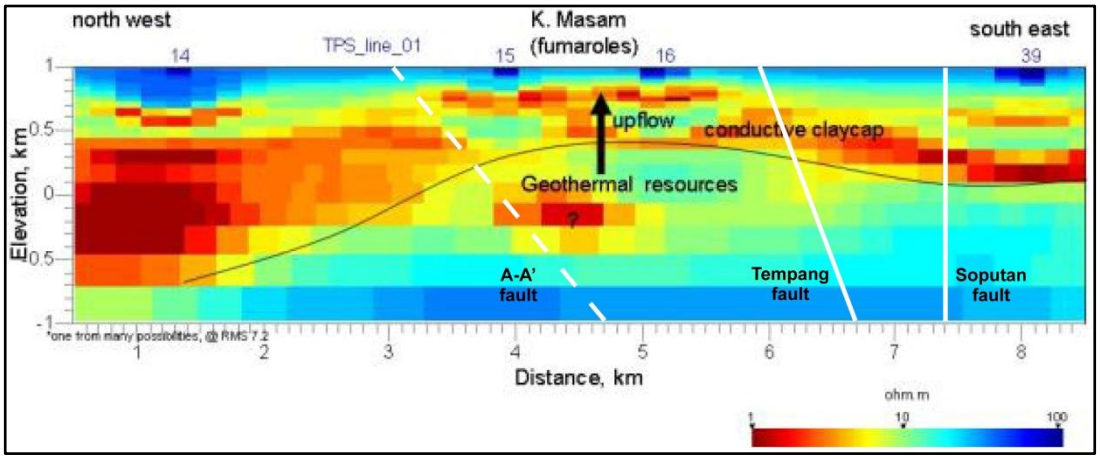

Figure 5.5. NW-SE cross section of Tompaso MT structure (modified from Handoko et al., 2010). Numbers at the top of the section are the MT stations (Fig. 5.5). The section does not intersect the A-A' fault (dashed line). The fault is to the NE of the section.

The western boundary of the system is in agreement with the orientation of A-A' fault (Fig. 5.4). As shown by the MT resistivity map (Fig. 5.4), the conductivity to the WNW of the fault A-A' is high and there is no indication of decreasing conductivity further to the WNW which

[3] The group of wells sharing the same location of well head. Refer to section 3.3.1 for the detailed description of well clusters in Tompaso.

suggests that fault A-A' could be the NW boundary of the prospected area of the Tompaso geothermal system. In LHD-26, the presence of A-A' fault is suggested by the anhydrite-hematite front (section 5.1.2.). The anhydrite-hematite front suggests that this fault acts as a channel for the descending cooler meteoric water to the east of the fault.

The present-day temperature structure of the Tompaso geothermal system is in agreement with the condition suggested by the anhydrite-hematite front for the A-A' fault. It is visible from the structure that the part of the system to the east of the A-A' fault is colder, although only the upper portion, than the part of the system to the west of the fault. However, the temperature increases at the eastern part of the system and Tempang Fault is likely to be the marker structure of this increasing temperature (Fig. 5.6).

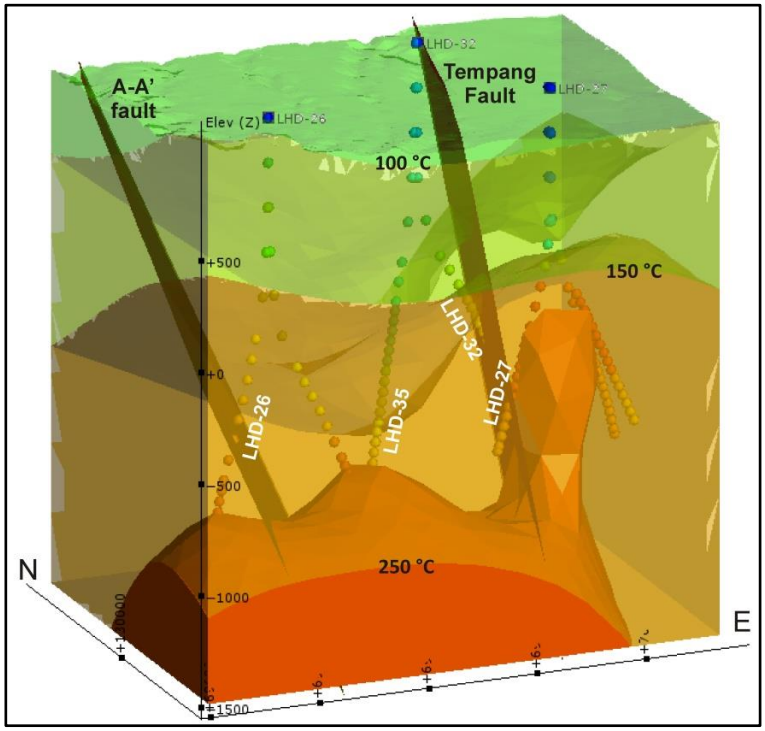

Figure 5.6. The A-A'-fault-updated temperature profile of Tompaso geothermal system. It is apparent that couple of Tempang and A-A' faults create a colder block in the middle. (See electronic appendix F-02 for the 3D 360°-rotated visualisation of the model).

The presence of the Tempang Fault is mainly identified by the temperature profile of the system since the lithologies of the well do not indicate the structure. There is a reverse temperature in LHD-27 (Fig. 5.6). The present-day temperature in this well increases down to 1554 m depth and then decreases downward (Pertamina Geothermal Energy, n.d.-d). At the deepest penetrated depth, epidote and illite is present as a replacement mineral at 1750 m depth coinciding with measured 208 °C. Epidote and illite are generally stable at 240 °C and 220 °C, respectively. Based on the temperature profile, the Tempang Fault has been inferred to have experienced a self-sealing mechanism so that the fault acts as an

impermeable structure inhibiting the hydrothermal fluid circulation. By assuming the self-sealing process of the Tempang Fault, it is likely that the A-A' fault introduces meteoric water into this part of the system especially at the shallow depth, but the movement of meteoric water is bounded to the east by the Tempang Fault.

5.2.3. Thermal history of Tompaso system

The history of hydrothermal activity in Tompaso geothermal system is reflected by secondary mineralisation. The coexistence of kaolinite and adularia at 200 m depth (~600 masl), for example, shows that there was a change of thermal regime in Tompaso geothermal system since these minerals cannot be in equilibrium. However, the thermal history of Tompaso are shown in more detail by the presence of several temperature indicator minerals (section 4.1.2.2) which provide information about the temperature when the mineral was formed. Epidote is normally stable at temperature higher than 240 °C with poorly crystalline epidote starting to form at ~200 °C (Reyes, 1990). In LHD-26, epidote is present at 1650 m depth in equilibrium with the measured 230 °C of the well at this depth (Fig. 5.7).

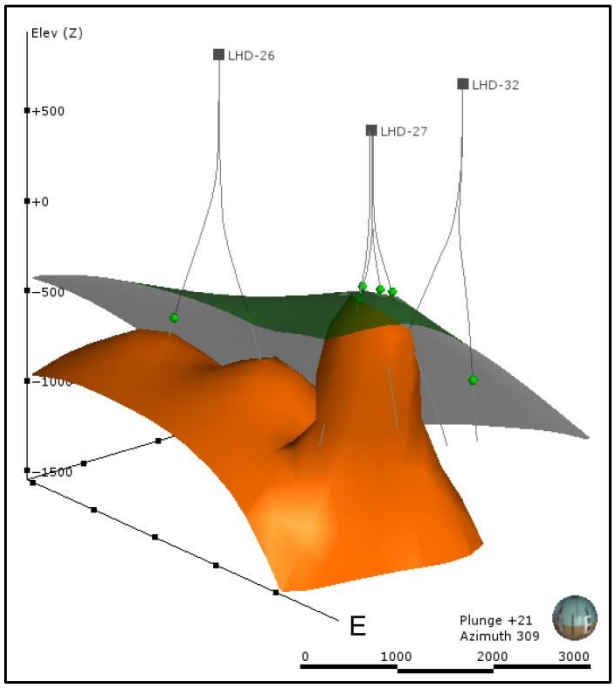

Figure 5.7. The first occurrence of epidote (green) represents the ancient 240 °C compared to present-day 240 °C (orange layer). The model is generated using Leapfrog Geothermal software. (See electronic appendix F-03 for the 3D 360°-rotated visualisation of the model).

The same condition is shown in LHD-27. Epidote is present at 900 m depth in LHD-27. The present-day temperature at this depth matches the formation temperature of epidote. Epidote is also present in other wells in LHD-27 cluster (LHD-31, LHD-33, and LHD-34) (Fig. 4.2; Fig. 5.7) (Pertamina Geothermal Energy, n.d.-e, n.d.-f, n.d.-g). The shallowest occurrence of epidote in these wells is present at measured ~250 °C which agrees with the formation temperature of epidote (Fig. 5.7). It is apparent that Tompaso system at the cluster of LHD-27 and LHD-26 has not been much modified since epidote has been formed. In contrast, epidote is found in LHD-32 at measured temperature of 57 °C colder than its formation temperature (Fig. 5.7) suggesting that LHD-32 has experienced cooling.

Cooling of the system in LHD-32 is also supported by the illite occurrences. The formation of illite occurs generally above 220 °C (Reyes, 1990). Illite is present in LHD-32 and LHD-26 at the depth where the measured temperatures are 159 and 171 °C, respectively (Fig. 5.8) (section 4.1.2). It is likely that the geothermal system experienced cooling in this area. The condition in LHD-26 shown by illite is in disagreement with epidote. However, the reason(s) for this disagreement is unknown without further investigation.

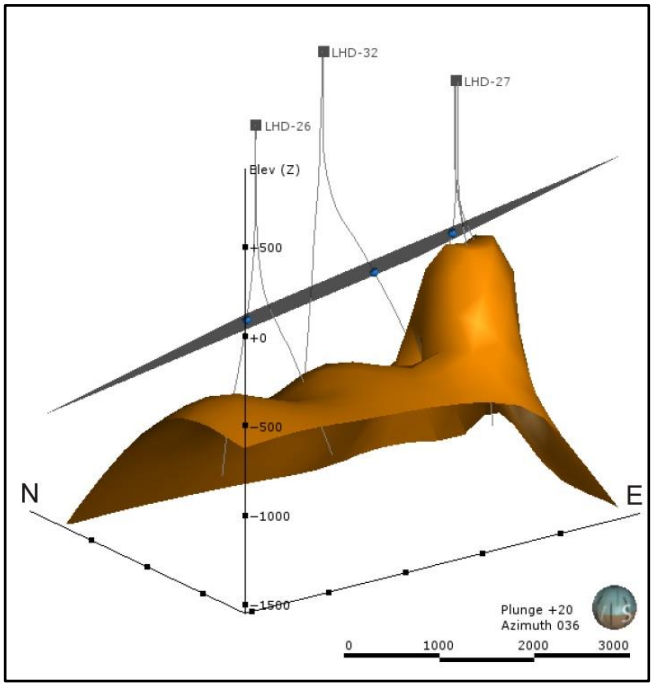

Figure 5.8. The first occurrence of illite (blue) represents the ancient 220 °C compared to present-day 220 °C (dark yellow layer). The model is generated using Leapfrog Geothermal software. (See electronic appendix F-04 for the 3D 360°-rotated visualisation of the model).

In LHD-27, illite was formed from 825 m depth. The depth of 800-900 m in LHD-27 is showing an abrupt increase of temperature from 128-254 °C (Pertamina Geothermal Energy, n.d.-d). It is plausible that 825 m depth shows a temperature of ~220 °C. Therefore, illite crystallisation is consistent with present-day temperature of LHD-27.

Smectite is another hydrothermal mineral commonly used as a temperature indicator. Smectite is stable up to ~180 °C. The deepest smectite in LHD-32 coincides with a measured temperature of ~165 °C (section 4.1.2). In the same cluster as LHD-32, smectite in LHD-35 is present at 70 °C (Pertamina Geothermal Energy, n.d.-d, n.d.-h). Both in LHD-32 and LHD-35, smectite appears in equilibrium with the present-day temperature of the geothermal system (Fig. 5.9).

The relationship of the deepest occurrence of smectite to present-day temperature in LHD-27 cluster shown by smectite is also consistent with the relationship shown by epidote and illite. Smectite is present down to 825 m depth in LHD-27. This depth is within the 800-900 m zone of abrupt temperature increase from 128-254 °C (Pertamina Geothermal Energy, n.d.-d) suggesting that it is likely that the measured temperature at 825 m matches the formation temperature of smectite. Therefore, epidote, illite, and smectite are in equilibrium with the present day temperature condition of LHD-27.

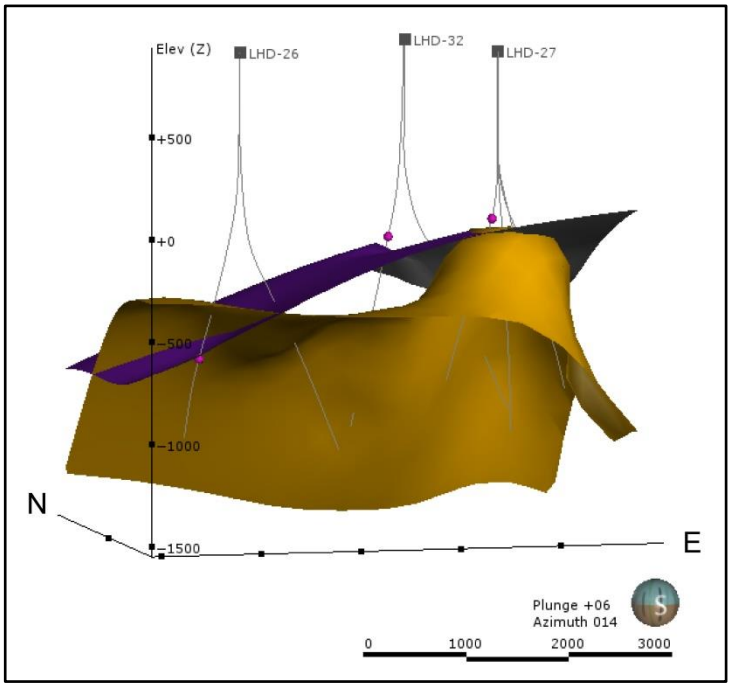

Figure 5.9. The deepest occurrence of smectite (purple) represents the ancient 180-200 °C compared to present-day 200 °C (yellow layer). The model is generated using Leapfrog Geothermal software. (See electronic appendix F-05 for the 3D 360°-rotated visualisation of the model).

In LHD-26, the deepest occurrence of smectite (1613 m depth) is below the present-day ~180 °C (Fig. 5.10). The temperature at this depth is 227 °C. Three possible scenarios can explain the occurrence of smectite at the present higher temperature in LHD-26. The first scenario is that there has been a recent heating in this part of the field and the smectite has not had a chance to respond and change to either illite-smectite or illite. This is in

disagreement with the observation drawn by the occurrence of illite suggesting cooling and epidote suggesting that the temperature is stable in this part of the system.

The second scenario requires low permeability in this part of the well, resulting in limited fluid movement. Fluid movement is needed to facilitate cation exchange. Tompaso geothermal system is hosted by andesitic lithologies where potassium levels in the rocks are low. Therefore, fluid movement is important for bringing potassium to form illite or interlayered illite-smectite. Consequently, lack of fluid movement leads to the formation of smectite in higher temperature.

The last scenario is that the identification was wrong. Unfortunately, EDS is not the best reliable method to determine clay composition. EDS can only qualitatively measure the chemical composition of sample. In addition, SWIR is not useful for identifying minerals in LHD-26 due to the natural colouration problem (section 3.3.5). Because the occurrence of smectite in LHD-26 is only inferred based on EDS, no favoured interpretation about the smectite stability is proposed.

Chalcedony is present in LHD-26 samples. Chalcedony is stable at low temperature up to ~180 °C (Fournier, 1985). In Karaha-telaga Bodas, chalcedony was formed at >250 °C as a result of rapid decompression of the geothermal system due to volcanic eruption (Moore et al., 2002). As indications of decompression are absent in Tompaso, the chalcedony is assumed to be formed in its equilibrium condition (up to ~180 °C). In LHD-26, chalcedony is present at measured 180 °C. It is apparent that the temperature of the system has not been modified since the formation of chalcedony. This condition is in agreement with the condition shown by epidote.

Based on the information provided by all the temperature indicator minerals, the thermal evolution of the system is proposed. The northern and western part of Tompaso geothermal system was hotter when it was initiated. Then, there was a cooling down of the system in the area of LHD-26 and LHD-32 clusters. The decreasing activity in this part of the system may be related to the self-sealing process in the A-A' and/or Tempang Fault. The cooling down processes is supported by the evidence of the epidote and illite occurrences.

The first occurrences of all hydrothermal minerals present in LHD-27 agree that this part of the system is stable.There has not been significantly changed since the geothermal system was initiated. However, it is apparent that the bottom part of LHD-27 is in disagreement to this conclusion. The present-day temperature at the bottom of LHD-27 is inconsistent with

the distribution of epidote. The temperature profile shows that there is a reverse temperature in LHD-27 (Fig. 5.3). The maximum measured temperature in this well is at 1554 m depth and then decreases downward (Pertamina Geothermal Energy, n.d.-d). The temperature at the deepest of the well is ~208 °C. Meanwhile, epidote and illite are present at ~1750 m depth, showing that this depth was once hotter. By assuming that the cooling is due to the sealing of the Tempang Fault, it is inferred that the self-sealing mechanism in this fault likely occurred after the formation of epidote and illite. The part to the west of the fault (i.e. the bottom part of LHD-27) then has undergone a recent cooling which may be related to the introduction of meteoric water by the A-A' fault.

5.2.4. Conceptual model of Tompaso system

A conceptual model is proposed in this work based on the discussion above (Fig. 5.10). It is apparent that the heat source of Tompaso system is the same magma system hosting the most recent volcanic activity in the area: Soputan Volcano (Morrice et al., 1983). Soputan Volcano is a Quaternary volcano showing its latest activity at January 4, 2016. The heat source supplies magmatic water into the system which then disproportionated, giving rise to fumaroles in the upflow zone, situated below the northern flank of the Soputan-Sempu-Rindengan volcano complex, as shown by surficial hydrothermal activity in manifestation zone 1. The hydrothermal fluids then flow laterally to the ENE following the Soputan Fault. The Soputan Fault acts as a channel facilitating the outflow of the hydrothermal system, reflected by manifestation zone 3. The hydrothermal fluids flow further to the ENE and apparently mix with the descending cooler meteoric water at the vicinity of Lake Tondano. The mixing between steam-heated fluids and meteoric water has resulted in the discharge of manifestation zone 4.

To the north of the upflow zone, the flow of hydrothermal fluids is bounded to the NW by the A-A' fault. The A-A' fault at once suspected to introduce cooler meteoric water to the depth in the eastern side of the fault, especially the upper portion, resulting in the cooling in this part of the system as suggested by hydrothermal mineralogy and present-day temperature structure in LHD-26 and LHD-32 clusters. However, the cold water does not flow all the way to the east because of the self-sealing process in the Tempang Fault. Thus, it is apparent that the eastern part of the Tompaso geothermal system (i.e. to the east of Tempang Fault) has not been much modified and there is no significant change in its

thermal structure (Fig. 5.10). Following this model, the pairing of Soputan Fault and Tempang Fault has created a thermal focus of Tompaso geothermal system at the intersection of these faults, where LHD-27 is located (Fig. 5.2, 5.10). However, this model is only one possible model of Tompaso geothermal system based on the results of this work. Further study is needed to draw a conclusion on this conceptual model.

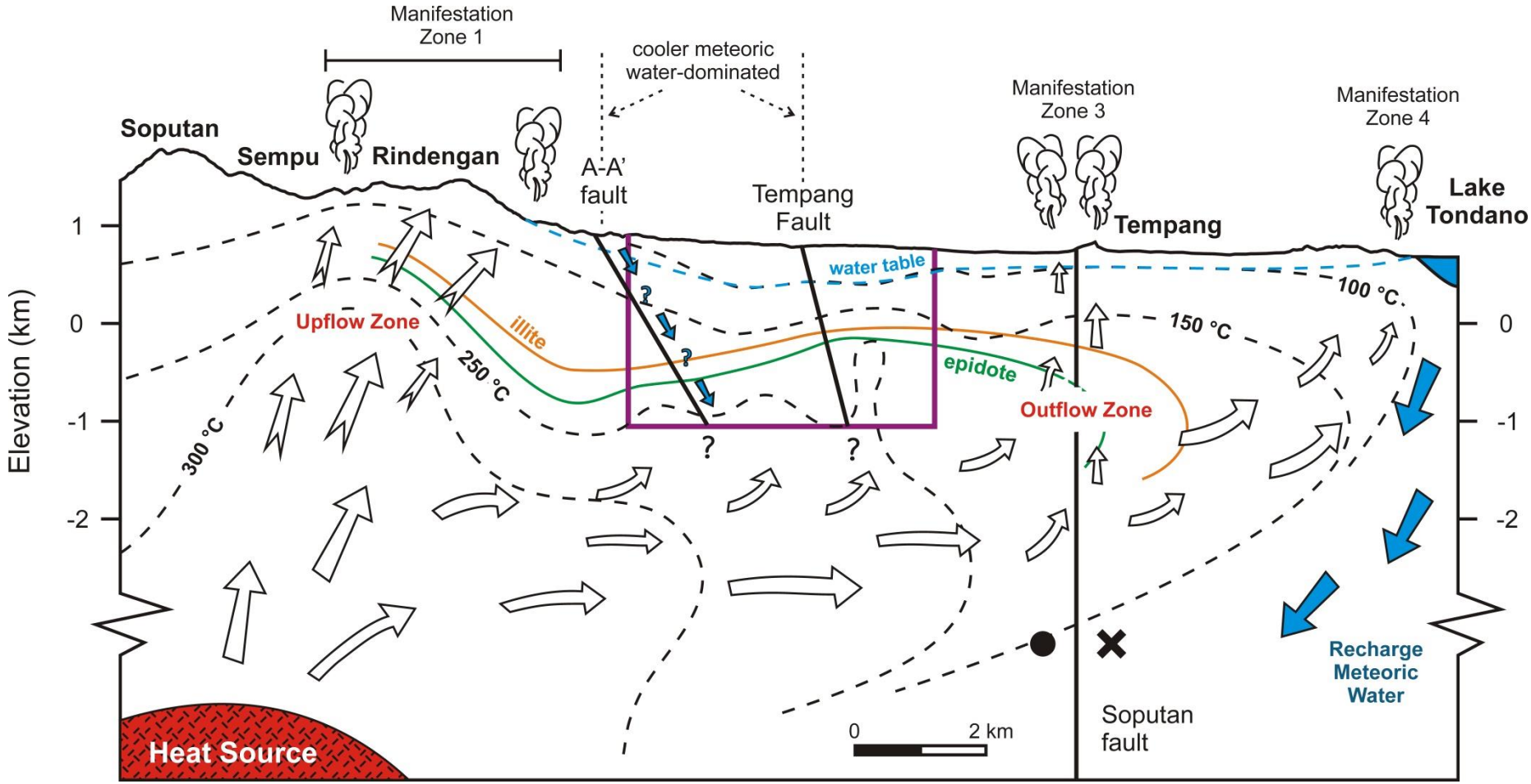

Figure 5.10. Proposed conceptual model of Tompaso geothermal system. White arrows represent hydrothermal fluids and blue arrows represent cooler meteoric water. Purple outline is the boundary of the 3D model (Fig. 5.3). The shallowest occurrence of illite and epidote is as marked.

5.3. Hydrothermal Alteration Processes in Andesite Lithologies

Observations on the distribution of hydrothermal alteration products with respect to textures of andesite lithologies have been undertaken in this thesis, investigating whether andesite textural properties may control the hydrothermal alteration processes. In active geothermal systems, lithologies have commonly been intensely altered so that it is difficult to identify their initial rock type. Therefore, the results of this observation were expected to give a contribution or guidance for future works on the identification of the altered rock type, especially andesite lithologies. Unfortunately, the results do not say much about the relationships between andesite textures and hydrothermal alteration.

Tompaso andesite lithologies are generally weakly altered as can be seen from the optical petrography and SWIR results. Most of the SWIR recordings contain only noise because of the natural colouration problem of the rock (i.e. the rocks are actually still fresh) (section 3.3.5). Therefore, Wairakei Waiora Valley Andesite (WVA) was used as comparison to Tompaso andesite lithologies. The WVA samples are generally more intensely altered than Tompaso's samples. Size of the samples is likely to be one of the limitations apart from the alteration intensity. Most of analyses in this work have been undertaken on fine-grained cuttings (<2 mm). Since the surface of samples is irregular, it is difficult to get a flat surface of cuttings in polished grain mounts. The BSE-EDS imaging thus could not produce good quality results. Further study using core is needed to support the results presented here.

Despite the challenges in this study, it is observed that hydrothermal alteration processes in andesite lithologies are likely influenced by mineralogy composition and texture. Volcanic glass, common in Tompaso andesites as groundmass, is very unstable and usually alters first. Following volcanic glass, ferromagnesian minerals are the next unstable minerals. In Iceland geothermal systems, Browne (1978) demonstrated that olivine and pyroxene had been altered first, compared to plagioclase. The pyroxene and hornblende of Tompaso and Wairakei systems show the same condition.

Another element of texture likely controlling the movement of hydrothermal fluids is the igneous textures. In both Tompaso and Wairakei samples, glomerocrysts of plagioclase+pyroxene are common. The glomerocrysts show higher IA than monomineralic plagioclase glomerocrysts (section 4.3.2). Plagioclase minerals, when they are present as single crystals or as monomineralic plagioclase glomerocrysts, are more stable and less susceptible to hydrothermal alteration processes. Meanwhile, plagioclase appears more

altered when it is associated with pyroxene in glomerocrysts. The higher IA of polymineralic glomerocrysts may suggest that bonding/grouping with less stable minerals reduce the resistance of a mineral to hydrothermal alteration. In addition, there are a number of plagioclase phenocrysts containing glass inclusions, forming sieve texture. These inclusions tend to alter more quickly than the rest of the crystal.

From the observation, crystal size does not affect the hydrothermal alteration preferences. Phenocrysts can be less altered than groundmass in some samples and the opposite in other samples. The phenocrysts are commonly more altered than groundmass since they have been fractured, although not always. It is apparent that the influence of structural weak zones (e.g. fractures and shears) is dominant in controlling hydrothermal alteration processes in massive lithologies, such as andesite volcanic rocks. The WVA sample of WK-122/584.4 m shows a flow-banding texture which was formed due to shearing during the emplacement of the rock (section 4.3). The sample demonstrates that the hydrothermal minerals replace first the micro fracture associated with the banding. Further study is needed to draw the conclusion on the andesite texture-hydrothermal alteration relationships.

CHAPTER SIX

SUMMARY

6.1. Evaluating Regional Geology of Tompaso Area

The regional stratigraphy of Tompaso area is dominated by products of the Tondano Caldera-forming eruption (the Tondano Tuff Formation). However, our understanding of the volcanic history of Tompaso area, especially Tondano Caldera, is vague since there has not been any geochemical analysis and/or age dating undertaken on Tondano Tuff Formation. There have been two different arguments on the general composition of this formation: intermediate and silicic, derived from different processes and mechanism. Therefore, geochemical analysis is the next essential study of this area so that the volcanic setting of Tompaso can be better constrained.

From the results of this work, eight units are present in the Tompaso area: from the oldest encountered unit — Tuff B unit, Rhyolite unit, Andesite B unit, Pitchstone unit, Pyroclastic Breccia unit,Andesite A unit, Pumice unit, and Tuff A unit. None of these units are dated. Consequently, subsurface stratigraphic correlations are difficult to assess. The silicic Pitchstone unit may correlate with Lengkoan Formation glassy obsidian. In addition, the similarity of the petrographic characteristics of the Pitchstone unit to those of Lengkoan Formation needs to be confirmed by age dating. If the two units are correlated, it is apparent that the Tondano Caldera forming eruption products are either present at deeper than 1400 m depth (~400 mbsl) or are not present at all. Consequently, this would help to reconstruct the volcanic setting of the area as the Tondano Caldera structure is present only ~7 km to the SE of the geothermal well locations.

Regardless of the similarity of the petrological characteristic of the Pitchstone unit to Lengkoan Formation, the distribution of this unit is likely reflecting a shallow rhyolitic magma chamber. The occurrence of the Rhyolite unit also suggests the presence of shallow rhyolitic magma chamber and both units are likely to be supplied by the same magma chamber. Even though there is no indication found of the greater Tondano silicic volcanic activity, the more localised rhyolitic volcanic activity is present in Tompaso area.

The NE-SW Soputan and NNE-SSW Tempang Faults have been widely recognised and named in regional geology, although there is no surficial indication of these faults observed during fieldwork. The other structures present in Tompaso area are NNE-striking lineaments, identified by topographic signatures. The orientation of these faults, as seen in the map (Fig. 5.2), suggests that their formation was related to the emplacement of Soputan Volcano. Soputan Fault does not intersect all studied wells, yet its presence is inferred from the alignment of surficial geothermal manifestations. Tempang Fault has also been accepted by previous workers. However, the fault is only indicated by present-day temperature structures and surface features of the geothermal system.

A fault located at the western end of the NNE-striking lineaments on the northern flank of Soputan Volcano is proposed to be the A-A' fault in this work. The fault has been estimated by the presence of an anhydrite-hematite front in LHD-26 as well as the MT resistivity structure of the area. However, none of the results collected in this work are strong enough to draw firm conclusions on this fault. Further research is needed to confirm the presence of the A-A' fault.

6.2. Conceptual Model of Tompaso Geothermal System

None of the units intercepted during the drilling of the studied wells appear to provide horizontal permeability for the geothermal system. The permeability of Tompaso system is predominantly controlled by faults. Surficial geothermal activity reflects the role of the NE-SW Soputan Fault in providing a channel for hydrothermal fluids and facilitates the discharge of the fluids at the surface. However, the extent of the Soputan Fault is not visible in the existing drilling wells.

The other faults controlling the hydrothermal fluids flow are the NNE-trending Tempang Fault. This fault has apparently been sealed and become a barrier of the uprising geothermal fluids to the east and descending cooler oxidising water to the west of the fault plane. In the western part of the system, the A-A' fault is likely the margin of the geothermal system as reflected by the MT resistivity profile separating the hotter geothermal system to the east from the cooler country rocks to the west of the fault. However, as suggested by the hematite-anhydrite front, this fault has likely become an

aquifer for the descending cooler meteoric water to the east of the fault. This may be the cause of the cooling down in this part of the system as reflected by hydrothermal mineralogy in LHD-26. The couple of Tempang and A-A' faults has created a block rich in cool meteoric water in the middle of the area marked as the prospective zone of the system by resistivity data. However, the colder block is likely to cover only the upper part of the system as reflected by present-day temperature profiles.

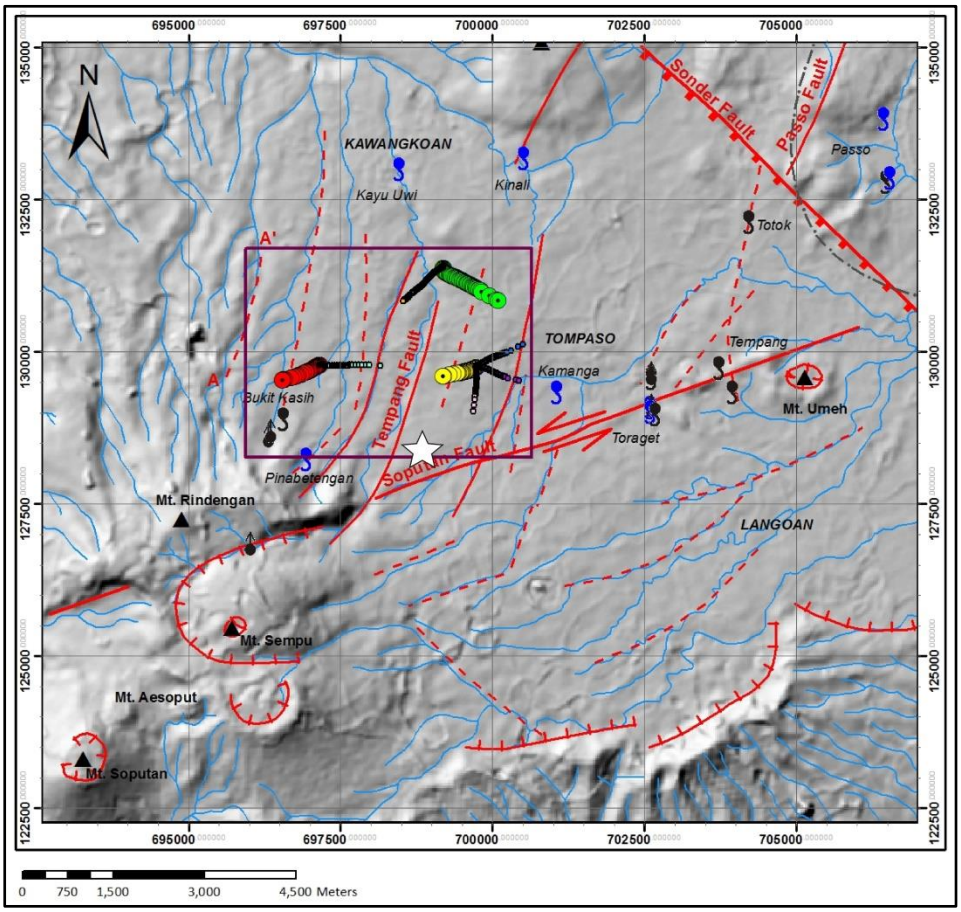

Figure 6.1. Map of the proposed targeted area. The most prospective targeted area is likely to be at the NE area of the intersections between Soputan and Tempang Faults (marked with a star symbol), close to LHD-27 cluster.

The conceptual model proposed in this work is only one of the possible models of Tompaso geothermal system. Further studies are required to evaluate this model. However, using this model, the next targeted production area can be proposed. For the purpose of targeting a well in geothermal energy production, depth is important. The shallowest possible depth is demanded in order to save the production costs. Since Soputan Fault is the main channel for the outflow of Tompaso geothermal system, heat transfer to near surface is located close to this fault. However, the presence of Tempang and A-A' faults inhibits the heat transfer from reaching the surface by allowing the accommodation of meteoric water in the area between these faults. Therefore, the most prospective targeted

area is likely to be at the NE area of the intersections between Soputan and Tempang Faults, near LHD-27 cluster. Drilling wells in this cluster show that present-day 250 °C profile is at slightly below sea level. Moreover, hydrothermal alteration products indicate that this part of the system is the most thermally stable, being the only cluster showing no changes in temperature since the geothermal system was initiated.

The area bounded by Tempang and A-A' faults could be a second prospective targeted area, especially in the southern part, close to the Soputan Fault. However, the wells would have to penetrate to deeper than 1000 mbsl as meteoric water dominates the upper portion of the block. The influence of meteoric water is stronger on the northern part of the block as shown by present-day temperature structure of the system as well as surficial geothermal activity in manifestation zone 3. Thus, only the southern part of this block represents a potential drilling target.

6.3. Andesite Textures and Hydrothermal Alteration Relationships

It was originally proposed that this work would contribute to knowledge of the preferential hydrothermal alteration of andesite by looking at the distribution of the secondary minerals related to the primary rock textures. This would allow easier identification of intensely altered andesite in hydrothermal areas. Unfortunately, samples available for this work were mainly fined-grained cuttings making comparisons challenging.

The results of this work indicate that the preference of hydrothermal alteration processes on andesite, except fractures, is influenced by mineral composition and arrangement. The abundance of ferromagnesian minerals correlates with the intensity of alteration. If the andesite rocks contain more ferromagnesian minerals, the rocks will be altered more easily. Bonding with ferromagnesian minerals also increases the susceptibility of plagioclase to hydrothermal alteration. Plagioclase in polymineralic glomerocrysts tends to be altered more quickly than plagioclase present in monomineralic glomerocrysts or as single crystals. In addition, glass inclusions in sieved-textured plagioclase crystals are altered more quickly than the rest of the crystals. Also, igneous rocks, both intrusive and extrusive, may have experienced shearing during emplacement creating flow-banding texture. Flow-banding texture in Wairakei Waiora Valley Andesite rocks shows that hydrothermal alteration

processes follow the orientation of the banding. The presence of a flow-banding texture gives pathways for the hydrothermal fluids, leaving the lenses of the banding to be the last component altered. Further study is definitely needed to draw the conclusion on the andesite texture-hydrothermal alteration relationships, especially on core samples.

REFERENCES

Alcaraz, S., Lane, R., Spragg, K., Milicich, S., Sepulveda, F. & Bignall, G. (2011). 3d geological modelling using new Leapfrog Geothermal software. In: *Proceedings of the 36th Workshop on Geothermal Reservoir Engineering, Stanford University, US*. Stanford, CA.

Allis, R. G. (1981). Changes in heat flow associated with exploitation of Wairakei Geothermal Field, New Zealand. *New Zealand Journal of Geology and Geophysics*, *24*, 1–19.

Árnason, K., Karlsdóttir, R., Eysteinsson, H., Flóvenz, Ó. G. & Gudlaugsson, S. T. (2000). The resistivity structure of high-temperature geothermal systems in Iceland. In: *Proceedings of the World Geothermal Congress 2000, Kyushu-Tohoku, Japan* (pp. 923–928).

AusSpec International. (2010). *AusSpec Workshop Manual for CD*. Australia: AusSpec International Ltd (http://www.ausspec.com/).

Bachri, S. (1977). *Geologi Lapangan Panasbumi Lahendong – Tompaso, Minahasa, Sulawesi Utara*. Jakarta, Indonesia: Seksi Penyelidikan Panasbumi, Subdit Volkanologi, Direktorat Geologi.

Barker, S. J., Wilson, C. J., Allan, A. S., & Schipper, C. I. (2015). Fine-scale temporal recovery, reconstruction and evolution of a post-supereruption magmatic system. *Contributions to Mineralogy and Petrology*, *170*.

Best, M. G. (2003). *Igneous and Metamorphic Petrology*. Berlin, Germany: Blackwell Science Ltd.

Bibby, H. M., Caldwell, T. G., Davey, F. J. & Webb, T. H. (1995). Geophysical evidence on the structure of the Taupo Volcanic Zone and its hydrothermal circulation. *Journal of Volcanology and Geothermal Research*, *68*, 29–58.

Bignall, G., Rosenberg, M. D., Kilgour, G. N., Milicich, S. D. & Rae, A. J. (2007). Stratigraphy of the western Wairakei Geothermal Field: insights from recent drilling in the greater Te Mihi area. In: *Proceedings of the 29th New Zealand Geothermal Workshop*. Auckland, New Zealand.

Bignall, G., Milicich, S. D., Ramirez, L. E., Rosenberg, M. D., Kilgour, G. N. & Rae, A. J. (2010). Geology of the Wairakei-Tauhara Geothermal System, New Zealand. In: *Proceedings of the World Geothermal Congress 2010* (pp. 25–30). Bali, Indonesia.

Bromley, C. J. (2009). Groundwater changes in the Wairakei–Tauhara geothermal system. *Geothermics*, *38*(1), 134–144.

Browne, P. R. L. (1970). Hydrothermal alteration as an aid in investigating geothermal fields. *Geothermics*, *2, Part 1*, 564–570.

Browne, P. R. L. (1978). Hydrothermal alteration in active geothermal fields. *Annual Review of Earth and Planetary Sciences*, *6*, 229–250.

Browne, P. R. L. & Ellis, A. J. (1970). The Ohaki-Broadlands hydrothermal area, New Zealand; mineralogy and related geochemistry. *American Journal of Science*, *269*(2), 97–131.

Cattell, H., Cole, J., Bignall, G. & Sepulveda, F. (2015). Influences of geological depositional processes and environments on geothermal strata from Wairakei-Tauhara

Geothermal Field, New Zealand. In: *Proceedings World Geothermal Congress 2015*. Melbourne, Australia.

Chambefort, I., Lewis, B., Wilson, C. J. N., Rae, A. J., Coutts, C., Bignall, G. & Ireland, T. R. (2014). Stratigraphy and structure of the Ngatamariki geothermal system from new zircon U–Pb geochronology: Implications for Taupo Volcanic Zone evolution. *Journal of Volcanology and Geothermal Research*, *274*, 51–70.

Chave, A. D. & Jones, A. G. (2012). *The Magnetotelluric Method: Theory and Practice*. Cambridge, UK: Cambridge University Press.

Cohen, K. M., Finney, S. C. & Gibbard, P. L. (2015). *International Chronostratigraphic Chart v 2015/01. International Subcommission on Stratigraphy*.

Cox, M. E. & Browne, P. (1998). Hydrothermal alteration mineralogy as an indicator of hydrology at the Ngawha geothermal field, New Zealand. *Geothermics*, *27*(3), 259–270.

Downs, D. T., Rowland, J. V., Wilson, C. J. N., Rosenberg, M. D., Leonard, G. S. & Calvert, A. T. (2014a). Evolution of the intra-arc Taupo-Reporoa Basin within the Taupo Volcanic Zone of New Zealand. *Geosphere*, *10*(1), 185–206.

Downs, D. T., Wilson, C. J. N., Cole, J. W., Rowland, J. V., Calvert, A. T., Leonard, G. S. & Keall, J. M. (2014b). Age and eruptive center of the Paeroa Subgroup ignimbrites (Whakamaru Group) within the Taupo Volcanic Zone of New Zealand. *Geological Society of America Bulletin*, *126*(9-10), 1131–1144.

Eastwood, A. A., Gravley, D. M., Wilson, C. J. N., Chambefort, I., Oze, C., Cole, J. W. & Ireland, T. R. (2013). U-Pb dating of subsurface pyroclastic deposits (Tahorakuri Formation) at Ngatamariki and Rotokawa Geothermal Fields. In: *Proceedings of the 35th New Zealand Geothermal Workshop*. Rotorua, New Zealand.

Effendi, A. C. & Bawono, S. S. (1997). Geological Map of the Manado Sheet, North Sulawesi. Jakarta, Indonesia: Geological Research and Development Centre.

Flegler, S. L., Heckman, J. W. & Klomparens, K. L. (1993). *Scanning and Transmission Electron Microscopy: An Introduction*. Oxford University Press.

Fournier, R. O. (1985). The behavior of silica in hydrothermal solutions. *Reviews in Economic Geology*, *2*, 45–61.

Ganda, S. & Sunaryo, D. (1982). *Laporan Pendahuluan Geologi Daerah Minahasa, Sulawesi Utara* (Internal Company Report). Jakarta, Indonesia: Divisi Geothermal Pertamina, Dinas Geologi, Seksi Geologi, PT Pertamina.

Geological Resource Centre. (2014). *Executive Summary: Pemutakhiran Data dan Neraca Sumber Daya Energi Status 2014* (p. 20). Bandung, Indonesia: Geological Resource Centre, Geological Agency, The Ministry of Energy and Mineral Resources of Indonesia. Retrieved from http://psdg.bgl.esdm.go.id/images/stories/neraca/neraca_2014/Executive%20Summary%20Neraca%20Energi%202014%20rev%20pusdatin.pdf

Giggenbach, W. F. (1992). SEG distinguished lecture: magma degassing and mineral deposition in hydrothermal systems along convergent plate boundaries. *Economic Geology*, *97*, 1927.1944.

Giggenbach, W. F. (1995). Variations in the chemical and isotopic composition of fluids discharged from the Taupo Volcanic Zone, New Zealand. *Journal of Volcanology and Geothermal Research*, *68*(1), 89–116.

Gravley, D. M. (2004). *The Ohakuri pyroclastic deposits and the evolution of the Rotorua-Ohakuri volcanotectonic depression.* (PhD Thesis). University of Canterbury, Christchurch, New Zealand. Retrieved from http://ir.canterbury.ac.nz:80/handle/10092/5465

Grindley, G. W. (1965). *The Geology, Structure and Exploitation of the Wairakei Geothermal Field, Taupo, New Zealand*. New Zealand Geological Survey Bulletin 75. Department of Scientific and Industrial Research, Wellington, New Zealand.

Hall, R. (1996). Reconstructing Cenozoic SE Asia. *Geological Society, London, Special Publications*, *106*, 153–184.

Hall, R. (2009). The Eurasian SE Asian margin as a modern example of an accretionary orogen. *Geological Society, London, Special Publications*, *318*, 351–372.

Hall, R. & Smyth, H. R. (2008). Cenozoic arc processes in Indonesia: identification of the key influences on the stratigraphic record in active volcanic arcs. *Geological Society of America Special Papers*, *436*, 27–54.

Handoko, B. T. (2010). *Resource assessment of Tompaso Geothermal Field, Indonesia* (No. 30) (pp. 647–674). Reykjavik, Iceland: United Nation University.

Henley, R. W. & Ellis, A. J. (1983). Geothermal systems ancient and modern: a geochemical review. *Earth-Science Reviews*, *19*(1), 1–50.

Hochstein, M. P. & Sudarman, S. (2015). Indonesianvolcanic geothermal systems. In: *Proceedings World Geothermal Congress 2015*. Melbourne, Australia.

Houghton, B. F., Wilson, C. J. N., McWilliams, M. O., Lanphere, M. A., Weaver, S. D., Briggs, R. M. & Pringle, M. S. (1995). Chronology and dynamics of a large silicic magmatic system: Central Taupo Volcanic Zone, New Zealand. *Geology*, *23*(1), 13–16.

Jaffe, L. A., Hilton, D. R., Fischer, T. P. & Hartono, U. (2004). Tracing magma sources in an arc-arc collision zone: Helium and carbon isotope and relative abundance systematics of the Sangihe Arc, Indonesia. *Geochemistry, Geophysics, Geosystems*, *5*, Q04J10.

Ji, J. & Browne, P. R. (2000). Relationship between illite crystallinity and temperature in active geothermal systems of New Zealand. *Clays and Clay Minerals*, *48*(1), 139–144.

Kamah, M. Y., Hartanto, D. B. & Thamrin, M. H. (2010). The evidence used in targeting wells in a geothermal reservoir using fracture zones and erratic structure at Lumut Balai and Tompaso Geothermal Area, Indonesia. In: *Proceedings World Geothermal Congress 2010*. Bali, Indonesia.

Kavalieris, I., Van Leeuwen, T. M. & Wilson, M. (1992). Geological setting and styles of mineralization, north arm of Sulawesi, Indonesia. *Journal of Southeast Asian Earth Sciences*, *7*(2), 113–129.

Lawless, J. V., White, P. J. & Bogie, I. (1997). *Important Hydrothermal Minerals and Their Significance* (7th ed.). Geothermal and Mineral Services Division, Kingston-Morrison Ltd.

Lécuyer, F., Bellier, O., Gourgaud, A. & Vincent, P. M. (1997). Tectonique active du Nord-Est de Sulawesi (Indonésie) et contrôle structural de la caldeira de Tondano. *Comptes Rendus de l'Académie Des Sciences-Series IIA-Earth and Planetary Science*, *325*(8), 607–613.

MacKenzie, W. S., Donaldson, C. H. & Guilford, C. (1982). *Atlas of Igneous Rocks and Their Textures*. England: Longman Group Limited.

Marini, L., Moretti, R. & Accornero, M. (2011). Sulfur isotopes in magmatic-hydrothermal systems, melts, and magmas. *Reviews in Mineralogy and Geochemistry*, *73*(1), 423–492.

Martin, R., Rodgers, K. A. & Browne, P. R. L. (1999). The nature and significance of sulfate-rich, aluminous efflorescences from the Te Kopia geothermal field, Taupo Volcanic Zone, New Zealand. *Mineralogical Magazine*, *63*(3), 413–413.

Martin, R., Rodgers, K. A. & Browne, P. R. L. (2000). Aspects of the distribution and movement of aluminium in the surface of the Te Kopia geothermal field, Taupo Volcanic Zone, New Zealand. *Applied Geochemistry*, *15*(8), 1121–1136.

McPhie, J., Doyle, M. & Allen, R. L. (1993). *Volcanic Textures: A Guide to The Interpretation of Textures in Volcanic Rocks*. Australia: CODES-University of Tasmania.

Mielke, P., Bignall, G. & Sass, I. (2010). Permeability and thermal conductivity measurements of near surface units at the Wairakei Geothermal Field, New Zealand. In: *Proceedings of the World Geothermal Congress 2010*. Bali, Indonesia.

Milicich, S. D. (2013). *Aspects of the Chronology, Structure and Thermal History of the Kawerau Geothermal Field*. (PhD Thesis). Victoria University of Wellington, Wellington, New Zealand. Retrieved from http://researcharchive.vuw.ac.nz/handle/10063/3044

Milicich, S. D., Bardsley, C., Bignall, G. & Wilson, C. J. N. (2014). 3-D interpretative modelling applied to the geology of the Kawerau geothermal system, Taupo Volcanic Zone, New Zealand. *Geothermics*, *51*, 344–350.

Milicich, S. D., Wilson, C. J. N., Bignall, G., Pezaro, B. & Bardsley, C. (2013a). Reconstructing the geological and structural history of an active geothermal field: A case study from New Zealand. *Journal of Volcanology and Geothermal Research*, *262*, 7–24.

Milicich, S. D., Wilson, C. J. N., Bignall, G., Pezaro, B., Charlier, B. L. A., Wooden, J. L. & Ireland, T. R. (2013b). U–Pb dating of zircon in hydrothermally altered rocks of the Kawerau Geothermal Field, Taupo Volcanic Zone, New Zealand. *Journal of Volcanology and Geothermal Research*, *253*, 97–113.

Milloy, S. F., Newson, J. & Sepulveda, F. (2014). Geothermal surface features at Geyser Valley, Wairakei, New Zealand. In: *38th Stanford Workshop on Geothermal Reservoir Engineering Proceedings*. Stanford University, California.

Moore, D. M. & Reynolds, R. C. (1989). *X-ray Diffraction and the Identification and Analysis of Clay Minerals*. Oxford, England: Oxford University Press.

Moore, J. N., Allis, R., Renner, J. L., Mildenhall, D. & McCulloch, J. (2002). Petrologic evidence for boiling to dryness in the Karaha-Telaga Bodas geothermal system, Indonesia. In: *Proceedings of the 27th Workshop on Geothermal Reservoir Engineering* (pp. 98–108).

Morrice, M. G., Jezek, P. A., Gill, J. B., Whitford, D. J. & Monoarfa, M. (1983a). An introduction to the Sangihe arc: Volcanism accompanying arc—arc collision in the Molucca Sea, Indonesia. *Journal of Volcanology and Geothermal Research*, *19*(1), 135–165.

Morrice, M. G., Jezek, P. A., Gill, J. B., Whitford, D. J. & Monoarfa, M. (1983b). An introduction to the Sangihe arc: Volcanism accompanying arc—Arc collision in the

Molucca Sea, Indonesia. *Journal of Volcanology and Geothermal Research*, *19*(1–2), 135–165.

Nelson, S. T. & Montana, A. (1992). Sieve-textured plagioclase in volcanic rocks produced by rapid decompression. *American Mineralogist*, *77*, 1242–1249.

Nicholson, K. (1993). *Geothermal Fluids: Chemistry and Exploration Techniques*. Berlin, Germany: Springer Verlag Inc.

Pertamina Geothermal Energy. (n.d.-a). *Data file for Tompaso: [Rekap data manif TPS.xls] version of 15 May 2013*. Jakarta, Indonesia: Unpublished report on file at PT Pertamina Geothermal Energy.

Pertamina Geothermal Energy. (n.d.-b). *Data file for LHD-32: [Data Excel LOGPLOT LHD-32.xls] version of 16 January 2013*. Jakarta, Indonesia: Unpublished report on file at PT Pertamina Geothermal Energy.

Pertamina Geothermal Energy. (n.d.-c). *Data file for LHD-26: [Data Excel LOGPLOT LHD-26.xls] version of 11 January 2013*. Jakarta, Indonesia: Unpublished report on file at PT Pertamina Geothermal Energy.

Pertamina Geothermal Energy. (n.d.-d). *Data file for Tompaso: [P & T Tompaso.xls] version of 20 January 2014*. Jakarta, Indonesia: Unpublished report on file at PT Pertamina Geothermal Energy.

Pertamina Geothermal Energy. (n.d.-e). *Data file for LHD-31: [Data Excel LOGPLOT LHD-31.xls] version of 15 January 2013*. Jakarta, Indonesia: Unpublished report on file at PT Pertamina Geothermal Energy.

Pertamina Geothermal Energy. (n.d.-f). *Data file for LHD-33: [Data Excel LOGPLOT LHD-33.xls] version of 16 January 2013*. Jakarta, Indonesia: Unpublished report on file at PT Pertamina Geothermal Energy.

Pertamina Geothermal Energy. (n.d.-g). *Data file for LHD-34: [Data Excel LOGPLOT LHD-34.xls] version of 17 January 2013*. Jakarta, Indonesia: Unpublished report on file at PT Pertamina Geothermal Energy.

Pertamina Geothermal Energy. (n.d.-h). *Data file for LHD-35: [Data Excel LOGPLOT LHD-35.xls] version of 15 January 2013*. Jakarta, Indonesia: Unpublished report on file at PT Pertamina Geothermal Energy.

Pirajno, F. (2009). *Hydrothermal Processes and Mineral Systems*. East Perth, Western Australia, Australia: Springer Science & Business Media.

Prasetyo, I. M., Sardiyanto, H. K. & Thamrin, M. H. (2015). Clay alteration study from wells of Tompaso Geothermal Field, North Sulawesi, Indonesia. In: *Proceedings of World Geothermal Congress 2015*. Melbourne, Australia.

Prijanto, Fauzi, A., Lubis, L. I. & Suwana, A. (1984). Geochemistry of the Minahasa Geothermal Prospect, North Sulawesi. In: *Proceedings of the 13th Indonesian Petroleum Association Annual Convention*, 473–485.

Pubellier, M., Spadea, P., Pouclet, A., Solidum, R., Desprairies, A., & Cambray, H. (1991). 34. Correlations of tephras in Celebes and Sulu sea basins: Constraints on geodynamics. In *Proceedings of the Ocean Drilling Program: Scientific results* (Vol. 124 pp. 459-465). College Station, Texas (Ocean Drilling Program).

Raharjo, I. B. (2012). *Geophysical signatures of volcano-hosted geothermal systems.* (PhD Thesis). University of Utah, Utah, US. Retrieved from http://gradworks.umi.com/34/99/3499205.html

Ramirez, L. E., Rae, A. J. & Bignall, G. (2009). Geochemistry of buried rhyolite lavas, Western Steamfield, Wairakei Geothermal Field, Taupo Volcanic Zone, New Zealand. *Geothermal Resources Council Transactions*, *33*, 949–952.

Rangin, C., & Silver, E. A. (1991). Neogene tectonic evolution of the Celebes-Sulu basins: new insights from Leg 124 drilling. In *Proceedings of the Ocean Drilling Program, Scientific Results* (Vol. 124, pp. 51–63). College Station, Texas (Ocean Drilling Program).

Reed, S. J. B. (2005). *Electron microprobe analysis and scanning electron microscopy in geology*. Cambridge, UK: Cambridge University Press.

Reyes, A. G. (1990). Petrology of Philippine geothermal systems and the application of alteration mineralogy to their assessment. *Journal of Volcanology and Geothermal Research*, *43*(1), 279–309.

Reyes, A. G., Giggenbach, W. F., Saleras, J. R., Salonga, N. D. & Vergara, M. C. (1993). Petrology and geochemistry of Alto Peak, a vapor-cored hydrothermal system, Leyte Province, Philippines. *Geothermics*, *22*(5), 479–519.

Risk, G. F., Rayner, H. H., Stagpoole, V. M., Graham, D. J., Dawson, G. B. & Bennie, S. L. (1984). *Electrical resistivity survey of the Wairakei geothermal field* (No. 200). Wellington, New Zealand: Geophysics Division, DSIR.

Roberts, J. J., Bonner, B. P. & Duba, A. G. (2000). Electrical resistivity measurements of andesite and hydrothermal breccia from the Awibengkok geothermal field, Indonesia. In *Proceedings of the 25th Annual Stanford Geothermal Reservoir Engineering Workshop* (pp. 339–344).

Robinson, B. W. (1985). Sulfur and sulfate-oxygen isotopes in New Zealand geothermal systems and volcanic discharges. Studies on sulfur isotope variations in nature. In: *Proceedings of an Advisory Group Meeting*. Vienna, Austria.

Rosenberg, M. D., Bignall, G. & Rae, A. J. (2009). The geological framework of the Wairakei–Tauhara Geothermal System, New Zealand. *Geothermics*, *38*, 72–84.

Rowland, J. V. & Sibson, R. H. (2004). Structural controls on hydrothermal flow in a segmented rift system, Taupo Volcanic Zone, New Zealand. *Geofluids*, *4*(4), 259–283.

Rowland, J. V., Wilson, C. J. & Gravley, D. M. (2010). Spatial and temporal variations in magma-assisted rifting, Taupo Volcanic Zone, New Zealand. *Journal of Volcanology and Geothermal Research*, *190*, 89–108.

Sanders, F., Chambefort, I., Rosenberg, M., Bignall, G., Rae, A. & Sepuvelda, F. (2013). Characterisation and stratigraphic correlation of the andesites encountered in the Wairakei Geothermal Field. In: *35th New Zealand Geothermal Workshop Proceedings*. Rotorua, New Zealand.

Sardiyanto, Nurseto, S. T., Prasetyo, I. M., Thamrin, M. H. & Kamah, M. Y. (2015). Permeability control on Tompaso Geothermal Field and its relationship to regional tectonic setting. In *Proceedings of World Geothermal Congress 2015*. Melbourne, Australia.

Seebeck, H., Nicol, A., Giba, M., Pettinga, J. & Walsh, J. (2014a). Geometry of the subducting Pacific plate since 20 Ma, Hikurangi margin, New Zealand. *Journal of the Geological Society*, *171*, 131–143.

Seebeck, H., Nicol, A., Villamor, P., Ristau, J. & Pettinga, J. (2014b). Structure and kinematics of the Taupo Rift, New Zealand. *Tectonics*, *33*(6), 1178–1199.

Sepulveda, F. R., Siega, C., Bixley, P. F., Mannington, W. I., Milloy, S. F., Soengkono, S. & Andrews, J. (2014). Wairakei Geothermal Field Boundary: Insights from Recent Geophysics and Reservoir Information. In *Proceedings of 39th Workshop on Geothermal Reservoir Engineering*. Stanford University, Stanford, California.

Shinohara, H., Giggenbach, W. F., Kazahaya, K. & Hedenquist, J. W. (1993). Geochemistry of volcanic gases and hot springs of Satsuma-Iwojima, Japan: Following Matsuo. *Geochemical Journal*, *27*(4/5), 271–285.

Siahaan, E. E., Soemarinda, S., Fauzi, A., Silitonga, T., Azimudin, T. & Raharjo, I. B. (2005). Tectonism and volcanism study in the Minahasa Compartment of the North Arm of Sulawesi related to Lahendong Geothermal Field, Indonesia. In: *Proceedings of World Geothermal Congress 2005*. Antalya, Turkey.

Sigurdsson, H., Houghton, B., McNutt, S., Rymer, H., & Stix, J. (2000). *Encyclopedia of Volcanoes*. San Diego, California: Academic Press.

Simpson, M. P., Mauk, J. L., Bowyer, D. & Worland, R. J. (2006). Alteration mineral studies of an epithermal prospect and a geothermal field using the TerraSpec. In: *Proceedings of the 39th Annual Conference of the New Zealand Branch of the AusIMM* (pp. 247–256).

Simpson, M., Rae, A., Ganefianto, N. & Sepulveda, F. (2013). Short wavelength infrared (SWIR) spectral characterisation of smectite, illite-smectite and illite for geothermal fields of the Taupo Volcanic Zone, New Zealand. In: *35th New Zealand Geothermal Workshop Proceedings* (pp. 17–20). Rotorua, New Zealand.

Siratovich, P., Davidson, J., Villeneuve, M., Gravley, D. M., Kennedy, B., Cole, J., Wyering, L & Price, L. (2012). Physical and mechanical properties of the Rotokawa Andesite from production wells RK 27_L2, RK28 and RK30. In: *34th New Zealand Geothermal Workshop Proceedings*. University of Auckland, Auckland, New Zealand.

Steiner, A. (1977). The Wairakei geothermal area, North Island, New Zealand: its subsurface geology and hydrothermal rock alteration. *New Zealand Geological Survey Bulletin 90*. New Zealand Dept. of Scientific and Industrial Research, Wellington, New Zealand.

Ussher, G., Harvey, C., Johnstone, R. & Anderson, E. (2000). Understanding the resistivities observed in geothermal systems. In: *Proceedings World Geothermal Congress 2000* (pp. 1915–1920). Beppu - Morioka, Japan.

Utami, P. (2011). *Hydrothermal Alteration and the Evolution of the Lahendong Geothermal System, North Sulawesi, Indonesia* (Unpublished PhD Thesis). University of Auckland, Auckland, New Zealand.

Utami, P., Siahaan, E. E., Azimudin, T., Suroto, Browne, P. R. L. & Simmons, S. F. (2004). Overview of Lahendong Geothermal Field, North Sulawesi Indonesia: a progress report. In: *Proceedings of the 26th NZ Geothermal Workshop* (pp. 6–11). Taupo, New Zealand.

Vandergoes, M. J., Hogg, A. G., Lowe, D. J., Newnham, R. M., Denton, G. H., Southon, J., Barrell, D. J. A., Wilson, C. J. N., McGlone, M. S., Allan, A. S. R., Almond, P. C., Petchey, F., Dabell, K., Dieffenbacher-Krall, A. C. & Blaauw, M. (2013). A revised age for the Kawakawa/Oruanui tephra, a key marker for the Last Glacial Maximum in New Zealand. *Quaternary Science Reviews*, *74*, 195–201.

Van Padang, M. N. (1951). *Catalogue of the Active Volcanoes of the World Including Solfatara Fields Part 1: Indonesia*. Napoli, Italy: International Association of Volcanology and Chemistry of the Earth's Interior.

Villamor, P. & Berryman, K. R. (2006). Late Quaternary geometry and kinematics of faults at the southern termination of the Taupo Volcanic Zone, New Zealand. *New Zealand Journal of Geology and Geophysics*, *49*(1), 1–21.

Wallace, L. M., Beavan, J., McCaffrey, R. & Darby, D. (2004). Subduction zone coupling and tectonic block rotations in the North Island, New Zealand. *Journal of Geophysical Research: Solid Earth, 109*. B12406.

Williams, H. & McBirney, A. R. (1979). *Volcanology*. San Francisco: Freeman Cooper.

Wilson, C. J. N. (2001). The 26.5 ka Oruanui eruption, New Zealand: an introduction and overview. *Journal of Volcanology and Geothermal Research*, *112*(1), 133–174.

Wilson, C. J. N. & Rowland, J. V. (2016). The volcanic, magmatic and tectonic setting of the Taupo Volcanic Zone, New Zealand, reviewed from a geothermal perspective. *Geothermics*, *59, Part B*, 168–187.

Wilson, C. J. N., Rogan, A. M., Smith, I. E. M., Northey, D. J., Nairn, I. A. & Houghton, B. F. (1984). Caldera volcanoes of the Taupo volcanic zone, New Zealand. *Journal of Geophysical Research: Solid Earth (1978–2012)*, *89*(B10), 8463–8484.

Wilson, C. J. N., Houghton, B. F., McWilliams, M. O., Lanphere, M. A., Weaver, S. D. & Briggs, R. M. (1995). Volcanic and structural evolution of Taupo Volcanic Zone, New Zealand: a review. *Journal of Volcanology and Geothermal Research*, *68*(1), 1–28.

Wilson, C. J. N., Gravley, D. M., Leonard, G. S. & Rowland, J. V. (2009). Volcanism in the central Taupo Volcanic Zone, New Zealand: tempo, styles and controls. In: *IAVCEI Proceedings in Volcanology 2* (pp. 225–247). London: Geological Society of London.

Wilson, C. J. N., Charlier, B. L. A., Rowland, J. V. & Browne, P. R. L. (2010). U–Pb dating of zircon in subsurface, hydrothermally altered pyroclastic deposits and implications for subsidence in a magmatically active rift: Taupo Volcanic Zone, New Zealand. *Journal of Volcanology and Geothermal Research*, *191*(1–2), 69–78.

Wood, C. P. (1996). Basement geology and structure of TVZ geothermal fields, New Zealand. In: *Proceedings of the 18th New Zealand Geothermal Workshop* (pp. 157–162). University of Auckland, Auckland, New Zealand.

Zhang, Y. (1999). H2O in rhyolitic glasses and melts: measurement, speciation, solubility, and diffusion. *Reviews of Geophysics*, *37*(4), 493–516.